Experimental Investigation of the Impact of Binder Composition and Hemp Hurd Particles on the Mechanical and Hygrothermal Performance of Hempcrete

by
Elmira Ataebi

Under the supervision of
Dr. Miroslava Kavgic

Co-supervisor
Dr. Reza Foruzanmehr

Thesis submitted to the University of Ottawa
in partial Fulfilment of the requirements for the
Master of Applied Science in Civil Engineering

uOttawa

Department of Civil Engineering
Faculty of Engineering
University of Ottawa

Abstract

Hempcrete, as a lightweight bio-based material, is increasingly gaining attention due to its decarbonization potential in the construction sector. The wooden-structured hemp hurd, combined with a lime-based binder and cementitious materials in the presence of water, forms a durable composite with excellent insulation properties and the ability to provide indoor hygrothermal comfort. This study aims to minimize the environmental impact of hempcrete by using locally sourced materials and increasing the proportion of bio-aggregate in the mixture. The research also seeks to address a gap in the literature by offering a more reliable comparison between various hempcrete binder compositions. This objective is achieved by isolating variables such as density, hemp hurd particle size distribution, and the dominant molar ratio in the binder mix design. The experimental study was conducted using standardized, finely ground hemp hurd, with a hemp-to-binder ratio of 1:1 by weight and a target density of 190 kg/m^3. Fifteen distinct hempcrete mix designs were developed using hydrated lime paired with five different supplementary cementitious materials (SCMs), including metakaolin, pumice, silica fume, slag, and Portland cement (as the reference SCM). The mixtures were formulated based on an innovative approach, using the CaO/SiO_2 molar ratio of the binders, and compared with conventional percentage-based binder formulations. Furthermore, hempcrete made with finely ground hemp hurd was compared to that made with conventional, as-received hemp hurd to further investigate the effect of particle size distribution. The comparisons were conducted in terms of mechanical and hygrothermal properties.

The results indicated an improvement in mechanical strength with the introduction of SCMs into the binder mixture. However, after reaching an optimal point, further increases in SCM content led to a decline in mechanical performance. Replacing hydrated lime with SCMs based on the CaO/SiO_2 molar ratio of the binder resulted in more consistent mechanical behaviour compared to conventional percentage-based mix designs. Furthermore, increasing the SCM content was found to increase thermal conductivity while reducing the heat capacity of the hempcrete. The incorporation of SCMs in the hempcrete composition

demonstrated improved performance in both mechanical and hygrothermal properties compared to the control samples, with metakaolin outperforming all other SCMs. In addition, hempcrete made with finely ground hemp hurd exhibited lower mechanical behaviour but superior insulation performance. Overall, the outcomes of this study provide new insights into more effective comparison methods for hempcrete components and contribute to a better understanding of the material's properties.

Keywords: Hempcrete, Hemp-lime concrete, Bio-based construction material, Hygrothermal properties, Mechanical properties, Metakaolin, Pumice, Silica fume, Slag, CaO/SiO_2 molar ratio

Acknowledgements

I would like to express my sincere gratitude to my supervisor, Dr. Miroslava Kavgic, for her continuous support and encouragement throughout this research. I also extend my appreciation to my co-supervisor, Dr. Reza Foruzanmehr, for his insightful advice and invaluable guidance.

Special thanks are due to Dr. Muslim Majeed for his support during the experimental phase and to Leo Denner for his help with the mechanical testing.

I would like to acknowledge my fellow graduate students, Dario Alonso Ramirez and Kamesh Solaiappan, for their thoughtful feedback and assistance with the structure and content of this thesis.

Finally, I wish to thank my colleagues, friends, and family for their unwavering support and encouragement throughout the course of this research.

I dedicate this thesis to my grandfather, who dares to challenge conventional ideas and inspires me to do so.

Table of Contents

List of Figures

List of Tables

List of Abbreviations

SCM	Supplementary Cementitious Material
NHL	Natural Hydraulic Lime
CL	Calcic Lime
OPC	Ordinary Portland Cement
C-A-S-H	Calcium Aluminum Silicate Hydrate
GGBS	Ground Granulated Blast-furnace Slag
SEM	Scanning Electron Microscope
GHG	Greenhouse Gases
DPC	Damp-Proof Course
UTM	Universal Testing Machine
DAQ	Data Acquisition System
TPS	Transient Plane Source
PLA	Poly Lactic Acid
MK	Metakaolin
PU	Pumice
SF	Silica fume
SL	Slag (Ground Granulated Blast-furnace Slag)
PC	Portland cement
XRF	X-ray Fluorescence
HFM	Heat Flow Meter
WVP	Water Vapour Permeability
THC	Tetrahydrocannabinol

Chapter 1

Introduction

1.1 Background

The increasing global awareness of climate change has shifted its perception from a future concern to an urgent, ongoing reality. Human-induced alterations witnessed since the mid-20th century have resulted in rising greenhouse gas levels in the atmosphere (Climate Change - NASA Science, 2024). Figure 1 illustrates the increase in atmospheric CO_2 levels since the beginning of the century, reaching values unprecedented for millennia (Carbon Dioxide Concentration | NASA Global Climate Change, 2024). Carbon dioxide emissions in North America are notably high, contributing 16.6% to the world's total output. This level surpasses the combined contributions of Europe, South America, and Central America (Bp Statistical Review of World Energy, 2022). Therefore, Canada has committed to the Paris Agreement by setting ambitious targets to reduce greenhouse gas emissions, aiming for net-zero emissions by 2050 and taking immediate action to limit global warming to well below 2°C, with efforts to pursue 1.5°C (The Paris Agreement, 2015).

The construction industry contributes over 37% of global CO_2 emissions (Building Materials and the Climate, 2023). A building's carbon footprint throughout its lifespan includes operational carbon, from energy used by occupants, and embodied carbon, resulting from material production and construction activities (GlobalABC Roadmap for Buildings and Construction, 2020-2050, 2020). Operational carbon has been addressed by building energy codes and standards worldwide that are becoming more stringent to reduce the energy consumption of the built environment. The most common strategies to improve building energy performance include increasing insulation in cold climates, balancing insulation and thermal mass in temperate climates, and enhancing thermal mass in hot and dry climates (Stanwix & Sparrow, 2014). However, increasing insulation (e.g., rock wool, fibreglass) and thermal mass (e.g., concrete, masonry,

stone) also raise a building's embodied energy. As energy performance standards increase, there is growing recognition of the need to reduce embodied energy and carbon, encompassing the materials, products, systems, and technologies used in construction.

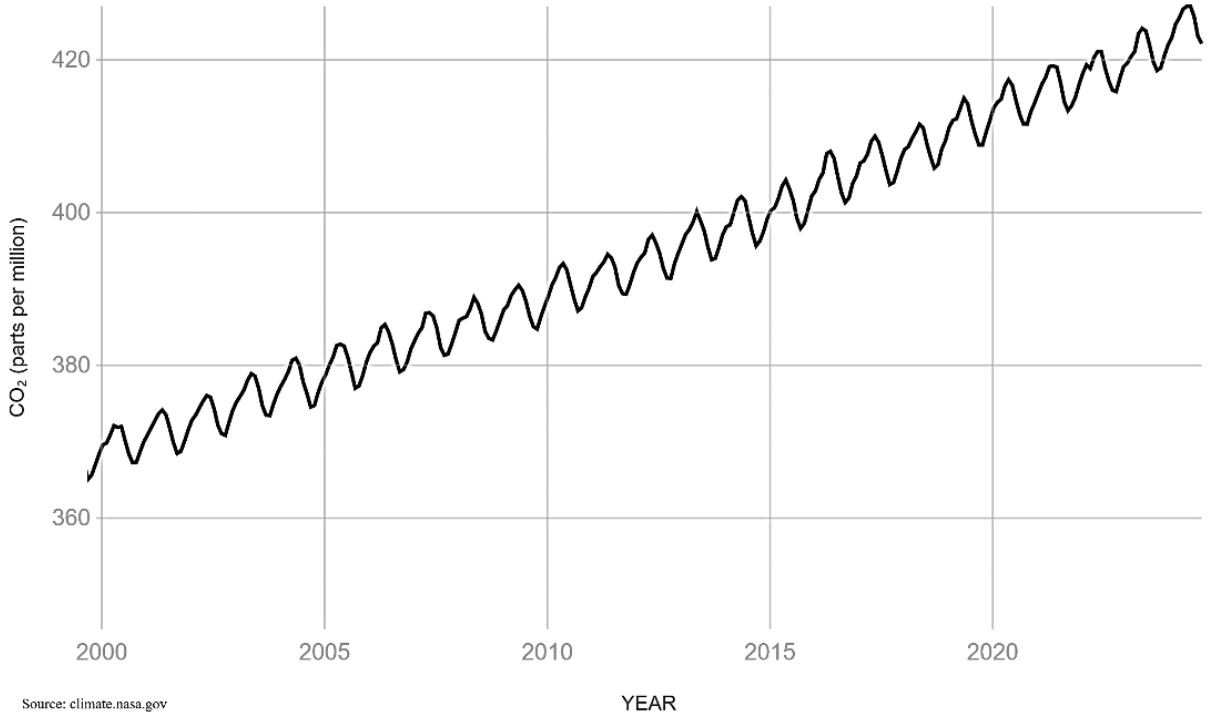

Figure 1- NASA's direct measurements of atmospheric CO_2 levels per year (*Carbon Dioxide Concentration | NASA Global Climate Change*, 2024)

The embodied energy of building materials arises from the energy consumed during their extraction, processing, transportation, and construction throughout their lifecycle (Grazieschi *et al.*, 2021; Karimpour *et al.*, 2014). Most traditional insulation materials, such as expanded polystyrene (EPS), polyisocyanurate/polyurethane (PIR/PUR), and extruded polystyrene (XPS), are derived from fossil fuels and carry high embodied energy. Given the reference value of 1 m^2 of area with 1 m^2K/W of thermal resistance and a 50-year lifespan design, which can be referred to as a functional unit (FU), the embodied energy and carbon vary across different materials. For instance, EPS ranges from 44- 78 MJ/FU and 1.9-

3.5 kg CO_2eq/FU, PIR/PUR from 63.1- 147 MJ/FU and 2.63- 10.4 kg CO_2eq/FU, and XPS from 47.3- 144 MJ/FU and 5.21- 13.22 kg CO_2eq/FU (Grazieschi *et al.*, 2021). Advanced super-insulating materials like aerogels can achieve similar thermal performance with less material yet carry a higher embodied carbon footprint (aerogels: 251- 372 MJ/FU and 11.6- 18.7 kg CO_2eq/FU) (Grazieschi *et al.*, 2021). Similarly, materials frequently used for thermal mass, such as concrete, are energy-intensive, mainly due to the high use of Portland cement, which contributes around 5- 7% of global CO_2 emissions (Cabeza *et al.*, 2021; Shobeiri *et al.*, 2021).

Lignocellulosic materials like hemp, flax, bamboo, and wood particles are abundant agricultural and forestry by-products with strong potential to help decarbonize the construction industry due to their carbon-storing capabilities. These bio-aggregates can be blended with cementitious binders, such as hydrated lime and Supplementary cementitious materials (e.g., metakaolin, slag, pumice), to create high-performance bio-based composites (Amziane & Sonebi, 2016; Ardanuy *et al.*, 2015; Chellapandian *et al.*, 2024). Studies have shown that these cementitious lignocellulosic composites offer excellent thermal insulation, high moisture-buffering capacity, enhanced energy efficiency, and indoor hygrothermal comfort (Lagouin *et al.*, 2019; Rahim *et al.*, 2016).

A prime example is the hemp-lime composite, commonly known as "hempcrete," composed of hemp's woody core (hurd or shive), a lime-based binder, and water. This lightweight and porous bio-composite is recyclable and has significant carbon storage properties. In this respect, hempcrete sequesters more atmospheric CO_2 through photosynthesis than it emits over its lifecycle, making it capable of achieving carbon neutrality (Shea *et al.*, 2012). It also offers superior thermal insulation, heat storage capacity, and airtightness (Abdellatef *et al.*, 2020; Stanwix & Sparrow, 2014). Additionally, hempcrete boasts excellent acoustic insulation, moisture regulation, durability, and resistance to pests and fire (Amziane & Sonebi, 2016; Collet *et al.*, 2013; Kinnane *et al.*, 2016a; Stanwix & Sparrow, 2014). These properties enable hempcrete walls to meet building code requirements and facilitate timber-frame construction, making it particularly suitable for use in high-performance, low-carbon buildings.

Numerous authors have investigated the properties of hempcrete, with a primary focus on the mechanical behaviour of the material (Arnaud & Gourlay, 2012; Elfordy *et al.*, 2008; Murphy *et al.*, 2010; T.-T. Nguyen *et al.*, 2009). Other studies have also examined the hygrothermal properties of hempcrete. Hence, Elfordy *et al.* (2008) concentrated on the mechanical properties and the relation between thermal conductivity and density of hempcrete, while Walker & Pavía (2014b) discussed the hygrothermal properties of the material in greater detail. However, most studies focused on higher-density (above 300 kg/m^3) hempcrete, whereas the low-density (150 to 300 kg/m^3) formulas remain less explored (Mahmood *et al.*, 2024).

Furthermore, selecting the optimal binder to pair with hemp hurd has been a subject of ongoing debate among authors. Even though the influence of different binder types has been investigated in several studies (Arnaud & Gourlay, 2012; Murphy *et al.*, 2010), most comparisons have focused primarily on various types of lime. Moreover, comparisons in review papers are not entirely reliable between specimens chosen from different studies, as it is rare to find two hempcrete samples with identical conditions across different research. Variations in binder type, hemp hurd origin and process, binder-to-hemp ratios, hemp hurd particle sizes, casting techniques, curing conditions, and test apparatus complicate direct comparisons. Some studies conducted a more comprehensive examination of the effect of various binders on hempcrete properties (Walker *et al.*, 2014; Walker & Pavía, 2014a, 2014b). However, the binders were chosen according to the material availability in Europe.

This study advances the understanding of how different binders affect hempcrete's mechanical strength and hygrothermal properties while minimizing the influence of hemp hurd variations. Additionally, it introduces a novel method for more efficiently comparing binder performance. The binder selection process focuses on the options currently available in Canada.

1.2 Objectives and Contribution to the Body of Knowledge

The primary aim of this thesis is to establish an innovative approach to develop the mix design with enhanced consistency, based on the binders' CaO/SiO_2 molar ratio, to allow direct and more effective

comparison between different mix designs. An additional objective is to develop a novel hempcrete composition with excellent hygrothermal properties, using locally available ingredients in Canada, in order to reduce environmental impact.

This study presents a novel comparison of various hempcrete binders available in Canada, addressing the limited research on this relatively new material within the country. In particular, it focuses on identifying and evaluating properties of binders made from locally sourced raw materials, filling a critical gap in existing knowledge. As highlighted in 1.1, only a few studies have directly compared different binder types under uniform casting and curing conditions. This study uniquely addresses this gap, providing a more reliable and controlled evaluation than typically found in previous research. Numerous studies have indicated the dominance of hemp hurd in influencing sample properties due to its substantial proportion in the mixture and its variable particle size compared to the binders. Focusing on binder comparison in hempcrete, the notable influence of hemp hurd in the mix prevents a favourable comparison. Therefore, in this study, the hemp hurd particles are finely ground to minimize the impact of the aggregate variable and provide a solid foundation for a more effective binder comparison. To the author's knowledge, this innovative approach has not been applied in other studies. Furthermore, this is the first study to introduce a novel approach to mix design using the binders' CaO/SiO_2 molar ratio for a more precise comparison, rather than the conventional method based on fixed percentages of hydrated lime and SCMs. Additionally, by creating the binder specimens with and without the hemp hurds, the effect of hemp shives has been presented on binder reactivity and properties.

Moreover, this study applied a considerable ratio of hemp hurd compared to most existing research to lower the carbon footprint and produce more lightweight material with superior hygrothermal performance suitable for insulation and wall filler applications. Additionally, this research compares finely ground hemp hurd particles' mechanical and thermal properties with conventional, as-received particle sizes. While few studies address this objective, this work further contributes by evaluating the energy required to process each type of hempcrete mix design.

1.3 Scope of the Work

The following steps have been undertaken to achieve the objectives:

- Four locally available Supplementary Cementitious Materials (SCMs) (metakaolin, pumice, slag, and silica fume) are selected as hardeners and combined with hydrated lime to create the different binder mix designs.
- The hemp hurd (shive) sourced from Canadian suppliers is ground to reduce its impact on the mixture as an aggregate.
- Specimens are created using selected binders and ground hemp hurd at a 1:1 ratio. Various binder combinations are considered for the mixtures. A mixing ratio of 7:3 (hydrated lime to SCMs) is applied for the conventional percentage-based approach. In addition, binders are prepared based on the CaO/SiO_2 molar ratio for each combination of hydrated lime and the selected SCMs. Where applicable, a mixture of Ordinary Portland Cement as the SCM with hydrated lime and pure hydrated lime is prepared as a reference for each set of samples.
- Each developed binder mix design is cast with and without aggregate to create hempcrete samples and binder specimens.
- Samples are prepared and cured under consistent conditions, including similar temperature and relative humidity. They follow similar dimensions, dry density, and age during testing.
- The specimens are tested for compressive strength, thermal conductivity, specific heat capacity, and water vapour permeability.
- The effect of hemp hurd presence and particle size, as well as binder types are investigated, and mixtures based on conventional percentages are compared with the CaO/SiO_2 molar ratio-based mixtures.

1.4 Thesis Structure

As a monograph thesis, this study includes five chapters and outlines the following structure:

Chapter 1: Presents a general introduction to the background of the study, including the primary problem that motivated this research to be conducted and the proposed solutions. It highlights the significance of the study, the main objectives, the novelties and contributions to the existing body of knowledge in the field, and the thesis structure.

Chapter 2: Offers a thorough literature review, beginning with an overview of hempcrete, its components, as well as the rationale behind choosing hempcrete for this study. The hempcrete properties, including mechanical, thermal, and moisture properties, are reviewed in detail. In addition, it presents a comprehensive examination of hempcrete, covering its applications, casting techniques, and mix designs. The chapter ends by identifying gaps in the literature that led to the selection of the specific objectives.

Chapter 3: Describes the raw materials utilized in the experiment, detailing the methods employed for sample preparation and maintenance. It also outlines the parameters for characterization, testing procedures, and the specifications of the apparatus used in the experiments.

Chapter 4: Provides the main findings of the study as well as a discussion of the rationale behind these results. It details the outcomes and related discussions regarding the characterization of the binders and hemp hurd. Most importantly, it compares the influences of hemp hurd and binder on hempcrete properties, including mechanical strength, thermal conductivity, specific heat capacity, and water vapour permeability. Furthermore, it thoroughly compares the effects of different SCMs used in hempcrete.

Chapter 5: Summarises the findings of the conducted research, indicates the existing limitations of the experiments, and provides suggestions for future studies.

Chapter 2

Literature Review

2.0 What is Hempcrete

Hempcrete, also known as lime-hemp concrete, is composed of hemp hurd as the bio-aggregate and hydrated lime as the primer binder. Hemp hurd, a by-product of the hemp plant, is primarily cultivated for the seed or fibre (Magwood, 2016). Hydrated lime, a low-impact binding agent, is commonly combined with materials such as hydraulic lime or supplementary cementitious materials (SCMs) with a reduced carbon footprint (Stanwix & Sparrow, 2014). Hempcrete is recognized as a durable and sustainable material, typically used as a wall, floor, or roof filler or as an insulation layer (Magwood, 2016). Owing to the high porosity ratio, the lightweight hempcrete exhibits remarkable hygrothermal and acoustic performance (Boulic *et al.*, 2013).

This chapter provides a comprehensive review of hempcrete, including the material's components, the rationale behind its selection, characterization, key properties (such as hygrothermal and mechanical), applications, casting techniques, and mix design.

2.1 Hempcrete Components

2.1.1 Hemp Hurd

2.1.1.1 Hemp History

Hemp refers to the Cannabis plant, a term derived from the Ancient Greek word *Kannabis*. The global varieties of hemp are categorized into three main types: *Cannabis Sativa*, the industrial hemp; *Cannabis Ruderalis*, the wild species; and *Cannabis Indica L.*, which contains a high concentration of tetrahydrocannabinol (THC). Among these three types of existing Cannabis, Cannabis Sativa has been

cultivated since the Neolithic era and is distributed worldwide (Boulic *et al.*, 2013; Stanwix & Sparrow, 2014).

Originating in China around 8000 BC, the plant has been proven to spread globally as its diverse applications were discovered afterward. Archaeological findings, such as ancient ropes and paper made from hemp, pottery with the depiction of individuals wearing hemp clothing, and the hemp seed itself, all indicate its widespread use (Boulic *et al.*, 2013; Jami *et al.*, 2019; Stanwix & Sparrow, 2014). A wealth of historical evidence underscores the crucial role of hemp, ranging from its compulsory cultivation by farmers in Britain to its contribution to Russia's victory over Napoleon's army (Stanwix & Sparrow, 2014). The plant was first introduced to North America in 1606 and became the most widely used fibre in the 19th and early 20th centuries prior to its prohibition (Liu *et al.*, 2023).

Hemp was recognized for both its beneficial properties as well as its potential for misuse. The material's decline began after World War I, when it was used as a drug, causing it to be prohibited and depriving society of its many other applications (Stanwix & Sparrow, 2014). However, modern industrial hemp production saw a resurgence, particularly in many European and Asian countries, followed by more limited adaptation in other continents, including North America. In Canada, agronomic industrial hemp was licensed again following its legalization in 1998 (Boulic *et al.*, 2013; Government of Canada, 2024; Magwood, 2016).

As hemp has been reintroduced to North America for less than three decades, its usage rate remains relatively limited. In November 2023, the area under hemp cultivation was reported to be 22,400 hectares (Government of Canada, 2024). Its broad range of applications, combined with the ability to capture carbon and heavy metals from the environment, positions it as an excellent candidate for industrial redevelopment (Boulic *et al.*, 2013). With the hemp industry progressing in North America, considerable price reductions for the material are anticipated due to the expected scale of future production (Magwood, 2016).

2.1.1.2 Hemp Structure and Specifications

Industrial hemp, which must contain less than 0.3% THC (Liu *et al.*, 2023), can be grown annually with stems measuring 2-4 metres in length and 1-3 cm in diameter. The stem is typically narrow and hollow, with its size and diameter influenced by the climate of the geographical cultivation area and the species type. It generally grows as a straight stem with minimal branching, maintaining similar morphology across different varieties. The stem consists of a central woody pith, known as the hurd, surrounded by a bark layer called the epidermis (fibre) (Boulic *et al.*, 2013; Jami *et al.*, 2019), as shown in Figure 2(a). The hurd, accounting for 60-70% of the hemp plant's weight, features a tubular porous structure with a large number of interconnected pores (Boulic *et al.*, 2013; de Bruijn *et al.*, 2009), as illustrated in Figure 2(b).

Hemp is a fast-growing crop, capable of reaching up to 30 cm in height weekly, which is advantageous for absorbing a notable amount of CO_2 in a short period. Cultivation typically starts in spring, with an 80–150-day vegetative period, leading to being harvested during summer. Harvesting the hemp in August, followed by chopping them into smaller pieces, the plants are left on the ground for a month to dry naturally under the sun. During this period, the fibre and hurd begin to separate through a process known as retting. After processing, hemp is compressed for efficient transportation. From one hectare of crop field, 12 tons of dry hemp with a moisture content below 15% can be achieved. If harvesting is delayed to collect seeds, there is a major shrinkage and drop in the quality of the stem (Boulic *et al.*, 2013; Stanwix & Sparrow, 2014).

The hemp plant shows a high capacity for adaptation to different climates and is highly tolerable. It can survive under challenging conditions, making it suitable for both hot and cold environments. Canada's climate, characterized by temperature, soil type, and precipitation, provides optimal conditions for hemp cultivation, and the plant has been successfully grown across the country (Boulic *et al.*, 2013; Liu *et al.*, 2023). Studies comparing hemp to other similar plants have highlighted its low environmental impact and minimal input requirements (Boulic *et al.*, 2013). For instance, hemp has a much lower chance of crop failure compared to flax, produces higher yields, and has less irrigation cost (Ahmed *et al.*, 2022).

Additionally, the energy utilized for hemp production is estimated to be half of that required for its parallels (Barbhuiya & Bhusan Das, 2022).

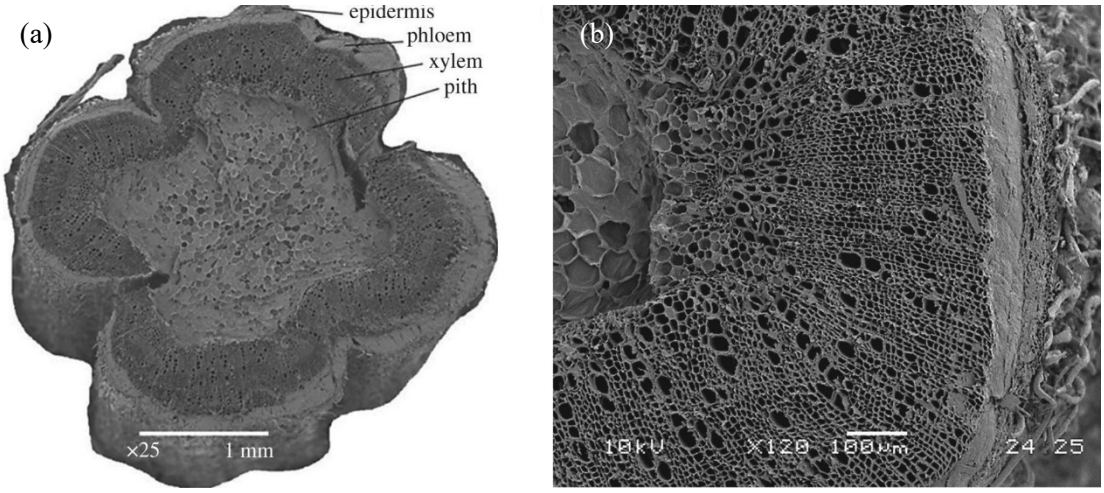

Figure 2- a) Hemp stem cross-section, b) Hemp stem micropores and macropores, (Jiang *et al.*, 2018)

The plant demands a relatively low amount of water, particularly when cultivated according to modern agricultural practices. It should be organically grown with organic fertilizers to obtain ideal fibre quality (Ahmed *et al.*, 2022). Due to its competitive nature for occupying the land and light, hemp does not require any weedkiller; in fact, it is deliberately cultivated to remove weeds that do not respond to chemicals. This characteristic, along with its soil-boosting properties, has made hemp a well-received choice in crop rotation systems among organic farming advocates. It is often cultivated before wheat and after legumes or can be paired with many other plants as well. Furthermore, being pest and fungus-resistant makes it a more sustainable and organic choice, as it requires no chemical interventions such as herbicides, pesticides, or fungicides (Boulic *et al.*, 2013; Stanwix & Sparrow, 2014).

Hemp, as opposed to most plants, has a wide variety of genetics (Liu *et al.*, 2023). The characterization and quality of hemp hurd as a bio-based material can vary, with factors such as the hemp's origin, harvest time, and retting process being crucial in determining the material's properties (L. Wang *et al.*, 2021). In France and Australia, standards to follow have been established for selecting hemp used in industry (Stanwix &

Sparrow, 2014), while most other countries, including Canada, lack regulatory specifications for characterizing industrial hemp or standardized processing methods since it is still considered a relatively new material. Various authors characterized hemp hurd in their experiments, and as expected, the results differ based on the type of material used. Table 1 summarises the gathered data from different studies.

Table 1- Hemp hurd specifications

Author	Apparent density (kg/m^3)	True density (kg/m^3)	Porosity	Water absorption	Moisture content
(Walker, 2013)	112.4 ± 2.2	-	-	350%	-
(Mahmood *et al.*, 2024)	94	-	-	-	7.2%
(Arnaud & Gourlay, 2012)	119	-	60%	200-300%	-
(Nguyen *et al.*, 2009)	113	-	93%	406%	12%
(Sinka *et al.*, 2014)	50	-	-	-	13.2%
(Abdellatef *et al.*, 2020)	110 ± 5	-	-	-	-
(de Bruijn *et al.*, 2009)	98	-	-	-	13.3%
(Bendouma *et al.*, 2023)	125.2 ± 2.9	1336 ± 0.2%	-	-	-
(Nozahic *et al.*, 2012)	103	-	-	406%	-
(Daher *et al.*, 2022)	104 ± 45	1438 ± 50	93 ± 5%	290 ± 15%	-
(Zerrouki *et al.*, 2022)	105	1256 ± 150	91 ± 5%	337%	-
(Jiang *et al.*, 2018)	80-160	1450	76.67 ± 2.03%	-	-

Furthermore, the chemical analysis of hemp hurd is presented in Table 2, which includes the weight percentage of compositions reported by four different authors.

Table 2- Chemical compositions of hemp hurd particles.

Author	Cellulose	Hemicellulose	Lignin	Extractives*	Ash	Others
(Magwood, 2016)	44%	25%	23%	4%	1.2%	2.8%
(Boulic *et al.*, 2013)	44%	18%	28%	7%	-	3%
(Jami *et al.*, 2019)	34-44%	18-37%	19-28%	5-8%	0-2%	0-2%
(Evrard, 2008)	50-60%	15-20%	20-30%	-	4-5%	-

As can be conceived, hemp hurd, as a bio-aggregate, is primarily composed of cellulose and hemicellulose. Cellulose contributes to the high tensile strength of the resulting product, whereas excellent moisture regulation of the material is inherited from the hemicellulose part. Additionally, the porous cellulose and hemicellulose nature result in significant porosity. The existing lignin acts as a natural binder, gluing the cell walls. It contributes to compressive strength while also protecting against microbial and chemical degradation as well as fire. Furthermore, extractives, including oil, protein, amino acid, pectin, and wax, influence the physical specifications of hemp hurd, such as colour and smell, and enhance its durability. These soluble compounds are also the premier reason for SCM reactions with aggregate, impacting the setting time and hardening process of hempcrete (Asghari & Memari, 2024; Laborel-Préneron *et al.*, 2018; Marceau & Delannoy, 2017; Wang *et al.*, 2021).

2.1.1.3 Hemp Applications

Hemp is among the agricultural products with a high yield potential. It has a wide range of applications, and many materials traditionally made from fossil fuels can be substituted with hemp constituents (Liu *et al.*, 2023).

The entire plant is utilized for various purposes, including biofuel or fuel for boilers, and the leaves are used as animal bedding and mulch. Canada, being the world's leading producer of hemp seeds, has numerous applications for them (Ahmed *et al.*, 2022; Liu *et al.*, 2023). The seeds are used as food for humans, birds, and animals. Moreover, the oil extracted from hemp seeds serves both edible and industrial purposes, such as oil paints, resins, solvents, industrial lubricants, inks, biodiesel fuel, and even in the pharmaceutical and cosmetic industries. Furthermore, hemp's cell fluid is utilized in the production of abrasive fluids (Boulic *et al.*, 2013; Stanwix & Sparrow, 2014).

Hemp bast fibre ranks second to be cultivated globally after jute (Ahmed *et al.*, 2022). It is a remarkably strong natural fibre compared to similar products (Liu *et al.*, 2023) and has a vast range of applications in scientific purposes, construction, automotive, and technical industries. Historically, the earliest uses of

hemp were related to its fibre, which was utilized to create thread. The fibre has also been used to produce paper for valuable books, banknotes, cigarette paper, coffee filters, and tea bags. Additionally, hemp fibre is employed in plastic production, replacing synthetic fibres to create fibre-reinforced plastics. It is combined with polymers to manufacture composites, mainly in the automotive industry, and is used to produce clothing fabrics, bags, shoes, rope, string, yarn, felt netting, and carpets. In construction, hemp fibre is applied in various forms, such as hemp wool for insulation, plasters, rendering, geotextile, and caulking textiles. Today, its most significant roles are in reinforcing plastics as a natural fibre and as an insulation material in construction (Boulic *et al.*, 2013; Stanwix & Sparrow, 2014).

Wooden hurd is a by-product of the hemp plant, whether cultivated for its bast fibre or seed and is typically discarded as landfill waste (Magwood, 2016). However, by a narrow margin, hurd is applied as animal bedding, mulch (for both horticulture and animal husbandry), packaging filler, and compressed into fuel pellets (Boulic *et al.*, 2013; Stanwix & Sparrow, 2014). Fine particles and dust from hemp hurd are also used in fishing bait and goods like mattress fillers. In recent years, hemp hurd has gained increasing use as an aggregate for hempcrete.

2.1.1.4 Hemp in the Construction Industry

Hemp was not the first plant used in construction history. Various types of hurd were utilized in combination with lime, particularly for finishing before the Industrial Revolution. In the mid-20th century, the widespread use of synthetic materials, due to their low cost, led to the use of non-permeable materials, harmful to the structure, and neglecting the bio-based alternatives (Stanwix & Sparrow, 2014). The earliest known application of hemp in construction dates back to 500 AD, with a bridge in France constructed using hemp mortar (Figure 3). In addition, a mansion built in Japan in 1698 is another historical example of hemp's use in construction. The durability and permeability of the material allow it to endure over time (Liu *et al.*, 2023).

Today, with the reconsideration of utilizing natural materials, there is increasing competition to identify the most suitable plant for construction applications (Boulic *et al.*, 2013). Hemp stands out among all other bio-composites and is currently the most widely used bio-based insulation material in construction (Jiang *et al.*, 2018; Liu *et al.*, 2023). Europe provides numerous examples of hemp's application in construction. In Canada, hemp was first utilized as a construction material in 2002 (Liu *et al.*, 2023). Both hemp fibre and hurd have diverse applications within the construction industry.

Figure 3- A bridge in France built in 500 AD with hemp (Liu *et al.*, 2023)

Hemp fibres, separated from the stalk's exterior, are primarily employed to enhance the rigidity and flexural properties of various products (Néron, 2019). Meanwhile, hemp hurd is mainly used as an aggregate, valued for its exceptional hygrothermal and acoustic performance (Magwood, 2016; Stanwix & Sparrow, 2014). Beyond hempcrete, which is comprehensively examined in this study, the following are examples of hemp's application in construction.

Hemp wool, derived from hemp bast fibres, is an eco-friendly substitute for conventional irritants and toxic mineral wool such as fibreglass and glass wool (Liu *et al.*, 2023). Distinguished by its durability compared to equivalent synthetics, hemp wool does not settle over time. It can maintain its structure for long ages thanks to the hemp fibre's strength. Moreover, the fibre cells excel in regulating humidity, particularly when

paired with permeable materials like hempcrete. Hemp wool insulation offers thermal performance comparable to synthetic parallels while noticeably reducing environmental impact (Boulic *et al.*, 2013; Stanwix & Sparrow, 2014).

Hemplaster is a lime plaster slurry reinforced with hemp fibre or a combination of fibre and hurd. The hemp improves the thermal properties of plaster by trapping air within the mixture. Furthermore, hemp increases the robustness of the plaster, making it well-suited for crack-prone areas. This reinforcement also reduces shrinkage and lowers the tending requirements of the plaster (Stanwix & Sparrow, 2014).

Hemp-reinforced concrete incorporates fibres as reinforcement, replacing a partial coarse aggregate in structural concrete. The concrete demonstrates a reduced environmental impact while maintaining comparable structural performance to conventional concrete. Moreover, it has been shown to exhibit enhanced ductility, making it a viable alternative in sustainable construction (Awwad *et al.*, 2014).

Overall, the application of hemp in the construction industry holds significant potential for reducing the sector's carbon footprint. Only in Canada, the availability of sufficient farmland and a favourable climate for hemp cultivation positions the country to expand its production capacity. By substituting hemp wool and hempcrete for conventional materials in all buildings, Canada could achieve an estimated 7.38% reduction in total carbon emissions (Liu *et al.*, 2023).

2.1.2 Binders

Lime is the primary binder in hempcrete and is often considered essential for at least a portion of the binder composition (Magwood, 2016). Although not an ideal choice (Ahmad *et al.*, 2021), Ordinary Portland Cement is known as the second most common binder in hempcrete due to its abundance and affordability (de Bruijn *et al.*, 2009; Delhomme *et al.*, 2022). In addition, commercial binders specifically formulated for hempcrete, commonly with hydrated lime as their primary component, along with hydraulic lime, pozzolans, and additives, have been widely used by researchers in producing hempcrete (Evrard, 2008; Murphy *et al.*, 2010; Nguyen *et al.*, 2009). However, the manufacturing processes of these binders

contribute to environmental impact and impose financial burdens. Several studies tried to develop alternative binders for hempcrete using materials such as wheat starch, gypsum, and gum Arabic (Bumanis *et al.*, 2020; Le *et al.*, 2014; Martínez *et al.*, 2024; Sinka *et al.*, 2015).

The permeability, low density, antimicrobial and antifungal properties, and low environmental impact of hydrated lime, as well as its abundance, are among the reasons it is the primary choice for pairing with hemp hurd. Despite the mentioned benefits, due to the late-setting and low strength of hydrated lime, it is preferred to be accompanied by a component to address its limitations. Hydraulic lime (NHL) has been the most common additive as the secondary binder component in hempcrete to date. NHL is produced by calcining limestone containing specific proportions of clay minerals and other impurities, which react with water to form hydraulic compounds. The suitability of limestone for this process depends on its chemical composition, which restricts the geographic availability of NHL. As a result, the NHL is not locally available in North America (Bendouma *et al.*, 2023; Magwood, 2016; Néron, 2019). Alternatively, numerous bio-based or chemical-based materials are available, each with different environmental impacts depending on their manufacturing process (Arrigoni *et al.*, 2017; Jami *et al.*, 2019). The following section provides an overview of hydrated lime and binders employed in this study, as well as a comparison of binders.

2.1.2.1 Hydrated Lime ($Ca(OH)_2$)

Although the use of hydrated lime as a natural glue in mixes dates back to Antiquity, it has gained significant attention in recent years (Néron, 2019). Hydrated lime or calcium hydroxide ($Ca(OH)_2$) is recognized as an extremely alkaline substance with a pH level of around 11. It is also referred to as air lime due to its reaction with air, in contrast to the reaction of hydraulic lime in the presence of water. Slaked lime, calcium lime, calcic lime (CL), pure lime, and fat lime are other terms used for the material (Stanwix & Sparrow, 2014). Hydrated lime is abundantly available and can be sourced across North America by many local suppliers (Bendouma *et al.*, 2023; Magwood, 2016).

The presence of hydrated lime in many ancient buildings specifies the durability of this material (Stanwix & Sparrow, 2014; Vyšvařil *et al.*, 2023). Its high alkalinity prevents the lime-based material from biological degradation (Brzyski, 2018). Nevertheless, being a natural, breathable substance, which indicates high water vapour permeability of lime, is a notable property that provides the material with long-term durability (Brzyski, 2018; Jami *et al.*, 2019; Néron, 2019; Stanwix & Sparrow, 2014; Walker, 2013). Furthermore, the late setting time of hydrated lime in hempcrete mixtures, owing to the wet conditions created by the binder's high alkalinity, allows the central parts of the produced material to dry properly and prevents interior rotting (Jami *et al.*, 2019; Walker, 2013). In addition, the hydrophilicity of hydrated lime and high moisture-buffering capacity are in alignment with the properties of hemp hurd, ensuring compatibility and enhanced performance in hempcrete applications (Jami *et al.*, 2019).

Even though hydrated lime is corrosive, harmful to inhale, and irritating to the skin during dry mixing, once dried, hempcrete is not dangerous or toxic to humans (Néron, 2019; Stanwix & Sparrow, 2014). It has no negative influence on the indoor environment and actively contributes to maintaining healthy indoor air quality for occupants (Magwood, 2016). Additionally, using lime as the binder prevents insect and vermin attacks and makes the resulting material fire-resistant. It also has natural antiseptic, antifungal, and disinfection properties (Magwood, 2016; Néron, 2019), and has been proven to enhance the antimicrobial activities of the produced hempcrete (Horszczaruk *et al.*, 2023). All the mentioned benefits, along with its abundance, make hydrated lime an excellent choice as a binder for hempcrete.

In the production process of hydrated lime, known as calcination, limestone heats up in a kiln, producing CO_2 and hydraulic lime (CaO), and then hydrated lime ($Ca(OH)_2$) is generated with the introduction of water. The resulting material, in the presence of air, reverts to its initial state of limestone, known as the carbonation process. Figure 4 illustrates the mentioned cycle. The natural chemical procedure of carbonation begins within the first 24 hours and continues gradually for up to 30 years, during which the material sets and hardens. Accordingly, the hempcrete strengthens over time through carbonation (Boulic *et al.*, 2013; Jami *et al.*, 2019; Néron, 2019; Stanwix & Sparrow, 2014).

Although both lime and cement are produced through limestone calcination, cement requires an additional clinkerization process at 1400 °C, resulting in higher embodied carbon. This makes lime the preferred choice over cement from a sustainability perspective (Jami *et al.*, 2019; Stanwix & Sparrow, 2014; Walker, 2013). While hydrated lime produces a relatively high carbon footprint of 0.78 $kgCO_2e/kg$, a considerable portion of these emissions is offset during the carbonation process (Magwood, 2016).

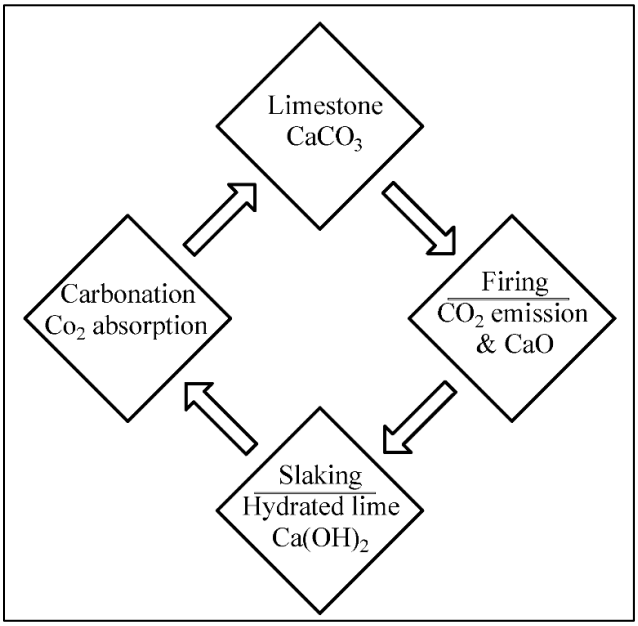

Figure 4- The hydrated lime cycle of production and carbonation- modified (Néron, 2019).

As mentioned earlier, the slow-drying property of hydrated lime is an advantage for hempcrete. However, the very long drying period makes the hydrated lime unsuitable as the sole binder for hempcrete, particularly in on-site applications (Stanwix & Sparrow, 2014). The excess moisture remaining for a long period may cause mould and decay within the core of the thick hempcrete. Furthermore, the lack of strength and structural integrity in hydrated lime, due to its deficiency in clay components, such as silica and alumina, poses challenges in hempcrete, especially at early ages (Brzyski, 2018; Stanwix & Sparrow, 2014). All in all, combining a Supplementary Cementitious Material with hydrated lime as the dominant component addresses the mentioned issues while retaining the compatibility of lime with hemp hurd properties.

2.1.2.2 Supplementary Cementitious Materials (SCMs)

The replacement of Ordinary Portland Cement (OPC) or hydraulic lime (NHL), the most common components to add to hydrated lime in hempcrete, with more sustainable SCMs is gaining attention among researchers (Magwood, 2016; Stanwix & Sparrow, 2014; World Energy Outlook 2022, 2022). SCMs are low-impact materials that reduce landfill waste. They exhibit relatively low specific gravity, as well as enhanced durability compared to OPC (Tale Masoule *et al.*, 2022), and can improve the resulting material's performance while increasing its airtightness (Murphy *et al.*, 2010; Néron, 2019; Pavía & Aly, 2016).

SCMs are classified according to their cementitious ingredients, such as CaO, SiO_2, and Al_2O_3. They either demonstrate cementitious properties, with a high calcium content exceeding 70% of calcium and silica in total, indicating their hydraulic nature, or they have pozzolanic properties characterized by low calcium and high silica and alumina content (Garcia-Lodeiro *et al.*, 2015a). Accordingly, the cementitious reaction is between the cementitious material, exhibiting intrinsic hydraulicity, and water, through hydration, forming calcium (aluminum) silicate hydrate C-(A)-S-H gel, comparable to gel produced during Portland Cement hydration. Pozzolanic materials, on the other hand, can have hydraulic behaviour in exposure to calcium hydroxide and water. Calcium hydroxide, resulting from the hydration process of hydrated lime, finally reacts with silica (and alumina if present in sufficient amounts) from pozzolans to form calcium (aluminum) silicate hydrate C-(A)-S-H gel, similar to gel in Portland Cement hydration. Binders such as slag and OPC exhibit cementitious behaviour, while materials like metakaolin, silica fume, fly ash, pumice, and rice husk ash are categorized as pozzolans, regardless of whether they originate from natural materials or industrial by-products (Garcia-Lodeiro *et al.*, 2015b; Panesar, 2019; Pavía & Aly, 2016).

2.1.2.2.1 Ordinary Portland Cement (OPC)

Portland cement was the key development in the attempt to create artificial lime in the 19th century. It was generated by calcining limestone and clay, followed by clinkerization at extremely high temperatures of 1400 to 1500°C (Stanwix & Sparrow, 2014). The resulting material typically has an angular shape (Provis *et al.*, 2010) and a specific gravity of 3.15 (Hedayatinia *et al.*, 2019; Zeyad *et al.*, 2022). Its accelerated

setting time, predictability with consistent results, and the ability to form stronger bonds compared to lime-pozzolanic mixtures are among the reasons for being massively replacing lime, despite initially being neither cost-effective nor widely available. However, Portland Cement's high carbon footprint is not the material's only drawback. Its lack of antifungal and antimicrobial qualities, as well as low water vapour permeability, are additional reasons for being less ideal as a binder for hempcrete, despite its relative durability and low price (Stanwix & Sparrow, 2014; Vyšvařil *et al.*, 2023).

2.1.2.2.2 Ground Granulated Blast-furnace Slag

Ground Granulated Blast-furnace Slag (GGBS) is a form of alkaline-activated slag (Oti *et al.*, 2024) with high calcium content, resulting from steel industry waste (Garcia-Lodeiro *et al.*, 2015a). During the process at 1500-1600°C, molten iron and slag are produced. High-pressure water is then used to quench the slag before being dried and ground to be used as a cementitious material (Panesar, 2019). It mainly consists of a high proportion of CaO and SiO_2, with smaller amounts of Al_2O_3 and MgO, influenced by the steel-making procedure (Garcia-Lodeiro *et al.*, 2015b). Slag is readily available (Jami *et al.*, 2019) and approximately one-third of this by-product is utilized in industry worldwide (Saleh Ahari *et al.*, 2015). Its properties and environmental benefits have made slag one of the most popular SCMs to be combined with hydrated lime to create hempcrete (Oti *et al.*, 2024). Table 3 provides the material's specifications.

Table 3- Slag specifications (Albidah, 2021; Panesar, 2019; Walker & Pavía, 2011)

Binder	Specific gravity	Structure shape	Amorphousness	Particle size (µm)	Specific surface area (M^2/g)	Water demand
Slag	2.85-2.95	Angular	Primarily amorphous	13.8-22.2	0.35-2.65	28 %

Slag largely consists of amorphous phases, with a minor presence of crystallinity, of which only the amorphous portion contributes to the cementitious behaviour of the material. The quicker the slag is quenched, the greater its amorphous properties, the finer the particle size, and the better its cementitious behaviour (Panesar, 2019). In a study, slag was described as a fully amorphous material. The author also

specifies it as a binder with relatively high specific gravity, low porosity, and high reactivity, which stems from its small particle sizes (Walker & Pavía, 2011). The fine particles fill the pores, leading to low water vapour permeability as well (Tale Masoule *et al.*, 2022). It should be taken into consideration that the particle specifications are highly influenced by the material's grinding method used (Panesar, 2019). Moreover, the hydraulic nature of slag allows it to set when mixed with water, similar to OPC, at a slower hardening rate (Panesar, 2019), while setting faster than other SCMs (Walker, 2013). It is a more durable precursor with lower water demand compared to OPC (Panesar, 2019) and exhibits good acoustic behaviour (Kinnane *et al.*, 2016a).

2.1.2.2.3 Metakaolin

Metakaolin is produced by calcining kaolin clay, a crystalline light-coloured rock, at temperatures ranging from 650 to 850°C, in which the material acquires its pozzolanic properties (Garcia-Lodeiro *et al.*, 2015a). As it requires to be combusted at high temperatures, metakaolin is more expensive than other SCMs, which limits its widespread use (Garcia-Lodeiro *et al.*, 2015b, 2015a). Given that metakaolin has to be mined and calcined, it is less environmentally friendly compared to other pozzolans (Tale Masoule *et al.*, 2022). However, the material consumes less energy in its production than OPC (Walker, 2013). This natural pozzolan is rich in SiO_2 and Al_2O_3, with a small amount of Fe_2O_3 (Garcia-Lodeiro *et al.*, 2015b).

As shown in Table 4, this amorphous and highly porous binder has a non-uniform platy shape. Having a high surface area and reactivity results in a high water demand, which can lead to shrinkage and cracking (Panesar, 2019; Provis *et al.*, 2010). In one study, the material was described as highly reactive compared to all other binders tested, achieving higher strength in a shorter duration (Walker, 2013). Moreover, since metakaolin is primarily produced rather than being a by-product like many other SCMs, its quality and properties can be more effectively controlled (Saleh Ahari *et al.*, 2015).

Several studies are focused on the effect of partially substituting hydrated lime with metakaolin in hempcrete binder. An SEM micrograph analysis is used by Daher *et al.* (2022) to reveal the enhancement

in the mechanical properties of the material with an increasing pozzolan-to-lime ratio as more hydrations occur. The replacement of 20% of lime with metakaolin resulted in a 41% increase in compressive strength. Furthermore, the durability of hempcrete with metakaolin and hydrated lime as binders was investigated by Zerrouki *et al.* (2022) through exposure to consecutive wet and dry cycles. The results indicated that metakaolin considerably enhances durability by confining the degradation of hempcrete.

Table 4- Metakaolin specifications (Panesar, 2019; Provis *et al.*, 2010; Walker, 2013; Zerrouki *et al.*, 2022)

Binder	Specific gravity	Structure shape	Amorphousness	Particle size (µm)	Specific surface area (M^2/g)	Water demand
Metakaolin	2.20-2.60	Platy shape	Amorphous	1-20	15-20	110 %

2.1.2.2.4 Pumice (Volcanic Ash)

The quick quench of volcanic lava with high silica content develops a hard glass structure. As a result, porous volcanic rock is produced with low density, as trapped gases inside the lava create holes and bubbles (Seraj *et al.*, 2017). Ancient Greeks and Romans utilized pumice in concrete production, combining volcanic ash with hydrated lime to create a durable material that has lasted for millennia (Seraj *et al.*, 2017). Pumice contains substantial quantities of SiO_2 and lower amounts of Al_2O_3, and its high silica content, along with its amorphousness, offers pozzolanic behaviour in a mixture (Garcia-Lodeiro *et al.*, 2015b).

The specifications of this pozzolanic ash are summarized in Table 5. Pumice is found to slightly decrease the lime water demand in the binder. Moreover, the addition of 40% pozzolan to hydrated lime in a binder has been observed to double the strength, while the density increases only minimally due to its porous and lightweight nature. It also enhances the durability of lime-based binders (Vyšvařil *et al.*, 2023). With a pH of 7.2, pumice exhibits notable chemical reactivity (Almalkawi *et al.*, 2017; Garcia-Lodeiro *et al.*, 2015b).

Table 5- Pumice specifications (Almalkawi *et al.*, 2017; Hedayatinia *et al.*, 2019; Seraj *et al.*, 2017; Vyšvařil *et al.*, 2023)

Binder	Specific gravity	Structure shape	Amorphousness	Particle size (µm)	Specific surface area (M^2/g)	Water demand
Pumice	2.35- 2.91	Spongy	Amorphous	1-400	0.96-10.9	103-107 %

2.1.2.2.5 Silica Fume

It is a by-product of silicon and ferrosilicon production, either elemental or alloys, during smelting at approximately 2000°C. This pozzolan is formed through the condensation of oxidized silicon dioxide vapour from quartz, which is now collected due to its toxicity rather than releasing the fume into the air (Albidah, 2021; Panesar, 2019; Walker, 2013). Silica fume, also referred to as micro silica or silica dust (Elzeadani *et al.*, 2022), mainly consists of silicon dioxide. The composition varies based on the source material; however, it must contain a minimum of 85% silicon dioxide (Panesar, 2019).

As shown in Table 6, silica fume's spherical structure, as noted in several studies, can result in a lack of particle interlock between the binder and hemp particles (Elzeadani *et al.*, 2022; Provis *et al.*, 2010). The high porosity and low apparent density in pozzolan are observed regardless of its very fine particle size. It has been reported that two-thirds of the particles are smaller than 0.1 µm, while 36% porosity was measured in a lime-silica fume mixture with a 1:1 ratio using mercury intrusion porosimetry (Walker, 2013). The pozzolan also exhibits high reactivity (Albidah, 2021; Elzeadani *et al.*, 2022; Panesar, 2019) and a setting time similar to OPC (Panesar, 2019).

Table 6- Silica Fume specifications (Panesar, 2019; Provis *et al.*, 2010; Walker & Pavía, 2011)

Binder	Specific gravity	Structure shape	Amorphousness	Particle size (µm)	Specific surface area (M^2/g)	Water demand
Silica Fume	2.20-2.30	Sphere	Amorphous	0.1-0.3	13-30	60%

2.1.2.2.6 SCMs Comparison

In a comprehensive study comparing nine SCMs, their reactivity was attributed to their amorphous nature. Accordingly, metakaolin, slag, and silica fume were the most reactive materials investigated, resulting in the highest mechanical strength. In addition, it was revealed that compressive strength increased with lower particle size in binders, despite having high porosity and low apparent density. The study also identified the chemical composition and silica content of the binder as the less determining variables on strength and reactivity (Walker & Pavía, 2011).

Regarding the setting time, when each SCM was combined with lime in a 1:1 ratio, slag exhibited the fastest setting time at only 9 hours. Metakaolin presented a medium performance of 34-hour hardening, while silica fume had one of the slowest setting times, taking 60 hours. Furthermore, slag achieved the highest strength among all SCMs within a one-year period (Walker & Pavía, 2011). The material also demonstrated the highest resistance to the freeze-thaw cycle, with approximately 35% greater resistance than the other binders (Walker, 2013).

Overall, based on several experiments, slag and metakaolin, followed by silica fume, have been identified as the binders with the best performance when combined with hydrated lime in hempcrete (Walker, 2013; Walker & Pavía, 2011).

2.1.2.3 CaO/SiO_2 Molar Ratio Rationale

CaO contains a considerable portion of hydrated lime, while pozzolans primarily consist of SiO_2 and Al_2O_3 (Garcia-Lodeiro *et al.*, 2015b, 2015a). However, silica participates more than alumina in enhancing the mechanical properties of binders (Panesar, 2019; Ra *et al.*, 2023). Moreover, pozzolans such as silica fume are rich in silica but include minimal alumina content. Considering the proportions of CaO and SiO_2 in hempcrete binders, the C-S-H gel is recognized as the main defining production (Tale Masoule *et al.*, 2022) and most critical binding phase (T.Mabah *et al.*, 2019). The produced gel contributes notably to the durability and compressive strength of the resulting material (Garcia-Lodeiro *et al.*, 2015b; Tale Masoule

et al., 2022). The characteristics of C-S-H gel, formed from the reaction between silica and calcium hydration in lime-rich hempcrete binder, can be evaluated by calculating the CaO/SiO_2 molar ratio (Garcia-Lodeiro *et al.*, 2015b).

Recent studies similarly highlight the effect of the molar ratio, particularly CaO/SiO_2, on the micro and nanostructures of cementitious and pozzolanic materials (He *et al.*, 2014; T.Mabah *et al.*, 2019; Wang *et al.*, 2024). The combination of each SCMs with hydrated lime produces diverse chemical compositions, whereas maintaining a fixed CaO/SiO_2 molar ratio can preserve the dominant composition and facilitate more effective comparisons. The CaO/SiO_2 molar ratio, as the most effective factor in the compressive strength of binders (Ra *et al.*, 2023), is also reported to be influential in the porosity and permeability of the material (Pandini *et al.*, 2020; X. Wang *et al.*, 2024).

2.1.3 Water

In a hempcrete mixture, hemp hurd can absorb significantly more water than necessary as a result of its porous structure. Excess water in the mixture results in an increase in the setting time of binders as well as an unbalanced distribution of binders in the composition, potentially leading to product failure. In addition, the extended drying time and excessive water exposure over the designated level can promote mould growth (Jami *et al.*, 2019; Magwood, 2016). Conversely, insufficient water amount does not allow the binder to react entirely and obtain the required hydraulic setting, causing a fragile and crumbly product (Magwood, 2016). Consequently, a specific amount of water must be introduced to the binder to ensure full reactivity while forming a paste with minimum workability. This approach also enhances the strength of the product, which is a determining factor in lightweight concretes that demonstrate low compressive strength by nature (Tale Masoule *et al.*, 2022).

Even when the same amount of hemp particles and binder are used as dry components in the mixture, varying the water ratios based on each SCM's requirement can considerably impact the outcome. Not only

does each SCM require a specific amount of water, but the same binders may also demand different amounts of water depending on their unique chemical and physical properties (Magwood, 2016).

In an experiment, it was observed that the water demand of cementitious materials depends on their porosity and apparent density. Accordingly, metakaolin and silica fumes with relatively low specific gravity have high water demand, whereas high-density slag requires a low amount of water. The author also revealed a direct correlation between water demand and specific surface area. This feature was considered to be more influential on water demand than particle size. The surface area for silica fume, metakaolin, hydrated lime, and slag was found to be 24, 18, 17, and 4 m^2/g, respectively. According to these values, if the surface area of lime and cementitious material differs significantly, the water demand of the mixture will vary from the lime's water demand. Furthermore, in a mixture of lime with SCMs at a 1:1 ratio, the binder-to-water ratio for metakaolin-lime, silica fume-lime, and slag-lime pastes was stated as 1:1, 1:0.73, and 1:0.57, respectively (Walker, 2013; Walker & Pavía, 2011).

2.2 Why Hempcrete

Hempcrete, as a bio-composite, consists of hemp hurd and lime, combining the benefits of both components. The material inherited durability along with antimicrobial and antifungal properties from lime (Marceau & Delannoy, 2017). The natural and non-toxic nature of its ingredients contributes to healthy indoor air quality for occupants. Furthermore, the excellent hygrothermal performance of hempcrete arises from the porosity of both the binder and aggregate. It's low thermal conductivity and high heat capacity (Jami *et al.*, 2019) make it a suitable choice for insulation in extremely hot and cold climates (Chau *et al.*, 2023; Magwood, 2016). Hempcrete is capable of regulating moisture effectively based on its high moisture buffering capacity. This property eliminates the risk of mould and fungi growth in high humidity, asthma or allergies in low humidity, and bacterial infections when relative humidity differs from the optimal range of 40 to 60% (Kaboré *et al.*, 2024; Stanwix & Sparrow, 2014).

The high porosity of hempcrete contributes to its excellent acoustic performance by absorbing sound through its porous structure (Boulic *et al.*, 2013). Hempcrete's lightweight nature makes it easy to work with and reduces the potential dead load in buildings. Being lightweight allows for the design of lighter foundations, which in turn require less concrete. In some cases, the foundation can even be built without Portland cement by replacing it with rock-filled gabions or compacted crushed limestone as a free-drained foundation (Stanwix & Sparrow, 2014). The porous matrix structure of hempcrete offers great compressibility with excellent ductile behaviour, making the material an ideal choice for construction in seismic areas. Incorporating hempcrete with these properties can reduce the number of layers in building assemblies, thereby minimizing environmental impacts (GlobalABC Roadmap for Buildings and Construction, 2020-2050, 2020; Magwood, 2016). In section 2.3, hempcrete properties have been discussed in more detail.

The hurd from a fast-growing, multi-purpose hemp plant (Jami *et al.*, 2019), combined with low-impact binders, results in a fully biodegradable hempcrete (Magwood, 2016). The production, utilization and disposal processes of the material have no negative impact on the environment (Stanwix & Sparrow, 2014). In addition, many publications highlight hemp's advantages over other bio-aggregate-based competitors. For instance, while flax shivs are more widely available in Canada, the material exhibits higher thermal conductivity compared to hemp hurd (Benmahiddine, Cherif, *et al.*, 2020). Moreover, rice husk is denser as an aggregate, with a maximum of 50% porosity, compared to hemp hurd, which has approximately 80% open pores (Chabannes *et al.*, 2014). Also, under similar conditions, the compressive strength of hempcrete is higher than rice-husk or wheat-husk concrete (Barbieri *et al.*, 2020). Hemp also stands out among all other bio-aggregates for its exceptional thermal performance, which remains consistent even with varying humidity levels. Between the dry state and the relative humidity of 60%, the material's thermal conductivity increases by only an average of 8% (Rosa Latapie *et al.*, 2024). Table 7 highlights the specification of common bio-aggregates in construction available in North America.

Table 7- Comparison of bio-aggregates used in construction

Material	Source	Particle density (Kg/m^3)	Particle porosity (%)	Thermal conductivity (W/m.K)
Hemp hurd	Agricultural co-product	200-250	80-88	0.05- 0.09
Flax hurd	Agricultural co-product	400-450	68-75	0.12- 0.145
Sunflower stem	Agricultural by-product	400-450	68-76	0.12- 0.145
Miscanthus stem	Co-product (ethanol)	370-400	70-78	0.125- 0.135
Wheat (straw & husk)	Agricultural by-product	320-440	66-77	0.14- 0.145
Corn cob	Agricultural by-product	400-450	65-75	0.095- 0.145
Rice husk	Agricultural by-product	430-470	30-50	0.07–0.10

Hempcrete is a carbon sink with a biogenic contribution of carbon sequestration by absorbing carbon through the hemp plant, along with non-biogenic carbon sequestration through lime carbonation (Jami *et al.*, 2019). Exceeding 100 kg of carbon dioxide can be sequestrated per cubic metre of hempcrete (Murphy *et al.*, 2010). Furthermore, a life cycle analysis conducted on a 1-metre-high hempcrete wall with 0.3 metres of thickness, using hydrated and hydraulic lime as the binder without rendering, showed that the material sequestrated 82.71 kg of CO_2e (Ip & Miller, 2012). Being carbon-negative with a negative embodied carbon value is the feature many publications agree on (Arehart *et al.*, 2020; Arrigoni *et al.*, 2017; Ip & Miller, 2012; Jami *et al.*, 2019; Liu *et al.*, 2023). It locks up more carbon dioxide than is released in the atmosphere during the raw material preparation, manufacturing, transportation, processing, disposal and any other associated steps (Stanwix & Sparrow, 2014). Figure 5 indicates this matter.

The embodied carbon of hempcrete is reported to be -2.73 $kgCO_2e/kg$ for a density of approximately 300 kg/m_3, with -121.4 kg per 4 × 8 inch wall area for the carbon footprint (Magwood, 2016). Additionally, an experiment using relatively high-impact binders, such as dolomite lime ($CaMg(CO_3)_2$) and Portland cement,

showed that the overall life cycle assessment still resulted in a negative CO_2 production value when the carbonation process was taken into account (Arrigoni *et al.*, 2017).

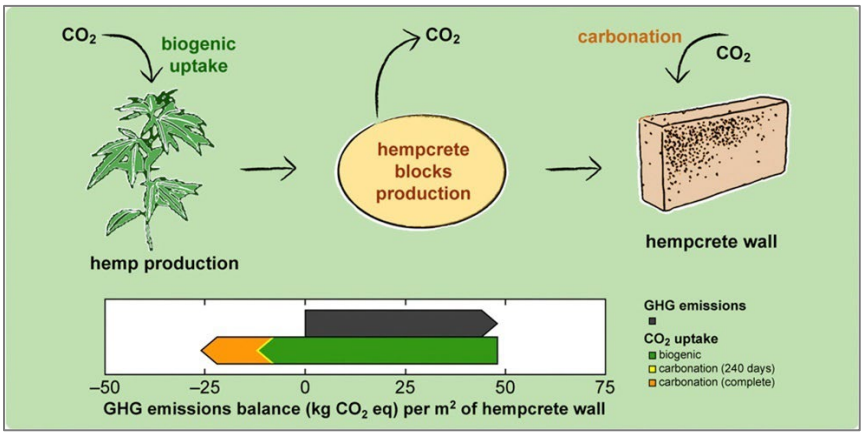

Figure 5- Hempcrete's GHG emissions (Arrigoni *et al.*, 2017 Graphical abstract)

Due to not being massively produced, local natural materials are often less cost-effective than synthetic alternatives, which benefit from bulk price reductions in their manufacturing. However, Hempcrete remains affordable in Canada (Magwood, 2016). As awareness of this unique material continues to grow, so does its market potential (Stanwix & Sparrow, 2014).

2.3 Properties of Hempcrete

2.3.1 Density

Unlike standardized materials such as concrete made with OPC and rock aggregate, the density of hempcrete varies in a wide range. The variation arises because, in hempcrete, the binder adheres hemp particles together, whereas, in concrete, the binder fills all the gaps between aggregates (Magwood, 2016). Binder ratio and compaction are identified as the two critical factors influencing density (Elfordy *et al.*, 2008). In addition, the size and orientation of hemp hurd particles, chemical composition, and production process are also among the factors for achieving density variation (Barbhuiya & Bhusan Das, 2022; Jami *et al.*, 2019). As an example, for a sample with an apparent density of 380 kg/m^3, true densities of

approximately 2050 kg/m^3 for coarse hurd and 2150 kg/m^3 for finer aggregates have been reported (Brzyski *et al.*, 2020).

The trapped air within the hempcrete structure forms three types of pores: binder intra-pores measuring approximately 1 μm, hemp intra-pores around 10 μm, and interconnected pores between particles ranging from 1 to 10 mm in diameter. Micropores constitute one-fourth of the total porosity, while the remaining portion consists of macropores (Arnaud & Gourlay, 2012; Evrard & De Herde, 2010; Song *et al.*, 2024; Walker, 2013). Walker (2013) reports the mean open porosity of hempcrete samples as 73-74% for a 30/70 slag/lime binder and a 20/80 metakaolin/lime binder composition, using a binder-to-hemp ratio of 2:1 by weight and an average density of 360 kg/m^3. The author further stated that the interconnected porosity accounts for the fluid permeability behaviour of hempcrete. In another study, a total porosity of 82% was observed for a 20/80 metakaolin/lime binder hempcrete with a binder-to-hemp ratio of 2:1 and a density of 380 kg/m^3 (Brzyski *et al.*, 2020). Across various experiments, the mean total porosity has been reported to range between 71% and 84% (Dhakal *et al.*, 2017).

In a comprehensive experiment, the pore structure in a hempcrete was analyzed, and the volume of each type of pore was measured. The hemp hurd intra-porosity was estimated to range between 60-70%. The study also revealed that the high porosity of hempcrete, particularly, the pores between the hurd and binder, contributes to the material's excellent thermal and acoustics properties. Accordingly, the porous nature of hempcrete, attributed to its low compaction, reduces the material's density, thereby enhancing its thermal and acoustic performance (Song *et al.*, 2024).

2.3.2 Compressive Strength

A combination of hemp hurd, a highly porous aggregate, and a medium-strength binder generates a non-load-bearing construction material (Boulic *et al.*, 2013; Magwood, 2016; Stanwix & Sparrow, 2014). Efforts to enhance the structural integrity of hempcrete have been made; however, these attempts were unsuccessful due to the trade-off with its thermal properties (Stanwix & Sparrow, 2014). Accordingly, the

compressive strength of hempcrete is primarily required for transportation and installation in the case of precast blocks. Otherwise, the material needs only to support its own weight (Mahmood *et al.*, 2024).

Unsurprisingly, there is a wide range of values for the compressive strength of hempcrete due to its dependency on various factors. A review study revealed that ultimate strength values influenced by density, binder composition, production process, hemp hurd specifications, and age of the specimen range between 0.025 and 5 MPa (Barbhuiya & Bhusan Das, 2022). Furthermore, the modulus of elasticity in hempcrete is reported to be relatively low (Jami *et al.*, 2019), covering a wide range (Khan, 2020; Walker, 2013), with its values associated with the material's dry density (Mahmood *et al.*, 2024).

Numerous studies have demonstrated that changes in density, either through compaction or variations in the binder-to-hemp hurd ratio, have a direct impact on the mechanical properties of hempcrete (Arnaud & Gourlay, 2012; Elfordy *et al.*, 2008; Murphy *et al.*, 2010; Nguyen *et al.*, 2009). Several authors have also identified a correlation between binder strength and the resulting hempcrete strength (Abdellatef *et al.*, 2020; Murphy *et al.*, 2010; Nguyen *et al.*, 2010), while others have found this relationship less relevant (Walker & Pavía, 2014a). Water content and curing conditions are recognized as additional factors in determining the material's strength (Abdellatef *et al.*, 2020; Arnaud & Gourlay, 2012). In addition, compressive strength is known as a subject to hempcrete age due to ongoing hydration and carbonation processes (Ahmad *et al.*, 2021; Walker *et al.*, 2014). Magniont *et al.* (2012) reported a ninefold increase in strength between 7 days and 1 year of curing. Finally, the quality, particle size, and arrangement of hemp hurd are named among the determining factors in hempcrete's strength (Jami *et al.*, 2019; Mahmood *et al.*, 2024; Stanwix & Sparrow, 2014). Accordingly, an experiment involving 13 different types of hemp hurd yielded varying mechanical properties, indicating the importance of hemp hurd characterization (Niyigena *et al.*, 2018).

Table 8 represents the test results for compressive strength and modulus of elasticity values after 28 days, as reported in various studies. The tests utilized either 200 × 100 mm cylindrical moulds or 100 × 100 ×

100 mm cubic moulds. Since the failure point on the load-displacement curve is often difficult to distinguish, many studies consider at 10% strain for compressive strength calculation in accordance with British Standards (Mahmood *et al.*, 2024; Sassoni *et al.*, 2014; Sinka *et al.*, 2014; Walker, 2013). Other researchers determined the maximum load based on the observed decrease in the force-displacement curve (Abdellatef *et al.*, 2020; Khan, 2020) or relied on visual judgement to assess the damage and instability of the sample during testing (Brzyski *et al.*, 2020). Similarly, the modulus of elasticity was calculated either based on a specific percentage of maximum stress (de Bruijn *et al.*, 2009; Khan, 2020) following ASTM Standards (*ASTM C469/C469M-22, Standard Test Method for Static Modulus of Elasticity and Poisson's Ratio of Concrete in Compression*, 2022) or simply from the slope of the linear part of the curve (Murphy *et al.*, 2010).

Hempcrete exhibits unique reactions and failure mechanisms compared to other materials. Deformation occurs rather than fracturing or cracking during compressive strength testing (Stanwix & Sparrow, 2014). Due to the high flexibility of hemp hurd, the test displacement can exceed 50% of the sample's height (Boulic *et al.*, 2013). This remarkable ability to withstand significant deformation without cracking is an appealing property, especially in seismic-prone areas (Jami *et al.*, 2019; T.-T. Nguyen *et al.*, 2009).

Comparing hempcrete with different particle sizes has intrigued several authors. Brzyski *et al.* (2020) tested fine and coarse aggregates with similar binders and revealed distinct behaviours between the two. Early damage occurred in the fine-aggregate sample with brittle behaviour, while with the ductile behaviour of the coarse-aggregate sample, no damage was observed at the equivalent deformation. Mahmood *et al.* (2024) observed that fine-ground particle hempcrete demonstrated more consistency compared to hempcrete made from larger particles. Similar to the previous study, the author discovered different mechanical behaviours for fine-particle hempcrete with lower maximum strength and equivalent modulus of elasticity compared to coarse-particle hempcrete. Moreover, finer hemp particles were shown to have lower strength than coarser hurd at 28 days despite having less porosity. However, the finer particles showed better long-term compressive strength, as they were more thoroughly covered by the binder (Arnaud &

Gourlay, 2012). In addition, the existence of fibres in the hemp particles was examined, but no considerable difference in mechanical properties was observed. de Bruijn *et al.* (2009) suggest that, considering lower processing costs, the presence of fibre content can be harmless.

Table 8- Compressive strength and modulus of elasticity in various studies based on the 28-day test

Study	Mould	Binder / hemp	SCM type	SCM/ lime	Density (kg/m^3)	σ_{max} (MPa)	E (MPa)
(Walker, 2013)	Cube	2:1	MK	20/80	360	0.1	1.23
(Walker, 2013)	Cube	2:1	Slag	30/70	360	0.13	1.63
(Khan, 2020)	Cylinder	1:1	MK	20/80	327	0.24	9.0
(Mahmood *et al.*, 2024)	Cube	1:1	Slag	20/80	200	0.111	3.96
(Elfordy *et al.*, 2008)	Cube	2:1	COM	30/70	290-485	0.18-0.85	4-35
(Abdellatef *et al.*, 2020)	Cylinder	1:1	Varies	Varies	304-372	0.11-0.47	3.16-10.84
(Daher *et al.*, 2022)	Cylinder	1:3 (v)	MK	20/80	445 ± 20	0.42 ± 0.05	78 ± 2
(Daher *et al.*, 2022)	Cylinder	1:3 (v)	-	0/100	420 ± 20	0.29 ± 0.08	62 ± 2

MK=Metakaolin, Com=Commercial binder, (v)=Calculated by volume, σ_{max} = Maximum compressive strength, E= Modulus of elasticity

The binder content has also been widely discussed among researchers. One experiment investigated the correlation between the mechanical properties of hempcrete and mix design. The study considered the hydraulicity of the binder to increase the setting time, which in turn contributed to early strength (Murphy *et al.*, 2010). Furthermore, to evaluate the effect of SCMs in hempcrete, different ratios of metakaolin in the lime-based binder were used, ranging from 10% to 70%. As the metakaolin ratio increased, a non-linear behaviour in compressive strength was observed. However, the compressive strength and modulus of elasticity increased proportionally (Abdellatef *et al.*, 2020). In another study, the introduction of 20% metakaolin in the lime-based binder improved mechanical strength and enhanced the material's robustness, delaying failure (Daher *et al.*, 2022). Similarly, it was revealed in another study that the addition of pozzolan to the binder composition increased compressive strength. The mechanical behaviour was found to be influenced by the binder selection (Nguyen *et al.*, 2010). However, in a long-term experiment, it was

established that although the addition of SCMs improved early strength, the compressive strength of hempcrete, regardless of binder choice, did not significantly differ after a one-year period (Walker & Pavía, 2014a).

2.3.3 Thermal Conductivity

Hempcrete's most important aspect, in terms of energy savings and gaining attention, particularly in cold climates like Canada, is its excellent thermal performance. This includes relatively low thermal conductivity, which defines its insulating properties (GlobalABC Roadmap for Buildings and Construction, 2020-2050, 2020). The highly porous hemp hurd, with a thermal conductivity range of 0.048 to 0.072 W/m.K (Rosa Latapie *et al.*, 2024), is classified as a low-conductive component for hempcrete. Considerable outcomes have been achieved both in laboratory studies and in practical applications. Several studies have indicated that the true performance of hempcrete is often better than the reported values, as steady-state comparisons of materials can be unrealistic (Magwood, 2016; Stanwix & Sparrow, 2014). Depending on the thickness of the hempcrete wall, it can meet the code standards in Canada (Magwood, 2016).

Density is known to be the most determining factor in the thermal conductivity of hempcrete, exhibiting roughly linear behaviour (Abdellatef *et al.*, 2020; Dhakal *et al.*, 2017; Elfordy *et al.*, 2008; Walker & Pavía, 2015). Studies have shown that increases in temperature or relative humidity directly correlate with higher thermal conductivity (Barbhuiya & Bhusan Das, 2022). Also, hempcrete, being exposed to moisture with gaining 75% of relative humidity, its thermal conductivity is reported to rise by 30% (Boulic *et al.*, 2013). Furthermore, the thermal conductivity value is highly influenced by hemp particle orientation (Barbhuiya & Bhusan Das, 2022; Tran-Le *et al.*, 2019). Some studies suggested that the hemp hurd particle size contributes to thermal conductivity (Dhakal *et al.*, 2017), while others detect no significant impact (Barbhuiya & Bhusan Das, 2022). However, the choice of binder is confirmed to have the minimum effect on hempcrete thermal properties (Barbhuiya & Bhusan Das, 2022; Nguyen *et al.*, 2010).

The average thermal conductivity of hempcrete is typically reported between 0.05 and 0.12 W/m.K (Walker & Pavía, 2015). Table 9 presents thermal conductivity values from various studies, with some derived as mean values calculated based on different temperatures (Evrard, 2008; Mahmood *et al.*, 2024). In an experiment based on the observations, for a 50 kg/m^3 increase in density, the thermal conductivity was suggested to increase by around 0.005 (Sinka *et al.*, 2014). However, this result does not align with findings from other studies, potentially due to the limited sample size used to conclude in the cited experiment.

Table 9- Thermal conductivity value for hempcrete in various studies

Study	Binder/ hemp	SCM type	SCM/ lime	Thickness (mm)	Density (kg/m^3)	Thermal Conductivity (W/mK)
(Walker, 2013)	2:1	MK	20/80	300	530	0.117
(Walker, 2013)	2:1	Slag	30/70	300	564	0.126
(Evrard, 2008)	2:1	Com	25/75	30 ± 0.7	300-350	0.115 ± 0.006
(Mahmood *et al.*, 2024)	1:1	Slag	20/80	80	200	0.0605-0.0667
(Sinka *et al.*, 2014)	63:37	MK	40/60	-	330-540	0.070-0.086
(Brzyski *et al.*, 2020)	2:1	MK	20/80	50	380	0.0992
(Abdellatef *et al.*, 2020)	1:1	Varies	Varies	55	291-321	0.0868-0.0959
(Dhakal *et al.*, 2017)	1:1	Com	-	76	233	0.074
(Bendouma *et al.*, 2023)	1.5:1	MK	45/55	-	326±4	0.102

MK=Metakaolin, Com=Commercial binder

2.3.4 Specific Heat Capacity

Despite its lightweight nature, hempcrete's high heat capacity enables it to function as a thermal regulator. The material absorbs heat from the environment, stores it, and gradually releases it when temperatures drop. This buffering behaviour, accompanied by satisfactory thermal conductivity, makes hempcrete an excellent candidate as an insulating material (Dhakal *et al.*, 2017; Jiang *et al.*, 2018; Stanwix & Sparrow, 2014). Other natural materials typically offer only low thermal conductivity, such as straw bale, or high thermal mass, such as rammed earth or cob. These two thermal performances make hempcrete a thermally efficient interior material, reducing dependence on mechanical air conditioning systems (Stanwix & Sparrow, 2014).

The heat capacity of hempcrete is defined as a function of its density and the hemp-to-binder ratio (Mahmood *et al.*, 2024). Furthermore, Walker (2013) reported that the hydraulicity of the binder impacts the heat capacity value of hempcrete. The author also observed the increase in specific heat capacity with rising relative humidity. Table 10 shows a range of specific heat capacity values, spanning from 930 to 1600 J/kg.K, derived from different studies. Notably, the average heat capacity of hempcrete exceeds that of Ordinary Portland Cement (OPC) concrete, which typically has a mean value of 800 to 1200 J/kg·K, despite hempcrete being significantly lighter (Jami *et al.*, 2019).

Table 10- Specific heat capacity value derived from different studies

Study	Binder / hemp	SCM type	SCM/lime	Thickness (mm)	Density (kg/m^3)	Specific Heat Capacity (J/kg.K)
(Walker, 2013)	2:1	MK	20/80	100	360	1240
(Walker, 2013)	2:1	Slag	30/70	100	360	1240
(Evrard, 2008)	2:1	Com	25/75	30 ± 0.7	300-350	1560 ± 30
(Mahmood *et al.*, 2024)	1:1	Slag	20/80	80	200	931-957
(Brzyski *et al.*, 2020)	2:1	MK	20/80	50	380	1601
(Abdellatef *et al.*, 2020)	1:1	Varies	Varies	55	291-321	1250-1421

MK=Metakaolin, Com=Commercial binder

2.3.5 Water Vapour Permeability

The efficient moisture behaviour of hempcrete is another factor that establishes it as a low-impact material (Jami *et al.*, 2019; Kaboré *et al.*, 2024). Hempcrete exhibits various moisture-related properties, including vapour sorption, water absorption, free water saturation, water vapour diffusion, and moisture buffering capacity (Collet *et al.*, 2008; Dhakal *et al.*, 2017; Mahmood *et al.*, 2024; Saeidpour & Wadsö, 2016; Walker & Pavía, 2014b). However, its high capacity for water vapour permeability has gained significant attention among users to replace conventional insulations (Walker & Pavía, 2015). Water vapour travels through the interconnected pores in hempcrete, balancing vapour pressure within the structure. This property contributes to the resident's well-being as well as the durability of the building since it prevents the possible

mould growth, rotting, and degradation caused by moisture overloading (Magwood, 2016; Stanwix & Sparrow, 2014).

Although the concept of a permeable and vapour-open assembly has gained growing interest among researchers and individuals concerned with human and building health, it does not align with the National Building Codes of Canada yet (Magwood, 2016). Consequently, to prevent the entire assembly from being permeable, hempcrete should be applied either as an interior or exterior layer with a permeable finish. If used as both layers, a vapour barrier must be incorporated to separate the two groups (Magwood, 2016).

Hempcrete's highly hydrophilic nature, compared to other plant-based materials, is unique since it can maintain its strength when exposed to humidity (Magwood, 2016). However, when used as outdoor insulation, protective measures are necessary to protect it from direct precipitation. Hempcrete can be finished with a vapour-permeable material and not water-permeable to allow air to circulate and prevent decay, while preventing rain penetration . Moreover, installing a rainscreen with a gap in front of the hempcrete, which can effectively block heavy rains, is another strategy (Magwood, 2016). In an experiment by Dhakal *et al.* (2017), the hygrothermal performance of outdoor hempcrete walls in the Ontario climate was investigated. A wall with a vented rainscreen was compared to a rendered wall with a 20mm lime layer. The results indicated that, although both options were effective, the moisture was controlled more efficiently using a rainscreen. Furthermore, studies have explored the treatment of hempcrete to achieve hydrophobic properties, enabling resistance to water penetration while retaining high water vapour permeability (Hussain *et al.*, 2019).

In a hempcrete composition, hemp hurd is significantly more vapour permeable compared to the binder. However, the binder’s performance in this regard must align with the overall composition (Stanwix & Sparrow, 2014). Binder selection thus plays a crucial role in the water vapour permeability of hempcrete (Walker, 2013). Hydrated lime binders demonstrate greater permeability features than SCMs (Jami *et al.*, 2019; Strandberg-de Bruijn & Johansson, 2014). The water vapour permeability of hempcrete is considered

to be influenced more by the SCM component of the binder than by the structural macropores Walker (2013). The author also revealed metakaolin as the most vapour-permeable SCM compared to similar cementitious materials such as slag. Moreover, a study investigating water vapour permeability in various SCMs highlighted that pore size in the binder paste plays a crucial role in this property. Accordingly, limestone was identified as the most permeable, followed by pozzolan and slag (Alderete *et al.*, 2018). Another study extensively discussed factors influencing water vapour permeability, noting that this property decreases as the sample ages due to the ongoing hydration process. Consequently, the study emphasized the importance of specifying sample age when reporting water vapour permeability (Issaadi *et al.*, 2015).

Table 11 presents the water vapour permeability and water diffusion resistance factor values derived from various studies. While the water vapour permeability shows a wide range of variability, the water diffusion resistance factor appears relatively consistent. The cup test is a commonly used method for conducting these tests, employing either the desiccant method or the water method (*ASTM E96/E96M-24, Standard Test Methods for Gravimetric Determination of Water Vapor Transmission Rate of Materials*, 2024). In an experiment, hempcrete samples measuring 100 × 100 × 37 mm were tested using both the water and dry cup methods. The results indicated differing values depending on the method, with the dry cup test yielding a higher diffusion resistance factor and lower water vapour permeability (Brzyski *et al.*, 2020).

Table 11- Water vapour permeability and water diffusion resistance factor values from different studies

Study	Binder / hemp	SCM type	SCM/ lime	Thickness (mm)	Density (kg/m3)	μ-value	WVP (kg/m.s.Pa)
(Walker, 2013)	2:1	MK	20/80	100	360	5.5	4.21×10^{-10}
(Walker, 2013)	2:1	Slag	30/70	100	360	5.5	4.1×10^{-10}
(Evrard, 2008)	2:1	Com	25/75	30	300-350	4.85	1.56×10^{-7}
(Brzyski *et al.*, 2020)	2:1	MK	20/80	37	380	5.57	3.55×10^{-11}

MK=Metakaolin, Com=Commercial binder, μ-value= Water diffusion resistance factor, WVP= Water vapour permeability

Numerous studies have examined the water vapour permeability behaviour of hempcrete as part of a wall assembly within the building envelope, often utilizing hygrothermal simulation tools such as WUFI (Evrard

& De Herde, 2010; Jirgensone *et al.*, 2024; Kaboré *et al.*, 2024). Furthermore, the water vapour permeability performance of hempcrete has been analyzed under varying humidity and temperature conditions (Evrard, 2008; Issaadi *et al.*, 2015). However, another study reported that the water vapour permeability of hempcrete remains relatively consistent under low to medium relative humidity levels (Jami *et al.*, 2019).

2.3.6 Other Hempcrete Properties

2.3.6.1 Durability

Hempcrete is known for being a durable material with a lifespan exceeding a century (Barbhuiya & Bhusan Das, 2022). The only notable exception is its low freeze-thaw resistance, which is significantly improved in hempcrete with more SCM compared to lime-hempcrete, despite being less porous. Salt and microbe exposure do not have a deterioration effect on the material (Walker *et al.*, 2014). Termites may be present in the material, but cannot live long, and mould formation only occurs when the composition lacks minerals and is exposed to a very high relative humidity of 98% for a long period (Barbhuiya & Bhusan Das, 2022). Weathered and unweathered hempcretes are reported to exhibit roughly similar performance (Barbhuiya & Bhusan Das, 2022). However, in another experiment, it was observed that weathered hempcrete exposed to water demonstrated poorer mechanical behaviour over the ages. The study found an approximately 50% decline in compressive strength in hempcrete samples subjected to an immersion-drying cycle. Interestingly, the hygrothermal behaviour slightly improved. To be precise, water vapour permeability increased by 38%, and thermal conductivity decreased by 6% (Benmahiddine, Bennai, *et al.*, 2020).

2.3.6.2 Acoustics

Hempcrete is better acoustic than OPC concrete (Jami *et al.*, 2019). The pores on the surface of the material are the contributors to the absorption of sound wave energy (Boulic *et al.*, 2013). Studies on hemp hurd indicate that smaller particle sizes, due to the reduced pore size between particles, perform better acoustic features compared to larger particle sizes (Stanwix & Sparrow, 2014). Similar to the thermal properties, acoustic performance depends on the interconnected pore volume within the hempcrete structure. Accordingly, lower-density hempcrete, resulting from reduced compaction, enhances the acoustic

behaviour of the material (Song *et al.*, 2024). As for the binder, the chemical composition is the most crucial factor in sound absorption. Hydrated lime demonstrates better acoustic performance than SCMs, while slag shows higher sound absorption compared to metakaolin (Kinnane *et al.*, 2016b). An acoustic experiment tested two 150 mm layers of hempcrete walls with a 75 mm gap between them. As a result, a sound reduction of up to 58 dB was achieved, exceeding the code standard requirement of 53 dB in Canada (Magwood, 2016).

2.3.6.3 Fire Resistance

Considering hemp as a vegetal aggregate, hempcrete is often assumed to be highly flammable. However, the lime-binder layer surrounding the particles inhibits the supply of oxygen required for ignition to protect the material (Boulic *et al.*, 2013; Magwood, 2016). In a comprehensive study on the fire behaviour of hempcrete by Shewalul *et al.* (2023), the blocks exhibited a low tendency to burn or spread fire. The material only showed a reduction in mass along with fume diffusion and minimum smoke spread, with no flaming ignition observed. Hempcrete resisted fire exposure for two hours, demonstrating its high fire resistance capability. Additionally, as hempcrete is made from natural materials and free of chemicals, the fume generated during burning is non-toxic (Magwood, 2016). A 3 × 3 × 0.3 m hempcrete wall without rendering was tested in another experiment. The wall remained undamaged for 73 minutes under direct fire exposure at temperatures between 800 and 1000 °C. Owing to the material's excellent insulation properties, the average temperature on the opposite side of the wall remained below 60°C (Stanwix & Sparrow, 2014).

2.3.6.4 Airtightness

Even with a low thermal conductivity value, insufficient airtightness can significantly reduce the material's thermal performance due to heat transfer through the walls (Magwood, 2016). Hempcrete acts as a sealed obstacle to block air transmission flow toward the building and in converse. Despite its naturally porous structure, a satisfying level of airtightness can be achieved with the application of render finishing (Stanwix & Sparrow, 2014). Hempcrete's airtightness level also meets the building code standards in North America (Magwood, 2016).

2.4 Application of Hempcrete

Hempcrete is an ideal material for both renovations and new constructions. Since it is not load-bearing, it is always located around the structural frame (Murphy *et al.*, 2010; Stanwix & Sparrow, 2014), with timber being the optimal structure to be coupled with. Hempcrete's greater hygroscopicity compared to timber allows it to absorb moisture from the timber and emit it into the environment, helping to maintain the structural health of the building (Néron, 2019).

There are no specifications for hempcrete in the building codes or standards of North America (Magwood, 2016). However, obtaining permission to meet the National Building Code of Canada (Canadian Commission on Building and Fire Codes, 2022), is accessible through the "alternative compliance" pathway to utilize hempcrete in buildings. This process is relatively straightforward, as hempcrete is not a structural element (Magwood, 2016). According to Section 9 of the Ontario Building Code (2012- supplementary standard SB-12, Energy efficiency for housing), hemp can be authorized as an alternative solution for building applications (Dhakal *et al.*, 2017).

Hempcrete has a wide range of applications in buildings and can be used for elements such as interior and exterior walls, floors, roofs, wall insulation layers, and window insulation, serving as an alternative to expanding spray foam or batt insulation (Magwood, 2016). Table 12 shows the typical density range and hemp-to-binder ratio for each application of hempcrete. The proportions vary depending on the binder choice and building conditions.

Table 12- Hempcrete densities and binder ratios based on application (Stanwix & Sparrow, 2014)

Mix type	Density range (kg/m^3)	Hemp: Binder ratio	Application
Very Lightweight	150 - 200	1:1	Loose filler- flat attic surface
Lightweight	200 - 250	1:1.5	Roof filling- supported walls
Mediumweight	250 - 350	1:2	Walls
Heavyweight	350 - 500	1:3	Floor slabs

Wall: The application of hempcrete as a wall material is its most common use. The density of a hempcrete wall typically ranges from 250 to 350 kg/m^3 (Magwood, 2016). Different insulation levels can be achieved depending on the thickness and density of the hempcrete. The masonry plinth made from bricks or stones using lime or lime-pozzolan mortar, with a minimum height of 250 mm above the ground, is sufficient to elevate the hempcrete wall. A damp-proof course (DPC) should also be on top of the plinth to block moisture penetration. The high alkalinity of hempcrete is corrosive to materials like steel; therefore, alkali-resistant materials should be replaced, such as stainless steel or galvanized steel (Stanwix & Sparrow, 2014).

Hempcrete can be built as tall as a six-story curtain wall (Magwood, 2016). It can be cast or installed as the layer in between the studs, wall inside or outside the structural frame, paired with hemp wool to optimize the thermal performance or as an interior or exterior insulation layer (Costantine *et al.*, 2018; Néron, 2019). Apart from the casting techniques, the final product of hempcrete should be rigid enough so that a layer of plaster for finishing suffices (Magwood, 2016). Hempcrete usually finishes with lime plaster (using hydraulic lime and sand, to which hemp hurd and fibres may be added as additives) or limewash as a protective finish (Néron, 2019; Stanwix & Sparrow, 2014). Gypsum board and MgO boards are also used as the interior finishing materials for the hempcrete wall, being secured using wood screws (Magwood, 2016; Néron, 2019).

Floors: It is the least common among any other applications of hempcrete in construction, with a relatively high density of 375 to 500 kg/m^3 and a capacity of 1.1 to 2 MPa for supporting loads, while the thermal conductivity significantly increases. This is acceptable considering the difference in temperature between the earth and outdoor air in very cold and hot weather (Magwood, 2016). Not Strong enough by itself, a hempcrete floor should be combined with other breathable materials to be applied as a floor. The thickness is also reduced, similar to that of a typical floor, which allows it to dry more quickly. A lower hemp-to-binder ratio is used to increase stiffness; however, hempcrete floors are still not suitable for use between floors. Given hempcrete's vulnerability to standing still water, the hempcrete floor slab should be placed

on top of a free-drained sub-base layer without capillary action so that moisture cannot be able to penetrate the building fabric (Stanwix & Sparrow, 2014).

Ceiling and roof: Hempcrete reduces the roof's load. When applied to the roof, it is placed between the rafters, as shown in Figure 6, or used as a loose filler on top of the ceiling (Stanwix & Sparrow, 2014). It is more lightweight than walls, with a low density of approximately 150-250 kg/m^3 (Magwood, 2016; Stanwix & Sparrow, 2014). Although hempcrete increases the ceiling weight compared to conventional insulations, it repels pests and vermin, regulates the humidity and temperature, does not settle after ages, and absorbs moisture. Given that roof leakage is very common over time, this feature is among the many advantages of hempcrete to be chosen over other insulations (Magwood, 2016).

Figure 6- Hempcrete roof application (Stanwix & Sparrow, 2014)

2.5 Casting Techniques

To apply hempcrete in buildings, three main casting techniques are used by builders, as explained below.

2.5.1 Cast in Place

When mixing the ingredients, they should be handled, placed inside the form, and compacted. After the initial setting, when hempcrete can bear its weight, the form can be moved upward to follow the same process for the next level. This is the most common hempcrete casting technique, which eliminates thermal bridges and provides satisfactory airtightness, especially when the hempcrete wall combines with a floor slab or roof insulation (Jami *et al.*, 2019; Stanwix & Sparrow, 2014). Regarding the downsides of this method, inconsistent density and mechanical behaviour can be noted, especially with larger groups of workers. This technique requires providing forms and shuttering (Jami *et al.*, 2019; Stanwix & Sparrow, 2014). Furthermore, it is highly dependent on weather conditions. The temperature should not drop below 5°C, and the hempcrete must dry thoroughly prior to being subjected to freezing temperatures. However, A typical 300 mm wall takes approximately three months to dry completely (Néron, 2019). Precipitation, extremely high temperatures, and humidity are also limiting factors in this technique (Stanwix & Sparrow, 2014).

2.5.2 Precast and Predried Blocks or Panels

Blocks or framed panels can be created using the precast technique. The panels usually have a wooden mesh frame and hempcrete in between them (Magwood, 2016; Stanwix & Sparrow, 2014). The block assembly is based on basic common masonry, following the tongue and groove instructions or using a thin layer of lime-based bedding mortar consisting of hydraulic lime and sand (Néron, 2019). The advantage of the off-site drying procedure with quick-drying mortar eliminates the concern regarding the timelines, especially in cold weather and humid climates such as Canada (Williams *et al.*, 2017). The fast drying, along with achieving controlled properties of hempcrete, has made this technique more popular (Jami *et al.*, 2019). Despite the mentioned upsides, the precast hempcrete demonstrates poorer thermal performance compared to other techniques. The mortar can act like a thermal bridge, and also, the companies need to increase the density and mechanical properties, usually by adding to the binder ratio to minimize

transportation damage. This approach involves more material, has more wastage, and is less cost-effective than the in-place casting technique (Stanwix & Sparrow, 2014).

2.5.3 Projection

In this technique, sprinkled water is added to the dry mix right before being sprayed through the nozzle (Elfordy *et al.*, 2008). There is one temporary frame, with studs and plates in between, and one open side to be shaped and straightened after the spray (Néron, 2019; Stanwix & Sparrow, 2014). This technique requires a finer-grade hemp particle size to avoid blocking the hemp in the hose. The spraying distance and velocity are influential in the resulting material compaction grade. The added water is only enough to activate the binder while not being absorbed by hurd. This contributes to consuming considerably less water and a shorter drying period (Elfordy *et al.*, 2008). The procedure saves time as well as the number of labourers. Therefore, it is preferable for massive constructions, while it cannot be justified for small buildings since it requires specific machinery and skilled labourers (Stanwix & Sparrow, 2014).

2.5.4 Techniques Comparison

The particles in the projection process and precast technique are mainly oriented horizontally, while the cast-in-place technique has more vertically oriented particles. A thorough experiment on the mechanical and thermal properties of all three production techniques is conducted (Williams *et al.*, 2017). It was revealed that horizontally oriented particles in the projection technique, even with higher density, demonstrated the best thermal conductivity performance. However, the mechanical properties of the projection technique are the poorest due to uneven binder distribution. That is why the projection technique is a good choice in retrofitting since the mechanical properties are less important, and this technique can offer equal thermal performance as other techniques with less thickness (Williams *et al.*, 2017). In addition, the cast-in-place method provides the best mechanical performance, followed by the precast technique and projection. The precast method is not as environmentally friendly as both in-place methods due to extra processes, including transportation and energy used in the company. Consequently, the embodied energy is expected to be higher in this method (Stanwix & Sparrow, 2014).

2.6 Hempcrete Mix Design

The modified ancient Roman recipe for casting the concrete is applied to create hempcrete. The hemp hurd is used as an aggregate, replaced by the mineral parallel, while lime and SCMs are used as the binding agent (Néron, 2019). There are various mix designs applied in different experiments and by producers, as no standard procedure has been published to date (Mahmood *et al.*, 2024). Considering all three hempcrete components, which differ in terms of characteristics and their proportion in the mixture, comparisons between hempcrete specimens can be challenging. The curing type, the settling strategies, the amount of applied force for compaction, the temperature and humidity level at the time of casting and curing, and the mixing technique are all examples of variable conditions (Magwood, 2016).

As for the mixing technique, it is common to combine the binder with the required water to ensure its full reactivity and then add hemp hurd with the remaining portion of water (Néron, 2019; Stanwix & Sparrow, 2014). However, the method of dry mixing the components prior to adding the total water at the end is more widespread (Boulic *et al.*, 2013; Murphy *et al.*, 2010, 2010; Stanwix & Sparrow, 2014; Walker, 2013). Mixing is sufficient as long as all materials are blended uniformly with no lumps. The mixing should be conducted gently with the least possible duration to avoid excessive water absorption by hurd (Evrard, 2008). Evrard (2008) hand-mixed the ingredients for only 3-4 minutes, while Walker *et al.* (2014) pre-mixed the dry ingredients by hand, used the mixer for the final procedure, and spent 7 minutes mixing in total. Then, the cast mixture needs to be settled to achieve integrity and create a bond between particles, using manual tamping (Murphy *et al.*, 2010; Walker, 2013) or machines such as a vibration table (Mahmood *et al.*, 2024) or a cold-press machine (Nguyen *et al.*, 2009).

The curing process has been a controversial issue among authors. Many studies followed a certain curing process, either by changing the temperature or the humidity (de Bruijn *et al.*, 2009; Evrard, 2008; Khan, 2020; Mahmood *et al.*, 2024; Murphy *et al.*, 2010; Nguyen *et al.*, 2010). On the other hand, ambient temperature and relative humidity were applied by several authors as well (Abdellatef *et al.*, 2020; Brzyski, 2018; Dhakal *et al.*, 2017). They argued that hempcrete should lose moisture gradually for maximum

reactivity; however, maintaining moisture in the sample may cause mould growth and decay. Ambient conditions are said to provide the material with the required setting speed. In addition, ambient temperature curing can simulate construction environments (Tale Masoule *et al.*, 2022). The influence of curing conditions on binder settings has been examined in a study. The results indicate that storing the sample in a relative humidity higher than 75% or lower than 30% will delay both the SCMs and hydrated lime setting (Arnaud & Gourlay, 2012). It has also been revealed that curing in high relative humidity can have a negative effect on the mechanical behaviour of hempcrete (Pavía *et al.*, 2015). Furthermore, there is a relation between the drying duration and the final colour of the hempcrete. With the same ingredients and ratios, the product appears more yellow when the drying time is longer (Néron, 2019).

2.7 Research Gap

In spite of considerable advances in hempcrete research in recent years, certain aspects require additional investigation. To be specific, there is limited research focused on binder comparison and evaluation of their properties under consistent production and curing procedures. However, since most of these studies have been conducted in Europe (Walker, 2013), a knowledge gap exists regarding binder comparison, confining the locally sourced materials in Canada. The presence of several variables in available studies obscured the rationale behind the prioritization of one binder sample over another (Abdellatef *et al.* 2020, 2020; Daher *et al.*, 2022). The present study attempts to address the gap by isolating the influence of the binder and minimizing the impact of other variables, such as density and variations in hemp hurd particle size. Additionally, in contrast to previous literature that introduces a certain percentage of SCMs into hydrated lime, this study employs a more scientific comparison approach. By maintaining the main chemical composition (CaO and SiO_2) constant across all binders and ensuring equal potential for main gel production (C-S-H), the methodology facilitates a more efficient comparison than that achieved by conventional percentage-based formulations.

The examination of hemp hurd within this experiment is threefold. First, the study investigates the incorporation of hemp hurd particles into the binder paste and observes the resulting alterations in binder

properties, a topic that has received limited attention to date. Second, the hemp hurd-to-binder ratio is increased to maximize the hygrothermal performance of hempcrete and to fill the gap related to the relatively high thermal conductivity of hempcrete when used as insulation (Magwood, 2016). Finally, the study reduces the hemp hurd particle size to improve the result consistency and compares the result with conventional hempcrete, which is created with as-received hemp hurd. The comparison is based on evaluating the energy required for hempcrete deformation, a subject that has been scarcely studied in the literature.

Chapter 3

Materials and Methods

3.0 Chapter Outline

The following chapter has been divided into three main sections. The materials section introduced the materials used in the experiment, including hemp hurd and binder components. The second section describes the applied methodology for binder paste cubes as well as hempcrete samples, such as the mixing proportions and casting techniques. Finally, the properties section provides the method used to obtain the results for the component's characterization, along with the samples' properties.

3.1 Materials

The following section introduces hemp hurd and all binder components used in this study. These include hydrated lime as the primary binder and four different SCMs: metakaolin, pumice, silica fume, and slag, along with Ordinary Portland Cement (OPC), which served as the reference SCM. Hydrated lime was used as the reference as well, without the inclusion of any SCMs. Figure 7(a), (b) demonstrated all six binder components used in this study, as well as hemp hurd particles.

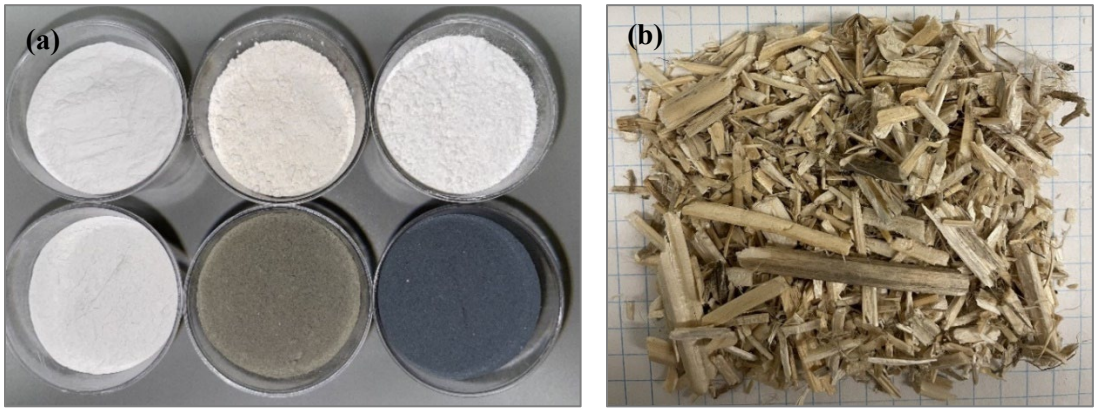

Figure 7- a) Binders, top row, left to right: pumice, metakaolin, hydrated lime. Second row: slag, Portland cement, silica fume, b) Hemp hurd particles as received.

3.1.1 Hemp Hurd

The hemp hurd was supplied by the BioComposites Group (BCG) through the Terrafibre Products Company, which mainly employs industrial hemp and flax to produce husbandry supplies. The company sources its raw materials from by-products of local hemp farmers grown in Alberta, Canada. They primarily use hemp fibres in manufacturing products, leaving hemp hurd as a by-product. In this study, all the hemp hurd used was obtained from the same batch of shipped parcels. The material was stored under ambient conditions at a temperature of 20 ± 2°C and a relative humidity of 55 ± 4%.

3.1.2 Hydrated Lime

The High Calcium Hydrated Lime ($Ca(OH_2)$), used as the main binder, was manufactured in British Columbia, Canada, and distributed by GRAYMOUNT INC., a local provider located in Québec. It comprises 90-100% calcium hydroxide and 0.0001-1% quartz. The material is a highly alkaline dry powder, classified as corrosive with the potential to cause skin and respiratory irritations. The product specification according to the company's datasheet is provided in Appendix A (a).

3.1.3 Metakaolin

The metakaolin, branded as PowerPozz™ (HRM), was locally sourced from Skycon Building Products Ltd., Ontario, Canada, and manufactured by Advanced Cement Technologies, WA, USA. It is made of 97.5-100% kaolin and less than 2.5% quartz. As a natural and calcined pozzolan, the material follows ASTM C-618-23 specifications and is categorized as Class N (ASTM C618 − 23, Standard Specification for Coal Ash and Raw or Calcined Natural Pozzolan for Use in Concrete, 2023). The physical and chemical properties of metakaolin are detailed in Appendix A (b).

3.1.4 Pumice

The white pumice (Grade: DS325) was supplied by HESS PUMICE Products, mined, refined, and manufactured in Idaho, USA. The product was received as an in-kind donation from the company; however, it was also available through a local distributor. Pumice is a non-toxic, natural pozzolan and classified as Class N based on ASTM C618 - 23 (Standard Specification for Coal Ash and Raw or Calcined Natural

Pozzolan for Use in Concrete, 2023). The material's direct application in cosmetic products (*Hess Pumice*, 2024) highlights its non-corrosive and non-irritant nature. Pumice specifications are available in Appendix A (c).

3.1.5 Silica Fume

The Dry Densified Silica fume admixture (MasterLife SF 100) was sourced by the local Lafarge Company in Ottawa, a major provider of cementitious materials across Canada. The product was manufactured by Master Builders Solutions Inc. in Ontario, Canada, and contains amorphous, crystal-free silica fume and quartz. It is hazardous if inhaled or comes into contact with the skin. The material datasheet is represented in Appendix A (d).

3.1.6 Slag

Ground Granulated Blast-furnace Slag (GGBS) type S was processed and collected from the Stoney Creek Plant, a local facility in Ontario, operated by Lafarge Company. The material complies with the specifications outlined in ASTM C989/C989M-24 (Standard Specification for Slag Cement for Use in Concrete and Mortars, 2024). The additional properties of this material, as documented in the Mill Certificate, are provided in Appendix A (e).

3.1.7 Ordinary Portland Cement (OPC)

Ciment Québec Inc., located in QC, Canada, was the distributor for the Type 1 general-use (GU) Portland Cement ELEMENT. The material meets the standards specified in ASTM C150/C150M - 24 (Standard Specification for Portland Cement, 2024). A detailed description of the OPC specifications is provided in Appendix A (f).

3.2 Methods

3.2.1 Binder Paste Cubes

3.2.1.1 Mixing Proportions

A combination of hydrated lime with four different SCMs was formulated for this experiment. Additionally, pure hydrated lime, as well as its mixture with OPC, were implemented as reference materials. In the first set of mixtures, 70% hydrated lime was combined with 30% SCMs by weight. The second set was designed based on the CaO/SiO_2 molar ratio of the total binder composition, resulting in unique hydrated lime-to-SCMs proportions for each mix. CaO/SiO_2 molar ratios of 0.8 and 3.0 were prepared for all mixtures, with the slag being an exception, where its high calcium content hindered achieving a CaO/SiO_2 molar ratio of 0.8. For each of the fifteen mix designs (shown in Figure 8), twelve specimens were prepared to conduct various tests, resulting in a total of 180 specimens.

Figure 8- All binder paste cube types created in the experiment

In addition, the water-to-solid ratio was determined according to the specific water demand of each material. Further details on the calculation of binder paste water demand are provided in the section 3.3.2.2. Table 13 presents the mix design for the specimens, with all quantities expressed as material weights.

Table 13- Mix proportions of binder paste cube samples

No.	Sample ID	SCM	Mixture type	Lime-to-SCM	Water: dry ratio
1	BP-MK-30	Metakaolin	Percentage based	70/30	0.8:1
2	BP-PU-30	Pumice	Percentage based	70/30	0.7:1
3	BP-SF-30	Silica Fume	Percentage based	70/30	0.75:1
4	BP-SL-30	Slag	Percentage based	70/30	0.65:1
5	BP-PC-30	Portland Cement	Percentage based	70/30	0.65:1
6	BP-MK-MR3	Metakaolin	Molar Ratio 3.0	69/31	0.8:1
7	BP-PU-MR3	Pumice	Molar Ratio 3.0	75/25	0.7:1
8	BP-SF-MR3	Silica Fume	Molar Ratio 3.0	79/21	0.75:1
9	BP-SL-MR3	Slag	Molar Ratio 3.0	49/51	0.6:1
10	BP-PC-MR3	Portland Cement	Molar Ratio 3.0	0/100	0.4:1
11	BP-MK-MR0.8	Metakaolin	Molar Ratio 0.8	36/64	0.85:1
12	BP-PU-MR0.8	Pumice	Molar Ratio 0.8	43/57	0.65:1
13	BP-SF-MR0.8	Silica Fume	Molar Ratio 0.8	49/51	0.75:1
14	BP-SL-MR1.1	Slag	Molar Ratio 1.1	0/100	0.4:1
15	BP-LIME	_	_	100/0	0.75:1

3.2.1.2 Casting Techniques and Curing Process

The preparation of binder paste cubes was adapted from the ASTM C109/C109M − 21 (Standard Test Method for Compressive Strength of Hydraulic Cement Mortars (Using 2-in. or [50 Mm] Cube Specimens), 2021). Casting was conducted under ambient conditions, with temperatures and humidity of 21 ± 1℃ and 52 ± 2%, respectively. Furthermore, all applied dry components were stored in closed containers at an average temperature of 20 ± 2℃ and relative humidity of 55 ± 4%.

The dry ingredients were weighed using an Electronic Digital Lab Analytical Balance Scale, manufactured by YYHEN Company. The scale featured a resolution accuracy of ± 0.01 grams and a maximum capacity of 3000 grams. Then the material was mixed for 30 seconds using a KitchenAid ARTISAN Series 5 Quart Tilt-Head Stand Mixer (Model No. KSM150PSBM). A flat beater attachment was used for mixing in a mixing bowl, with a capacity of 5 quarts (approximately 4.7 litres). The process was followed by adding

measured water to the dry mixture and combining the components for 3 minutes to achieve a homogeneous paste. The first layer of paste was transferred into the cubic mould, covering approximately half of its depth. Each side was tamped 32 times over 10 seconds in four sets per compartment, following the “hand tamping” procedure described in ASTM C109/C109M-21. This process was repeated for the final layer.

Four sets of 50 mm three-gang brass cubic moulds were employed for casting the specimens. The moulds were maintained at the ambient temperature used for casting, as specified earlier. A thin layer of lubricant was applied using a cloth, adapted from ASTM C109/C109M-21. Figure 9 illustrates the mould used in this experiment.

Figure 9- Binder paste cubes mould

The Specimens were de-moulded after 24 to 48 hours, depending on the specific setting time of each mix. Subsequently, the samples were stored under an ambient temperature of 20 ± 2℃ and relative humidity of 55 ± 4% until they were prepared for the required tests.

3.2.2 Hempcretes

3.2.2.1 Mixing Proportions

The hempcrete was created from three main components: the binder, finely ground hemp hurd, and water. 15 different mix designs were designed in this study, with the binder mix proportions equivalent to the

binder pastes described in 3.2.1.1 section. In addition, the HC-MK-30 specimen, consisting of metakaolin and hydrated lime in a 30/70 proportion, was prepared using coarse hemp hurd particles as received. For all samples, a target density of 190 ± 3 kg/m^3 was aimed for, with a binder-to-hemp ratio of 1:1 by weight. Considering using ground hemp hurd, this ratio was roughly equal to 1:4 by volume.

In total, this study tested 192 undamaged hempcrete samples, 6 cubic and 6 rectangular prism samples for each of the 16 mix designs. Due to the fragile nature of low-density hempcrete, additional specimens were prepared to account for potential damage.

Finally, the water ratio was derived from the combination of the water demand of the hemp hurd and that of the binder, as defined for each batch in Table 13. The water demand for the hemp hurd was considered to be three times its weight, based on the ball and finger test described in 3.3.3.2 section, which also aligns with findings from previous studies (Mahmood *et al.*, 2024; Murphy *et al.*, 2010). The final mix design is summarized in Table 14, with all proportions expressed by material weight.

Table 14- Mix proportions of hempcrete samples

No.	Sample ID	Hemp hurd particles	SCM	Mixture type	Lime-to-SCM	Hemp: binder: water
1	CHC-MK-30	As received	Metakaolin	Percentage based	70/30	1:1:3
2	HC-MK-30	Fine	Metakaolin	Percentage based	70/30	1:1:3.8
3	HC-PU-30	Fine	Pumice	Percentage based	70/30	1:1:3.7
4	HC-SF-30	Fine	Silica Fume	Percentage based	70/30	1:1:3.75
5	HC-SL-30	Fine	Slag	Percentage based	70/30	1:1:3.65
6	HC-PC-30	Fine	Portland Cement	Percentage based	70/30	1:1:3.65
7	HC-MK-MR3	Fine	Metakaolin	Molar Ratio 3.0	69/31	1:1:3.8
8	HC-PU-MR3	Fine	Pumice	Molar Ratio 3.0	75/25	1:1:3.7
9	HC-SF-MR3	Fine	Silica Fume	Molar Ratio 3.0	79/21	1:1:3.75
10	HC-SL-MR3	Fine	Slag	Molar Ratio 3.0	49/51	1:1:3.6
11	HC-PC-MR3	Fine	Portland Cement	Molar Ratio 3.0	0/100	1:1:3.4
12	HC-MK-MR0.8	Fine	Metakaolin	Molar Ratio 0.8	36/64	1:1:3.85

13	HC-PU-MR0.8	Fine	Pumice	Molar Ratio 0.8	43/57	1:1:3.65
14	HC-SF-MR0.8	Fine	Silica Fume	Molar Ratio 0.8	49/51	1:1:3.75
15	HC-SL-MR1.1	Fine	Slag	Molar Ratio 1.1	0/100	1:1:3.4
16	HC-Lime	Fine	_	_	100/0	1:1:3.75

3.2.2.2 Casting Techniques and Curing Process

As highlighted in various studies, no standard technique has been defined for hempcrete production (Mahmood *et al.*, 2024; Stanwix & Sparrow, 2014). The hemp hurd used in the specimens was ground according to the specifications described in 3.3.1.3. Both the ground hemp hurd and binder components were stored in containers at an ambient temperature of 20 ± 2°C and relative humidity of 55 ± 4% to simulate typical manufacturing conditions. Casting was performed under similar environmental conditions as well.

Batching begins with the dry mixing of the measured hydrated lime and SCM (Figure 10(a)) for 30 seconds. This step was followed by the addition of ground hemp and an additional 60 seconds of hand mixing (Figure 10(b)). Measuring the required water quantity, the mixture was blended using a Globe commercial food mixer, Model No. SP20 featured a ½ HP motor and a bowl with an 18.9-litre capacity (Figure 10(c)). The medium speed was used for 3 minutes until a uniform mixture was obtained (Figure 10(d)), yet to avoid providing excessive time for the hemp hurd to absorb excessive water. The mixer was paused 2-3 times during the blending process to ensure no lumps or dry particles remained in the mixture.

To achieve a consistent target density in all samples, a specific measured amount of mixture was placed into the defined moulds. This quantity varied slightly for each batch depending on the binder type and water demand. Due to the bulky nature of hemp hurd, the moulds were initially overloaded and then uniformly compacted to achieve the desired density within the mould's defined volume. To achieve this purpose, the moulds were equipped with height extensions and lids. The extension provided the material in the mould with additional room before being compacted downward, while the lid pressed down the material homogeneously to the specified height level. Figure 10(e) and (f) illustrate the process in detail.

For this experiment, two types of moulds were prepared based on the application. Eight rectangular prism moulds with internal dimensions of 150 × 150 × 50 mm were fabricated to test the thermal properties of hempcrete blocks. In contrast, the compressive strength tests were conducted using hempcrete cubes cast in six 100 × 100 × 100 mm moulds. Both mould types were constructed from plexiglass, whose slippery texture eliminated the need for lubrication prior to casting. Due to the fragile nature of hempcrete, all sides of the moulds were secured with screws to maximize control over the samples. Figure 11(a) illustrates the mould designs for both tests.

Figure 10- a) Binder components, b) Binder combination with hemp hurd, c) Hempcrete mixture in the mechanical mixer, d) Evenly distributed final mixture, e) Overloading hempcrete in mould, f) Uniformly slight compaction of hempcrete to the mould height.

The Samples were de-moulded after 24-48 hours, depending on their setting time, based on the estimation in the previous literature (Walker, 2013). They were stored under ambient environmental conditions with 20 ± 2°C temperature and 55 ± 4% relative humidity until the 25th day after casting. To enhance air circulation beneath the samples during curing, an elevated base with multiple holes was designed. This setup ensured uniform moisture loss from all sides of the specimens, thereby reducing the drying period without causing swift changes in humidity levels. Subsequently, the samples were transferred to an oven and dried entirely at a temperature of 60°C for three additional days. Before testing, it was ensured that the weight loss variation due to existing water in the hempcrete was below 1% during the final 24 hours. The oven-drying process of the hempcrete samples is depicted in Figure 11(b).

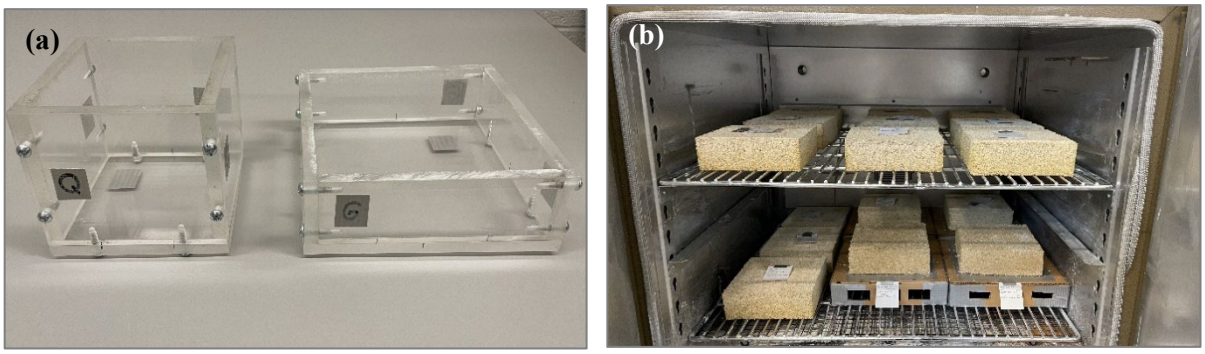

Figure 11- a) Cubic and rectangular prism plexiglass moulds, b) Placing the hempcrete samples in the oven

3.3 Properties

3.3.1 Components' Characterization

3.3.1.1 Composition

When preparing hemp hurd sourced from companies or local farmers, a portion of hemp fibres is inevitably mixed with the hurd (Magwood, 2016). However, no standardized methodology has been established to determine the fibre content in hemp particles used for creating hempcrete (Mahmood *et al.*, 2024). In this study, four separate samples, each weighing approximately 20 grams, were randomly selected from the received parcel of hemp particles. The fibres were manually separated from the hurd using a hand-picking

technique. The fibre content in the hemp particles was then calculated based on the average results from the four samples. Figure 12 distinguishes the separated hemp hurd and fibres.

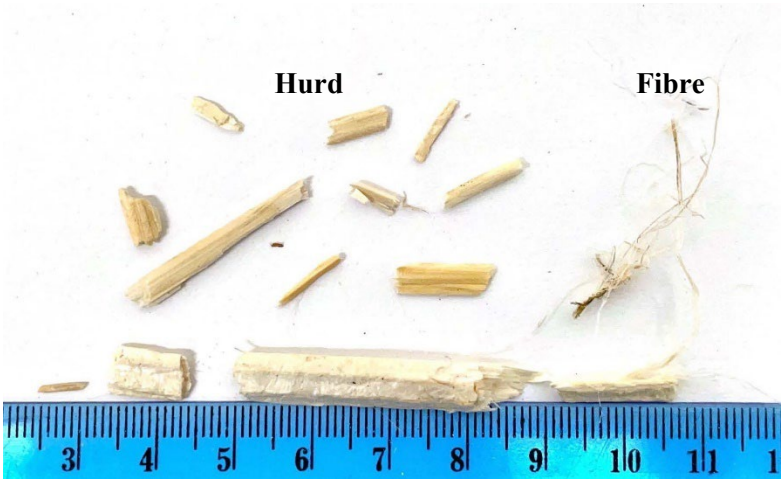

Figure 12- Hemp hurd and hemp fibres

In addition, the composition of the binder's components was determined using X-ray Fluorescence (XRF). A Rigaku Supermini200 benchtop sequential wavelength-dispersive spectrometer, incorporating a 200 W Pd-anode X-ray tube, was employed to perform sample analysis.

3.3.1.2 Apparent and True Density

The true density and apparent density (unit weight) of the binder components and hemp particles were determined in this study. The apparent density for loose materials was measured by gently placing the ingredients into a measuring container without compaction. By knowing the material's mass (m) as well as the occupied volume (v) in the container, the apparent density (ρ) was achieved using the following Equation 1.

$$\rho = m/v \qquad \textbf{Equation 1}$$

Furthermore, the true density of binder components and ground hemp hurd was measured using the Accupyc II 1345 gas pycnometer from Micromeritics Company (as shown in Figure 13). Helium gas was

employed as the analysis medium at a pressure of 19.500 Pounds per Square Inch Gauge (PSIG). To ensure accuracy, the test was repeated 10 times, achieving a volume precision of 0.02% and a temperature control accuracy of ±0.025°C. The pycnometer was connected to a data acquisition system for precise control and result recording.

Figure 13- Pycnometer

3.3.1.3 Particle Size

As previously mentioned, two hemp particle sizes were utilized in this study: large particles as received and finely ground hemp hurd particles. An ABORON Direct Grain Mill 150 was used for grinding (depicted in Figure 14), featuring a drill diameter of 150 mm and a speed range of 1400–2800 r/min. To prevent clogging, the material's diameter was maintained below 32 mm prior to grinding. The ground particles were produced by grinding hemp hurd twice using an unchanged grinder setting to ensure a homogeneous outcome. Various methods exist in the literature for determining the particle size distribution of hemp hurd, including sieve analysis and image processing. However, the elongated shape of hemp hurd makes image analysis the preferred method for determining particle size distribution over sieving (Walker, 2013). In this experiment, the particle sizes of both hemp grades were characterized by importing scaled images of the hemp particles into AutoCAD software and estimating the particle size distributions by averaging the

measured values. Four scanned images of particles were randomly selected and loosely spread on a paper sheet with a contrasting background. A ruler was included as a scale reference. The images were then imported into AutoCAD and rescaled based on the ruler. Particle lengths were measured and marked to prevent miscalculation, and the results were subsequently imported into an Excel spreadsheet to determine the minimum, maximum, and average particle lengths and widths. Initially, the particles were measured using ImageJ, a more conventional software for particle analysis. However, when compared with simultaneous actual particle measurements, using a calliper, AutoCAD was found to offer considerably higher precision and was therefore preferred.

Figure 14- Grinder

In addition, a Malvern Mastersizer 2000 was used to analyze the particle sizes of the binder components via laser diffraction. In this technique, a diffraction pattern is created when a laser beam targets a mass of particles, scattering light at an angle influenced by the particle size. However, since the method assumes all particles to be spherical, it introduces a significant margin of error. Furthermore, the interaction of light with multiple particles is disregarded in this measurement technique. The particle size results also included the materials' specific surface area.

3.3.1.4 Water Demand and Water Content

Hemp hurd exhibits a water demand that largely depends on its characterization and varies for each case. As outlined in the 2.1.3, the introduced water to the hemp hurd must be minimized to avoid delayed drying time and potential mould growth. Accordingly, the required water content for hemp hurd in a hempcrete mixture was determined using the ball and finger method, explained in 3.3.3.2 in detail. Furthermore, in this study, the hemp hurd was maintained at ambient temperature before measuring its water demand to replicate its behaviour under typical manufacturing conditions. The ambient temperature and relative humidity were controlled at 20 ± 2°C and 55 ± 4%, respectively.

Although minimal water was introduced to the hemp particles, the water absorption capacity of the hemp hurd was also measured by immersing it in water for 72 hours and periodically monitoring weight changes. Furthermore, the internal moisture content of the hemp hurd was determined by oven-drying the material at 90°C for six consecutive days, ensuring a weight variation of less than 0.1% over the final 24-hour period.

In addition, as highlighted in 2.1.3, the water introduced to the binders must be sufficient to facilitate complete hydration reactions while minimizing absorption by the hemp hurd. The water demand for each binder component was initially estimated based on data from prior studies to provide an overview. Subsequently, a slump test was performed for each binder component to determine its specific water demand. The slump test assessed material workability using a mini-slump cone with bottom and top diameters of 10 cm and 5 cm, respectively, and a height of 7.5 cm. Water was introduced gradually to achieve target workability, defined as forming a uniform paste while minimizing excessive flow. Following a method adapted from ASTM C143/C143M− 20 (Standard Test Method for Slump of Hydraulic Cement Concrete, 2020), the slump cone was filled in three layers, with each layer uniformly tamped 25 times using a tamping rod. Measuring the flow diameter of the binder paste on a flat surface, one minute after filling, the workability of the materials was identified. The resulting paste was ensured to be similar to the slump cone dimensions, with the maximum feasible height and minimum diameter. Moreover, the workability results were verified to be consistent for all binder components, in the achieved height and diameter.

3.3.2 Binder Paste Cubes Properties

3.3.2.1 Apparent Density

The apparent density of the cubes was calculated using their weight and volume. The scale specified in 3.2.1.2 was employed to measure the specimens' weight. The moulds for binder cubes had dimensions of 50 × 50 × 50 mm. However, due to varying shrinkage levels among different SCMs during the drying process, the exact volume of each specimen was determined using a calliper. With the mass (m) and volume (v) of the cubes measured, the apparent density (ρ) was calculated using Equation 1. The resulting density represents the average of six specimens from the same batch.

3.3.2.2 Water Demand

As explained in 3.3.1.4, the water demand for each binder component was determined. For mixtures containing two different binders, the overall water demand was calculated based on the individual water demand of each component, proportional to their respective ratios in the mixture. The water demand of the binder mix was calculated using the following Equation 2.

$$WDB = (WDL \times L) + (WDS \times S) \qquad \textbf{Equation 2}$$

Where *WDB* represents the water demand of the binder mix, *WDL* shows the water demand of hydrated lime, *L* indicates the hydrated lime proportion in the binder mix, *WDS* refers to the water demand of the SCM, and *S* is the SCM proportion in the binder mixture (Walker & Pavía, 2011).

3.3.2.3 Compressive Strength and Modulus of Elasticity

The 50 × 50 × 50 mm cube specimens were prepared to examine the compressive strength of different binder mix proportions, partially adapted from the ASTM C109/C109M − 21 (Standard Test Method for Compressive Strength of Hydraulic Cement Mortars (Using 2-in. or [50 Mm] Cube Specimens), 2021). Six specimens from each mix design batch were tested, and the results were calculated as the average values for maximum compressive strength and modulus of elasticity. The oven-dried cubes' weight was ensured to remain constant during the last 24 hours before testing. The specimens were tested at 90 days using a

68FM-100 INSTRON Universal Testing Machine (UTM), from the 6800 series, featuring a maximum load capacity of 100 kN load cell with ± 0.5% of reading accuracy class at a speed of 1.5 mm/min. Given that the materials in this study were classified as binder paste, this machine was selected over UTMs designed for testing concrete. The binder paste cubes were positioned inside a cube compression jig to achieve consistent load application across the samples. The instrument was paired with a data acquisition system (DAQ) to configure the test parameters, record data, and generate graphs. However, for the Portland Cement binder paste with the molar ratio of 3.0 (BP-PC-MR3), an automatic compression machine with a 400 kN load cell and a speed of 900 N/s was used since the 100 kN load cell was insufficient to determine the maximum possible load for these samples. Figure 15 exhibits the binder paste cube compressive strength test in the UTM.

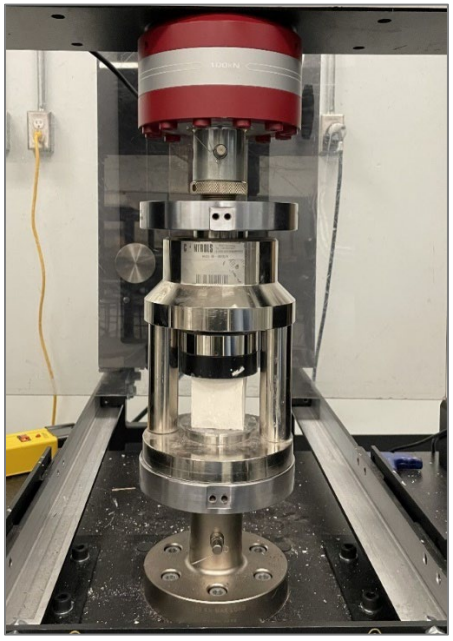

Figure 15- Compressive strength test of binder paste cube in UTM

The test was stopped when a major failure was observed in a specimen, indicated by a steep fall in the load-displacement curve. The compressive strength of each sample, measured in Mega Pascals (MPa), was

computed using the maximum load recorded in Newtons (N) before failure, divided by the cross-sectional area of the specimen in square millimetres (mm^2), according to the following Equation 3.

$$\sigma_{max} = \frac{F_{max}}{A} \quad \textbf{Equation 3}$$

When σ_{max} refers to the maximum compressive strength, F_{max} indicates the maximum applied load before failure, and A represents the cross-sectional area of the specimen.

Furthermore, the stress-strain curve was derived from the load-displacement data. The stress values were calculated by dividing the applied load by the cross-sectional area of the specimen. The strain was estimated by dividing the displacement data by the original length of the specimen, as no strain-measuring device was used in the experiment. However, since the displacement measured by strain-testing devices can differ from the UTM displacement, the modulus of elasticity was not scientifically precise and was computed solely to provide a general perspective for stiffness comparison between the samples. Therefore, the modulus of elasticity was determined using the slope of the linear region corresponding to 40% of the maximum stress in the stress-strain curve. This value was calculated using the following Equation 4.

$$E = \frac{\sigma}{\varepsilon} = \frac{F/A}{\Delta L/L} \quad \textbf{Equation 4}$$

When E represents the Modulus of elasticity (MPa), σ indicates the stress (MPa), ε shows the strain (-), F is the applied load (N), A denotes the cross-sectional area (mm^2), ΔL refers to the device displacement (mm), and L shows the initial length of the specimen (mm).

3.3.2.4 Thermal Properties

The thermal conductivity and specific heat capacity of the specimens were measured using a Trident thermal conductivity instrument, provided by C-Therm Company, with accuracies of ± 5% and ± 15-20%, respectively. A data acquisition system connected to the instrument enabled the configuration of test parameters, execution of tests, and storage of results through the Trident software. The samples were oven-

dried until a weight variation of below 1% was achieved over a 24-hour timespan. To ensure consistent and comparable results, all tests were conducted at the same specimen age. The apparatus simultaneously measured thermal conductivity and specific heat capacity using the Transient Plane Source (TPS) method, during which a sensor was sandwiched between two identical samples with no air gap in between (shown in Figure 16). To comply with the requirement that the minimum sample diameter must be at least 2.5 times the sensor diameter, a 13 mm diameter sensor was employed, as the binder paste cubes measured approximately 50 mm on each side. A power level of 0.08 W and a test duration of 80 seconds were selected based on the manufacturer's recommendations. Additionally, a five-filter validation of the acquired data was performed through the software to confirm the correctness of the procedure and settings.

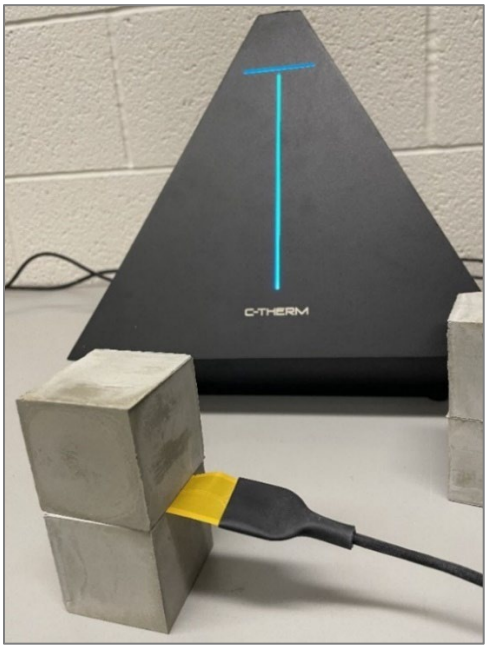

Figure 16- Binder paste cube thermal test conducted by Trident

3.3.2.5 Water Vapour Permeability

The cup test was employed to determine the water vapour permeability and water diffusion resistance factor of the binder paste cubes. The procedure was adapted from the ASTM E96/E96M-24 (Standard Test Methods for Gravimetric Determination of Water Vapor Transmission Rate of Materials, 2024). The test

dishes were designed and 3D printed using Poly Lactic Acid (PLA) materials, with external dimensions of 50 mm in length and width, a height of 40 mm, and a sidewall thickness of 1.6 mm. Using the water method, the dishes were filled with water to a height of 20 mm, and the binder paste samples were placed on top of the dishes. To ensure proper sealing, aluminum tape was applied along the edges, exposing only the top surface of the samples to the environment while the bottom surface was exposed to water vapour from the dish. The setup of a prepared sample is depicted in Figure 17(a). The assemblies were prepared and stored in an environmental chamber maintained at controlled conditions of 38 ± 0.7°C temperature and 30 ± 5% relative humidity, as shown in Figure 17(b). Six samples from each mix design were tested, five of which were placed on water-filled dishes for the experiment, with one blank specimen attached to an empty dish, used to monitor weight changes. The assemblies were weighted periodically every 48 hours until six consistent weight data points were collected. All samples were tested at a similar age to ensure that this factor did not influence the comparison of binders.

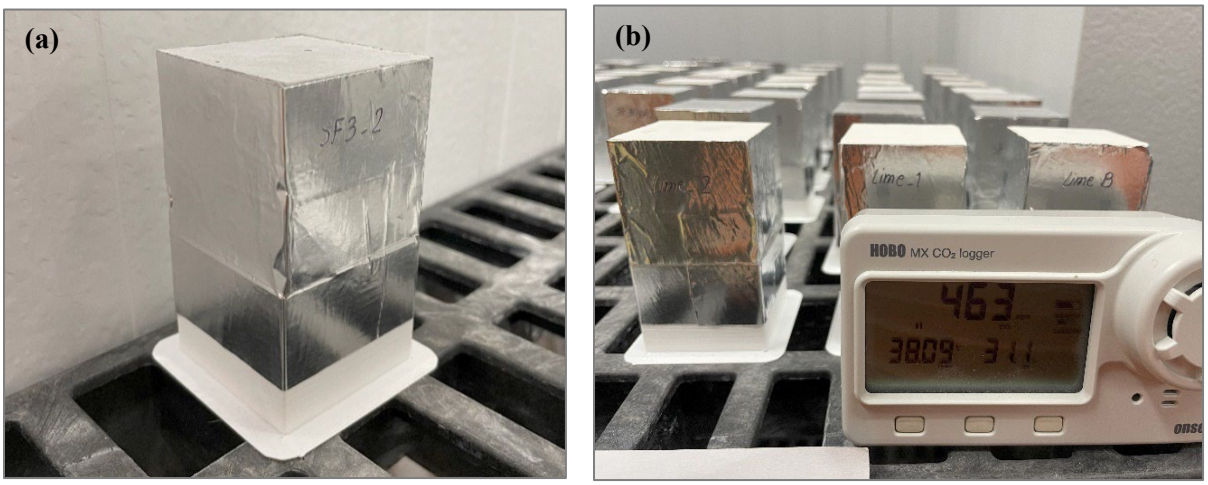

Figure 17- a) Prepared sample for the water method of cup test, b) Controlled environmental conditions

3.3.3 Hempcrete Property

3.3.3.1 Apparent Density

Since the porosity of hempcrete is a critical feature of its characteristics and properties, the apparent density is a key factor. The apparent density of hempcrete blocks was calculated by averaging the density of twelve specimens to enhance accuracy. It was computed by dividing the oven-dried weight of a specimen in kilograms (kg) by its volume, measured using a calliper in cubic metres (m^3), as outlined in Equation 1.

As highlighted in 3.2.2.1, the relatively low target density of 190 ± 3 kg/m³ was selected for this study. The justification for choosing this relatively low density can be threefold. Firstly, low-density hempcrete is commonly used as a ceiling filler or in insulation panels. Since hot air rises in the environment and the greatest heat exchange typically occurs in the ceiling area, the significance of its insulation properties becomes apparent, making hempcrete, as a low-conductive material, a suitable choice. Furthermore, the high moisture-buffering capacity allows for storing any potential leakage from the roof and gradually evaporating it, without settling over time, unlike other insulation materials. These features can be considered among hempcrete's primary advantages for ceiling applications. In addition, the binder impact in low-density hempcrete samples can be more evident compared to their high-density counterparts. Therefore, to better investigate the binder effect in hempcrete with a high hemp hurd ratio, low-density specimens were chosen. Finally, most hempcrete research has focused on suitable density for wall applications, whereas the properties of hempcrete with a density of less than 250 kg/m³ have been less investigated.

3.3.3.2 Water Demand

The water demand of a hempcrete sample comprises the water required for the binder mix and the hemp hurd particles to achieve a workable mixture with appropriate consistency without excessive water. The binder's mix water demand was determined for each binder following the explanation provided in 3.3.2.2. However, formulating the water ratio for hemp hurd is challenging due to its rapid and continuous absorption of water over a short period (Arnaud & Gourlay, 2012). To address this, the ball and finger test

was conducted to reveal the water demand of coarse and fine hemp hurd particle sizes separately, a method widely applied in various studies (Dhakal *et al.*, 2017; Mahmood *et al.*, 2024).

The procedure suggests forming a ball from a well-mixed batch, as shown in Figure 18. The water content is appropriate if the squeezed ball retains its integrity without extra leaking. In addition, when the ball is held, and a finger is pressed into it, it should split into two distinct halves, indicating the optimal water content (Magwood, 2016; Stanwix & Sparrow, 2014). This approach ensures the water amount is adequate to hydrate the binders and provide consistent flow for the mixture, while preventing the hemp hurd from absorbing excessive water, which could lead to mould growth and delayed drying times.

Figure 18- Ball and finger test to determine water demand

3.3.3.3 Compressive Strength and Modulus of Elasticity

The 100 × 100 × 100 mm samples were prepared to perform the compressive strength test. Six specimens were tested for each mix proportion, with the results originating from their average values. The tests were conducted 28 days after casting, providing a safe margin for the reactions of lime and SCMs to be substantially complete, given their varying setting times (Walker, 2013). Following the curing process and oven-drying, as described in 3.2.2.2, the samples were cooled for only 30 minutes before testing to minimize moisture absorption. The Universal Testing Machine (UTM), equipped with a 10 kN load cell and load measurement accuracy of ± 0.5% of reading and operating at a speed of 1mm/min, was used to compress

the specimens. The concentric metal discs were placed on both sides of the specimens to ensure uniform load distribution. Each test lasted approximately 1 minute for ground hemp hurd samples, whereas as-received hemp specimens sustained the test for over an hour without complete failure. The applied load and displacement were recorded throughout the test. Failure was defined as the point of maximum applied load for ground hemp hurd hempcrete. In contrast, for as-received hemp hurd blocks, the stress-strain curve exhibited a linear trend, continued by a horizontal plateau, and followed by a steeply rising line, indicating no distinct failure point. Therefore, the deformation at 10% of the sample length was considered the compressive strength value of coarse aggregate hempcrete. Figure 19 shows the compression test for a finely ground hemp hurd sample.

Figure 19- Hempcrete cubes' Compressive strength test

To provide a comparison of sample stiffness, the modulus of elasticity of the specimens was derived from the slope of the stress-strain curve within the elastic region. However, as noted in 3.3.2.3, this value does not represent the true modulus of elasticity due to the absence of a strain-measuring device for precise strain data acquisition.

3.3.3.4 Thermal Properties

A Fox 304 Heat Flow Meter (HFM), provided by TA Instruments Co., was utilized to measure the thermal properties of the hempcrete blocks. The instrument accommodated samples with maximum dimensions of 305 × 305 mm and a height of up to 102 mm, utilizing self-adjusting thickness measurements with an accuracy of ± 0.025 mm. It incorporated two thin-film heat flux transducers, facilitating rapid thermal equilibrium through advanced temperature control at a rate of 20 adjustments per second. These transducers, located at the centre of the plates, also served as sensitive temperature regulators with an accuracy of ± 0.01℃. The effective measurement area of the transducers was 100 × 100 mm, necessitating that sample dimensions exceed 100 mm in both length and width.

The 150 × 150 × 50 mm hempcrete blocks were surrounded by a layer of insulation to cover the margin gap between the specimens and the device walls on all four sides (as shown in Figure 20). The oven-dried sample was positioned centrally within the device, where the sensors were located, sandwiched between the bottom hot plate, set at 45℃, and the top cold plate, set at 20℃, to establish a gradient across the sample thickness. The induced heat flow was measured using internal heat flux transducers equipped with type E thermocouples embedded in the plates. To mitigate the effects of contact resistance and enhance precision, external thermocouples with auxiliary inputs were attached directly to the sample surfaces.

The HFM offered an accuracy of ± 1%, meeting the ASTM C518- 21 (Standard Test Method for Steady-State Thermal Transmission Properties by Means of the Heat Flow Meter Apparatus, 2021). The thermal conductivity value was calculated as the average of at least six specimens from the same mix proportion. Each thermal conductivity test lasted approximately 90 minutes and was repeated randomly to ensure result reliability. The device was coupled with a data acquisition system to run and configure the test settings using the WinTherm32 software and to store the obtained data. It is also accompanied by a PolyScience CA03A1T1-41AA1N DuraChill portable chiller to achieve lower temperatures, down to -10℃, with a temperature stability of ±0.1℃.

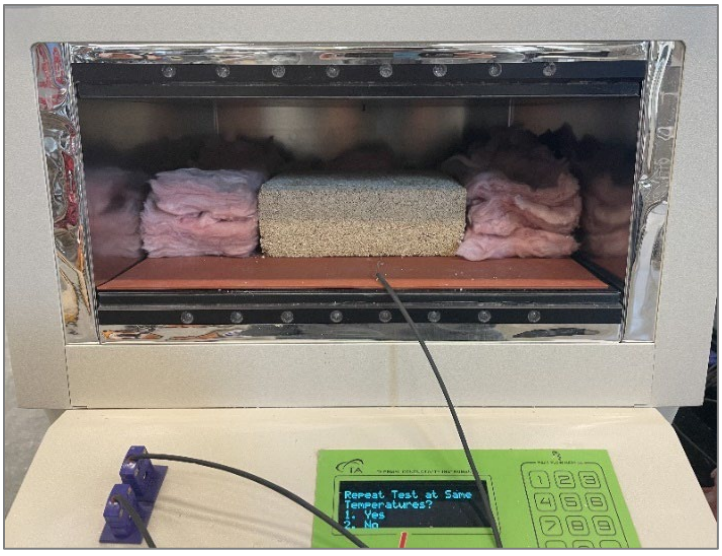

Figure 20- Placing the hempcrete sample in the heat flow meter

The HFM was also employed for determining the specific heat capacity. During the test, the top and bottom plate temperatures were set equally at 15, 25, and 35°C, with mean values of 20 and 30°C to ensure comparability. The test duration ranged from 300 to 330 minutes, during which the device automatically calculated the volumetric specific heat of the samples, unlike earlier versions, frequently referenced in prior studies (Abdellatef *et al.*, 2020; Brzyski *et al.*, 2020). The specific heat capacity was subsequently determined by dividing the volumetric specific heat value by the density of the specimen. Since all thermal property tests conducted in this research were non-destructive, the same specimens used for the thermal conductivity test were reused for the heat capacity test, with separate oven-drying.

Chapter 4

Results and Discussion

4.0 Pre-Discussion (Rationales)

As previously outlined, hydrated lime is paired with SCMs to create the hempcrete binder, enhancing hydration and accelerating setting time. As mentioned earlier, Portland cement and hydraulic lime are among the most frequently used materials, accompanied by hydrated lime in hempcrete (de Bruijn *et al.*, 2009; Delhomme *et al.*, 2022; Magwood, 2016; Stanwix & Sparrow, 2014). However, this research considered more eco-friendly alternatives and compared their behaviour in hempcrete with Portland cement as the reference. Among numerous options, slag, silica fume, pumice, and metakaolin were selected for their local accessibility, anticipated future availability, and environmental friendliness, while other candidates were excluded for various reasons. For example, fly ash is expected to have a limited operational lifespan, Leca exhibits a high carbon footprint, rice husk ash is not locally available, and black rice husk ash is produced in limited quantities and lacks potential for large-scale use.

In this study, the combination of hydrated lime and SCMs is formulated based on the overall molar ratio of binders in each mix design (the rationale is detailed in Section 2.1.2.3). This approach contrasts with the percentage-based combinations used in previous studies. The CaO/SiO_2 molar ratio of 3.0 was derived from the corresponding ratio in the chemical composition of the Portland cement used as the reference SCM. By achieving this molar ratio, the study aims to obtain the optimal mechanical strength characteristic of Portland cement. The results were compared to those from two different mix designs.

The first category employs a lower CaO/SiO_2 molar ratio of 0.8, which is known to be critical in previous studies (He *et al.*, 2014). This ratio ensures that hydrated lime accounts for at least half of the binder composition, thereby preserving its beneficial properties, as noted in the 2.1.2.1 section. An approximately

50/50 hydrated lime-to-SCM proportion is also regarded as an optimized binder ratio, according to studies (Bendouma *et al.*, 2023) approving the CaO/SiO_2 molar ratio of 0.8. On the other hand, a percentage-based binder mix design, with 70% hydrated lime to 30% SCMs, has been compared to binders characterized by a CaO/SiO_2 molar ratio of 3.0. In addition to closely matching the CaO/SiO_2 molar ratio of 3.0, this mix design is among the most commonly used proportions in binder compositions reported in previous studies (Al-Tamimi *et al.*, 2024; Issaadi *et al.*, 2015; Walker, 2013) or even in commercial binders (Elfordy *et al.*, 2008; Evrard, 2008).

In this experiment, hemp hurd was finely ground to produce the hempcrete samples. The elongation and orientation of hemp hurd particles are proven to significantly influence the pore structure and, consequently, the properties of hempcrete (Bennai *et al.*, 2018; Song *et al.*, 2024, p. 20; Williams *et al.*, 2018). Therefore, the use of finely ground hemp hurd, with the particle size chosen based on the findings in previous literature (Mahmood et al., 2024) was preferred in this study. The reduced hemp hurd particles resulted in more consistent specimens, minimized variability associated with the hemp hurd, and allowed the experimental focus to remain on the binder effects. Furthermore, a hemp hurd-to-binder ratio of 1:1 was maintained in all mix designs. The binder proportion was reduced relative to most previous studies to minimize environmental impact, improve energy efficiency in cold climates (Al-Tamimi *et al.*, 2024) and enhance hygrothermal performance (de Bruijn & Johansson, 2013). In contrast, exceeding the hemp hurd ratio beyond this proportion has been shown to lead to inconsistencies and reduced structural integrity in hempcrete samples (Mahmood *et al.*, 2024).

The following chapter presents the achieved results coupled with a discussion on the characterization of the binder paste and hempcrete samples, as well as their compositions. It also provides test results for compressive strength, thermal conductivity, heat capacity, and water vapour permeability on prepared samples, along with a comprehensive discussion of the influence of binders and hemp hurd on the mentioned properties.

4.1 Characterization

4.1.1 Binders

4.1.1.1 Density

Figure 21 illustrates the true density measured using a pycnometer alongside the apparent loose density of the hempcrete binder components. Silica fume, pumice, and hydrated lime exhibited low true densities, approximately 2330 to 2420 kg/m³, whereas metakaolin and slag displayed considerably higher true densities at 2900 and 2970 kg/m³, respectively, with Portland cement having the highest true density at 3160 kg/m³. However, the apparent loose density showed a different trend. Hydrated lime, metakaolin, and silica fume had the lowest apparent densities of 530 to 660 kg/m³, followed by pumice at 780 kg/m³, and finally Portland cement and slag, with apparent densities of 910 and 950 kg/m³, respectively. Table 15 presents the statistical analysis of density results, emphasizing the significance of the observed differences.

As can be perceived, hydrated lime and silica fume were the binders with the lowest density, characterized by low true and apparent densities, while Portland cement and slag were the highest density binders. Although pumice had a relatively low true density, its apparent density was above average. On the other hand, metakaolin exhibited one of the lowest apparent densities despite its high true density. A slight difference was also observed in the comparison between Portland cement and slag densities: although both possessed high true and apparent densities, Portland cement's true density exceeded slag's by 190 kg/m³, while slag demonstrated a higher apparent density. This gap between apparent and true densities indicates the volume of voids between the binder particles, which is attributed to the particle shape and arrangement of the materials (Walker, 2013). For instance, metakaolin particles appeared to create more voids between their particles than pumice.

Table 15- Statistical analysis for true and apparent densities of binder components- ANOVA

Densities (kg/m³)	*SS*	*df*	*MS*	*F*	*P-value*	*F crit*
True Density	6309076.52	5	1261815.30	48769.54	2.36E-97	2.39
Apparent Density	590133.33	5	118026.67	169.28	1.77E-14	2.77

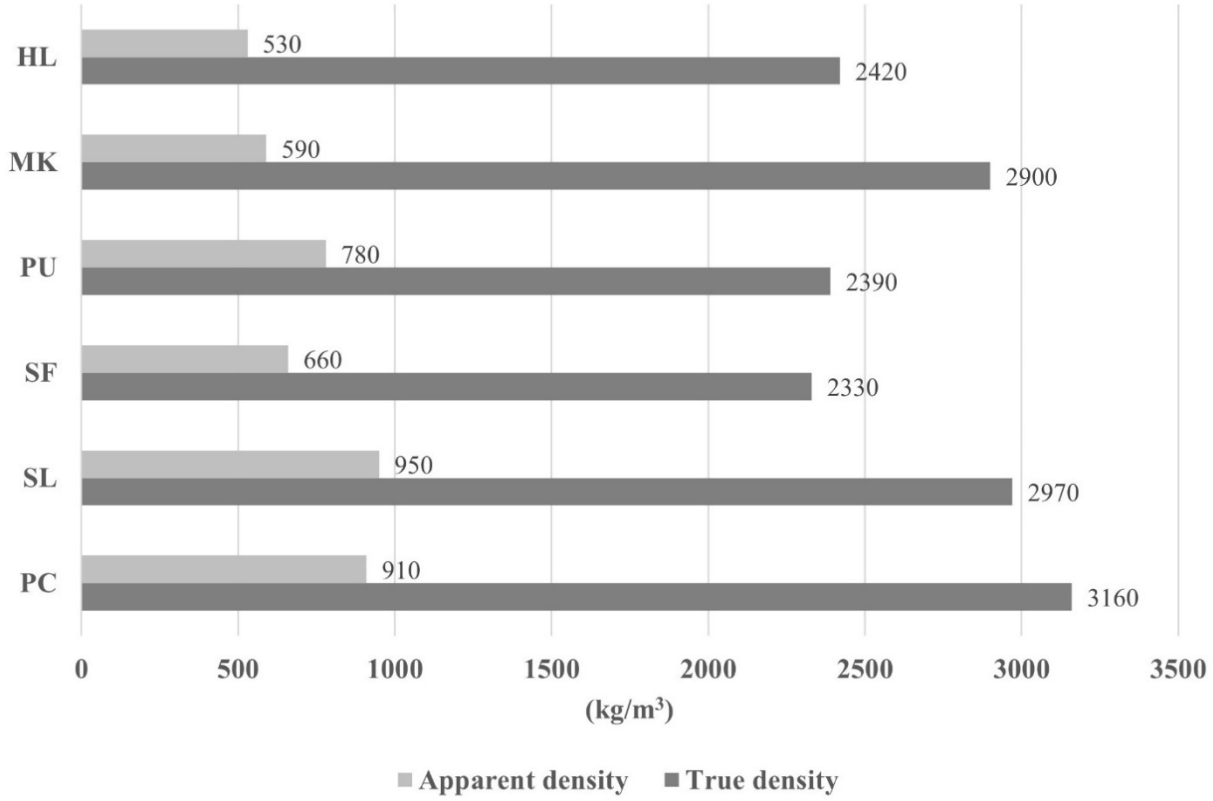

HL: hydrated lime, MK: metakaolin, PU: pumice, SF: silica fume, SL: slag, PC: Portland Cement

Figure 21- True and apparent density of binder compositions

Several methods exist to determine the apparent density (unit weight) of these materials (Walker, 2013), and variations in techniques and compaction levels can lead to significant differences in the results. For example, while the present study found the apparent density of metakaolin to be 590 kg/m³, Zerrouki *et al.* (2022) reported an apparent density of 400 kg/m³. In addition, since the determination of true density via pycnometry requires the particles to be very finely powdered, the resulting measurements may include a margin of error, particularly for binders with porous particles. The source and production process of the binders, whether as a by-product or being mined, can also influence their physical properties, such as density. For instance, a coarser ground porous particle may exhibit a lower true density in a pycnometer compared to the same material when more finely ground. Nonetheless, the results align reasonably well

with other studies and the product datasheet, indicating the reliability of the measurements. Table 16 summarizes the achieved data from the current experiment and compares it with other sources.

Table 16- The comparison of the achieved true density with other sources (Almalkawi *et al.*, 2017; Hedayatinia *et al.*, 2019; Panesar, 2019; Zeyad *et al.*, 2022)

True density (kg/m^3)	HL	MK	PU	SF	SL	PC
Current study value	2420	2900	2390	2330	2970	3160
Literature values	-	2200-2600	2350-2910	2200-2300	2850-2950	3150
Datasheet values	2300-2400	2600	2350	2100-2300	2910	3200

HL: hydrated lime, MK: metakaolin, PU: pumice, SF: silica fume, SL: slag, PC: Portland Cement

4.1.1.2 Water Demand

Table 17 lists the water demand values for a unit of binder components, showing that metakaolin exhibited the highest water demand, whereas slag and Portland cement had the lowest water demand among the binders. Hydrated lime, serving as the primary binder component, demonstrated a water-to-solid ratio of 0.75:1. In comparison, metakaolin had a higher water-to-solid ratio of 0.9:1, which increased the overall water demand in the binder mix. In contrast, pumice, slag, and Portland cement exhibited lower water-to-solid ratios of 0.575:1, 0.4:1, and 0.4:1, respectively, thus reducing the water demand in the resulting binder mix. Silica fume displayed a water demand equivalent to that of hydrated lime.

Table 17- Water demand proportion per unit of binder components

Binder	Hydrated lime	Metakaolin	Pumice	Silica fume	Slag	Portland Cement
Water demand	0.75	0.90	0.575	0.75	0.40	0.40

Although the water demand values obtained in this experiment did not exactly match those from other studies, they followed a similar trend. Walker & Pavía (2011) also identified metakaolin as having the highest water demand (with a ratio of 1.1) and slag as having the lowest (with a ratio of 0.28), while silica fume was found to be intermediate with a value of 0.6. Similarly, Elzeadani *et al.* (2022) reported that slag has a water demand between 0.3 and 0.4. Variations in water demand values can be attributed to differences

in the production processes and inherent physical properties of the materials, as well as the environmental conditions in which the binders were stored.

A direct relationship was observed between the binders' apparent density and their water demand. This finding corroborates previous studies, which reported the same finding (Walker, 2013). Low apparent densities typically reflect higher porosity, either within the particle structure or between particles, resulting in an increased capacity to absorb water. For example, Portland cement and slag, with their high apparent density, tended to exhibit low water demand, while metakaolin, hydrated lime, and silica fume, which had lower apparent densities, exhibited higher water demand.

4.1.1.3 Surface Area

Table 18 compares the surface area of the binder components. As observed, metakaolin exhibits the highest surface area, reflecting its fine particle size, whereas Portland cement shows the lowest. Some values, particularly for metakaolin and silica fume, fall outside the ranges reported in Table 3 to Table 6. This discrepancy can be attributed to differences in production processes and the degree of grinding. For example, the metakaolin used in the current study, manufactured by Advanced Cement Technologies Company, was water-washed and flash-calcined, while conventional production typically involves calcining in a multiple-hearth furnace or rotary kiln followed by post-grinding. Such variations in production methods may explain the differences in the measured surface areas.

Table 18- Specific surface area of the binder components

Binder	Hydrated lime	Metakaolin	Pumice	Silica fume	Slag	Portland Cement
Surface area (m^2/g)	1.47	2.6	0.7	0.51	1.12	0.39

The relationship between surface area and water demand for binder components has been discussed in previous literature (Walker & Pavía, 2011). Metakaolin, with the highest surface area, also exhibited the highest water demand, whereas Portland cement, with the lowest surface area, absorbed the least water amount. This direct relationship is consistent with the findings reported by Walker & Pavía (2011).

However, in both studies, some binders, such as slag and silica fume in the current study, fell slightly outside the expected range. As noted in Section 3.3.1.3, a margin of error is expected in the laser diffraction method, used to determine surface area in both studies.

4.1.1.4 Chemical Composition (XRF)

Table 19 indicates the chemical composition of the binder components used in this experiment, which generally aligns with the datasheets for each material. Hydrated lime primarily consists of approximately 73% CaO, with negligible amounts of SiO_2 and MgO. Regarding the SCMs, metakaolin is composed of about 55% SiO_2 and 40% Al_2O_3, with Fe_2O_3 and TiO_2 present at less than 2% each. Pumice is mainly constituted by 73% SiO_2 and 11% Al_2O_3, with minor amounts of CaO and Fe_2O_3 (approximately 1% each); additionally, 3% Na_2O and 5% K_2O act as extra activators, which distinguish its composition from that of other SCMs. Silica fume is predominantly SiO_2 at 93%, with Fe_2O_3 and CaO each contributing less than 1%. Slag contains roughly equal proportions of CaO (38%) and SiO_2 (37%), with MgO and Al_2O_3 accounting for 12% and 10%, respectively. Finally, Type 1 Portland Cement is characterized by 58% CaO and 21% SiO_2 as its primary components, with Al_2O_3, Fe_2O_3, and MgO present at approximately 5%, 4%, and 3%, respectively.

Table 19- Chemical composition of binder components

Chemical Compounds	Lime	Metakaolin	Pumice	Silica Fume	Slag	Portland Cement
CaO	72.80	0.19	0.89	0.70	37.83	58.15
SiO_2	1.46	54.55	73.38	93.07	36.80	20.58
Al_2O_3	0.25	40.47	11.32	0.06	10.20	4.77
Fe_2O_3	0.16	1.50	1.07	0.85	0.43	3.62
Na_2O	0.02	0.01	2.89	0.10	0.37	0.92
MgO	0.71	0.10	0.18	0.21	11.82	2.65
K_2O	0.09	0.21	4.68	0.40	0.49	0.80
TiO_2	0.04	1.73	0.03	0.01	1.44	0.30

According to Walker (2013), the overall active content of SiO_2 and Al_2O_3 is critical for binders because these components, in the presence of alkaline activators such as Ca^{2+}, K^+, and Na^+, participate in hydration and the formation of C(-A)-S-H gel. As shown in Figure 22, metakaolin, silica fume, and pumice contain the highest total amounts of SiO_2 and Al_2O_3, approximately 95%, 93%, and 85%, respectively, followed by slag and Portland cement at 47% and 25%, respectively, with hydrated lime exhibiting less than 2%. Furthermore, the active contents of CaO, Na_2O, and K_2O can serve as alkaline activators for SiO_2 and Al_2O_3 within the binder composition. Given the absence of Na_2O and K_2O in most binders, except in pumice, the CaO content becomes particularly significant. The substantial amount of CaO in hydrated lime (as shown in Figure 22) is one of the primary reasons for its extensive use in binder mixes.

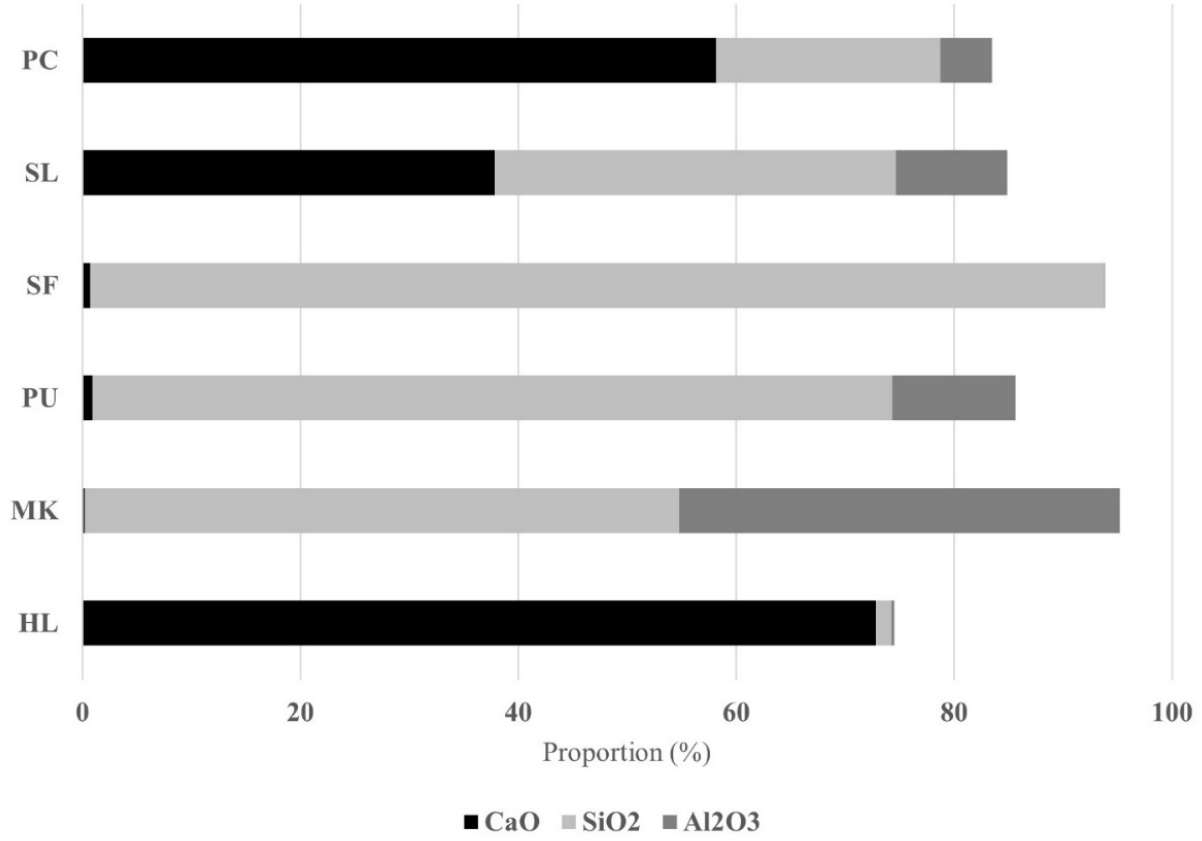

HL: hydrated lime, MK: metakaolin, PU: pumice, SF: silica fume, SL: slag, PC: Portland Cement

Figure 22- Main chemical composition of binder components

4.1.2 Hemp Hurd

4.1.2.1 Density

Table 20 presents the true density of hemp hurd particles, which were finely powdered to obtain more accurate results with a pycnometer. Figure 23 also provides a visual comparison of the true density values reported in previous literature and those obtained in the current study. The density values range from 1100 to 1550 kg/m³, with the current study reporting values above the average. This higher true density may be attributed to factors such as hemp species, environmental conditions during cultivation, and processing techniques. Additionally, the range of variation observed in this study is among the lowest reported, which may result from differences in measurement methods and the precision of the apparatus used.

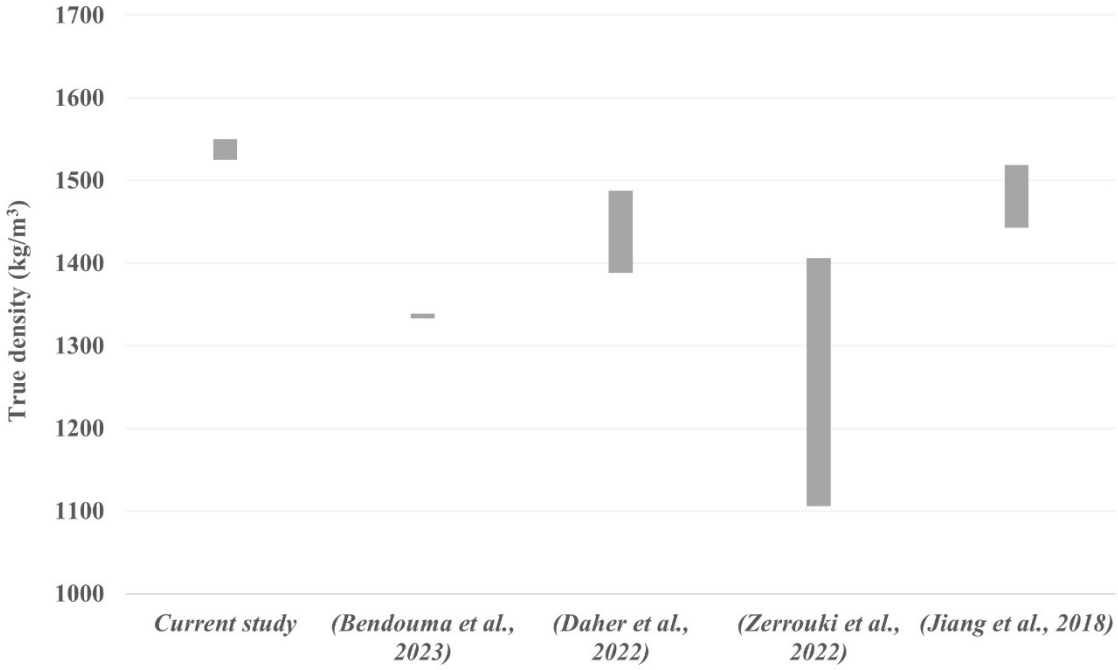

Figure 23- Comparison of true densities between this study and previous literature

The average apparent densities of both finely ground and as-received hemp hurd particles are summarized in Table 20 as well. Specifically, the apparent density of the finely ground particles was 120 kg/m³, which was higher than the as-received hemp hurd density of 87 kg/m³. This increase is likely due to the finer

particles filling voids more efficiently, resulting in a denser packing arrangement. In contrast, the larger and more elongated as-received hemp hurd particles tend to create significant voids when layered, thereby reducing the overall apparent density. Variations in particle orientation can lead to notable differences in the amount of void space, which in turn affects the apparent density. Similar observations have been reported in previous studies (Mahmood *et al.*, 2024; Niyigena *et al.*, 2018).

Table 20- Apparent and true densities of hemp hurd particles

As-received particles' apparent density (kg/m^3)	87
Fine particles' apparent density (kg/m^3)	120
Hemp hurd particles' true density (kg/m^3)	1535 ± 0.02%

Twelve different apparent density values, ranging from 50 to 160 kg/m³, are reported in the literature (see Table 1). The apparent densities measured in this study fell within the range reported by previous investigations. Factors such as composition, particle orientation, particle size, and moisture content all influence the magnitude of the apparent density (Khan, 2020). Additionally, the intensity of compaction plays a major role in determining the apparent density of hemp hurd particles.

4.1.2.2 Fibre Content and Particle Size Distribution

The results of the hemp hurd particle size distribution for both as-received and finely ground particles are summarized in Table 21. As explained in 3.3.1.3, for determining hemp hurd particle size distribution, the sieving method was avoided in this study due to the high margin of error, as reported in previous studies (Walker, 2013). As shown, the finely ground hemp hurd particles ranged from 0.1 to 2.5 mm in length, with an average of 0.85 mm, approximately ten times smaller than the as-received particle length, which ranged from 1 to 27 mm with an average of 7.47 mm. In addition, the width of the finely ground particles varied between 0.01 and 0.9 mm, with an average of 0.18 mm, whereas the as-received hemp hurd widths ranged from 0.2 to 6.8 mm, averaging 1.6 mm. Figure 24 provides visual representations of hemp hurd in both states.

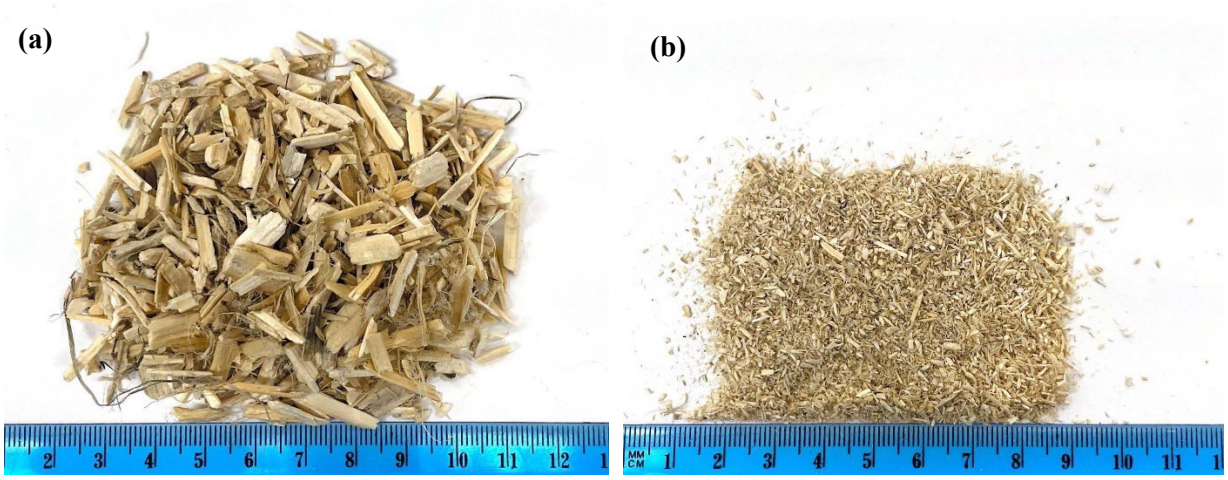

Figure 24- a) As-received hemp hurd particles, b) Finely ground hemp hurd particles

Table 21- Hemp hurd fibre content and particle size based on image analysis

	Minimum	Maximum	Average
As-received hemp hurd length	1 mm	27 mm	7.47 mm
Finely ground hemp hurd length	0.1 mm	2.5 mm	0.85 mm
As-received hemp hurd width	0.2 mm	6.8 mm	1.6 mm
Finely ground hemp hurd width	0.01 mm	0.9 mm	0.18 mm

Since most previous studies utilize the as-received particle size, the as-received range in this experiment is compared with values reported in Figure 25. This comparison reveals that the particle size range used in this study (1 to 27 mm) is consistent with those found in earlier research.

In this study, hemp is used with the existing fibres to mimic its industrial-scale application. This approach contrasts with some experiments where fibres and dust are removed from the hurd, and the material is washed and aired out before being incorporated into a mixture (Néron, 2019; Stanwix & Sparrow, 2014). Although the hemp hurds in this study were processed for defibration prior to shipment, approximately 5% of hemp fibres remained. This fibre content is lower than the values reported by Mahmood *et al.* (2024) and Nozahic *et al.* (2012), which were 9% and 20%, respectively. Several studies have investigated the influence of fibre content on the properties of hempcrete. While some have found that the presence of fibres

has little impact on hemp hurd characteristics (de Bruijn *et al.*, 2009), others report that fibres can be influential, specifically in increasing density and improving mechanical properties, although at the cost of longer drying times (Jahami *et al.*, 2024; Magwood, 2016).

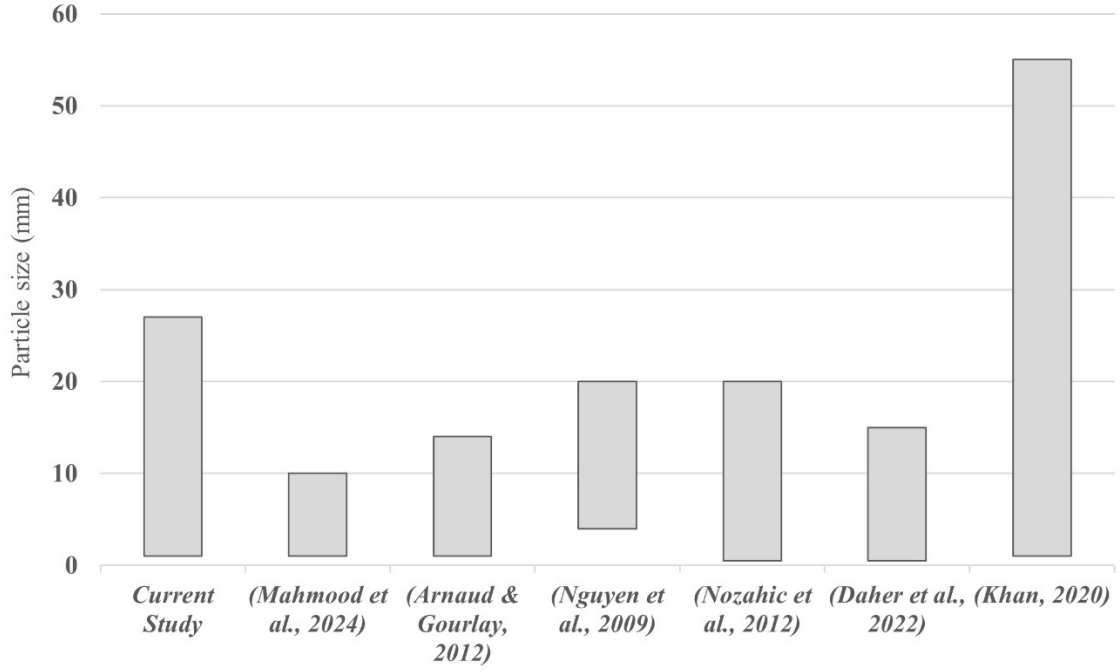

Figure 25- Hemp hurd as-received particle size comparison with other studies

4.1.2.3 Water Content, Demand, and Absorption Capacity

Table 22 lists the water content, water absorption capacity (both initial and after 72 hours), and minimum water demand of hemp hurd for both fine and as-received particles. The moisture content, ranging between 7.2% and 13.3%, is consistent with values reported in the literature (see Table 1), indicating that the storage conditions for the hemp hurd in this study were comparable to those in previous research.

Furthermore, the water absorption capacity reported in various studies ranges from 200% to 406% (Table 1). Although the 72-hour water absorption value observed in this study appears to exceed the literature range, this can be attributed to the shorter observation period (24- 48 hours) in the referenced studies. The initial water absorption results agree with other studies as well (Mahmood *et al.*, 2024). Notably, the initial

water absorption is higher in the finely ground particles, while the as-received particles gradually absorb more water over 72 hours. The higher surface area of the finely ground particles allows for a larger initial water uptake; however, over time, the porous structure of the larger as-received particles results in a higher overall water absorption capacity. In contrast, the grinding process reduces the internal porosity of the particles, limiting their water absorption after the initial uptake.

Table 22- Hemp hurd water content, water absorption capacity and water demand

Hemp Hurd Property	Finely-ground particles	As-received particles
Water content	9%	11%
Water absorption capacity (initial)	145%	112%
Water absorption capacity (72 hours)	433%	486%
Minimum water demand	300%	220%

Finally, the water demand for finely ground particles is three times their weight, whereas the as-received hemp hurd requires a minimum of 2.2 times its weight. This trend is consistent with the initial water absorption behaviour. The higher surface area of the finely ground particles leads to a greater volume of water being absorbed at the outset, thereby requiring a higher minimum water demand. Both water demand values for fine and as-received particles fall within the ranges reported in previous studies (Abdellatef *et al.*, 2020; Mahmood *et al.*, 2024; Walker, 2013).

4.2 Properties

4.2.1 Density

4.2.1.1 Binder Paste Cubes

Table 23 presents the average dry density and coefficient of variation for the binder paste cube samples, calculated from twelve samples for each mix design. Notably, the two samples without hydrated lime, BP-PC-MR3 and BP-SL-MR1.1, which consist of 100% Portland cement and slag, respectively, exhibit the highest densities of 1798 and 1564 kg/m³. In contrast, the specimen containing the highest ratio of silica

fume shows the lowest density at 966 kg/m³. Silica fume appears to be the only SCM whose addition reduces the binder's density compared to hydrated lime.

Table 23- Binder paste cube densities and coefficient of variations

No.	Sample ID	SCM	Lime-to-SCM	Dry Density (kg/m3)	Coefficient of variation
1	BP-MK-30	Metakaolin	70/30	1008	0.77
2	BP-PU-30	Pumice	70/30	1067	0.50
3	BP-SF-30	Silica Fume	70/30	983	1.30
4	BP-SL-30	Slag	70/30	1160	0.87
5	BP-PC-30	Portland Cement	70/30	1146	1.24
6	BP-MK-MR3	Metakaolin	69/31	1001	0.84
7	BP-PU-MR3	Pumice	75/25	1096	1.14
8	BP-SF-MR3	Silica Fume	79/21	996	0.90
9	BP-SL-MR3	Slag	49/51	1244	0.58
10	BP-PC-MR3	Portland Cement	0/100	1798	0.39
11	BP-MK-MR0.8	Metakaolin	36/64	992	0.45
12	BP-PU-MR0.8	Pumice	43/57	1114	1.07
13	BP-SF-MR0.8	Silica Fume	49/51	966	1.22
14	BP-SL-MR1.1	Slag	0/100	1564	0.85
15	BP-LIME	_	100/0	984	1.61

Table 24 compares the densities of 70/30 specimens with equal amounts of SCMs. Here, the sample with silica fume is the lightest, with a significant difference compared to metakaolin, while mixtures containing Portland cement and slag are the heaviest. These results are consistent with the true densities of the binder components (refer to Figure 21), with Portland cement and slag having the highest and silica fume having the lowest true densities. Interestingly, metakaolin, despite its relatively high true density, appears as the second lightest sample. This outcome may be due to the interaction between metakaolin, hydrated lime, and water, which leads to a more porous material, likely a result of the particle shapes and orientations creating numerous voids. Moreover, while both slag and Portland cement are heavy SCMs, the mixture

with slag was the heaviest when combined with 70% hydrated lime, even though Portland cement has the highest true density. However, as shown in Table 24, the difference between them is not considerable.

Table 24- Statistical analysis of samples with hydrated lime to SCM of 70/30

Comparison between samples	T-score	P-value
BP-SF-30 VS BP-MK-30	-5.00	< 5%
BP-MK-30 VS BP-PU-30	-17.41	< 5%
BP-PU-30 VS BP-SL-30	-14.98	< 5%
BP-PC-30 VS BP-SL-30	-2.37	< 5%

Binder pastes' density varies with mix design and chemical composition. Daher *et al.* (2022) reported a density of 840 kg/m³ for a binder paste consisting solely of hydrated lime and 872 kg/m³ when 20% of the hydrated lime was replaced with metakaolin. In contrast, Nozahic *et al.* (2012) calculated a binder paste density of 1310 kg/m³ for a mixture of pumice and hydrated lime. The coefficient of variation in the present study is considerably lower than those reported in previous literature (Daher *et al.*, 2022).

4.2.1.2 Hempcrete

As shown in Table 25, the density range is relatively narrow, spanning from 186.9 to 195.5 kg/m^3. These values were computed as the average density of twelve oven-dried hempcrete samples, including those used for mechanical and thermal property tests. The density range in this study is lower than most values reported in previous research, which typically fall between 300 and 800 kg/m³ (Al-Tamimi *et al.*, 2024; de Bruijn *et al.*, 2009; Elfordy *et al.*, 2008; Nguyen *et al.*, 2010). The low density in this study is affected by the minimal compaction applied during sample preparation. However, the significant increase in the hemp-to-binder ratio of 1:1 by weight (equivalent to 4:1 by volume) is the primary factor contributing to the lower density compared to most previous studies.

In addition, the very low coefficient of variation, ranging from 0.39% to 1.93% (as reported in Table 25), indicates the precision of the density measurements. The importance of maintaining a low-density variation

for achieving reliable comparisons has been emphasized in the literature (Abdellatef *et al.*, 2020; Al-Tamimi *et al.*, 2024). However, achieving uniform density is challenging due to factors such as binder ratio, binder type, compaction level, and particle size. If the binder content varies with its true density, the compaction must be adjusted to achieve similar densities. This is important, especially when binder true densities differ significantly, such as between Portland cement and silica fume.

Table 25- Hempcrete densities and coefficient of variations

No.	Sample ID	SCM	Lime-to-SCM	Dry Density (kg/m^3)	CoV
1	CHC-MK-30	Metakaolin	70/30	188.9	1.06
2	HC-MK-30	Metakaolin	70/30	190.0	1.36
3	HC-PU-30	Pumice	70/30	191.3	1.93
4	HC-SF-30	Silica Fume	70/30	189.4	1.78
5	HC-SL-30	Slag	70/30	193.4	1.04
6	HC-PC-30	Portland Cement	70/30	193.5	0.78
7	HC-MK-MR3	Metakaolin	69/31	193.1	1.04
8	HC-PU-MR3	Pumice	75/25	192.7	1.11
9	HC-SF-MR3	Silica Fume	79/21	190.7	1.05
10	HC-SL-MR3	Slag	49/51	187.8	1.61
11	HC-PC-MR3	Portland Cement	0/100	195.5	0.39
12	HC-MK-MR0.8	Metakaolin	36/64	192.6	1.59
13	HC-PU-MR0.8	Pumice	43/57	188.6	1.05
14	HC-SF-MR0.8	Silica Fume	49/51	186.9	0.83
15	HC-SL-MR1.1	Slag	0/100	194.0	1.39
16	HC-Lime	_	100/0	194.8	1.15

CoV= Coefficient of Variations

As highlighted in several studies, density is a primary factor impacting hempcrete properties (Abdellatef *et al.*, 2020; Dhakal *et al.*, 2017; Elfordy *et al.*, 2008; Walker & Pavía, 2015). Consequently, a wide range of densities in samples can significantly affect hempcrete properties. In this study, the narrow density range and low coefficient of variation confirm that density has minimal influence on the results. This allows for

a clearer focus on other key factors, such as the binder type and hemp hurd particle characteristics, when evaluating the hempcrete samples.

4.2.2 Chemical Composition

The resulting chemical composition of the three main binder components (CaO, SiO_2, and Al_2O_3) is demonstrated in Figure 26. In the samples with percentage-based binders, the amount of CaO appears relatively equal, but the ratio of CaO to SiO_2 varies. Since CaO is the main alkaline activator in the binders, the degree of hydration differs among them. Although CaO and SiO_2 are the key components in each binder, variation in Al_2O_3 content can also affect binder properties. A high ratio of Al_2O_3, especially in metakaolin binders, can contribute to the formation of C-A-S-H gel and result in improved mechanical properties compared to other binders.

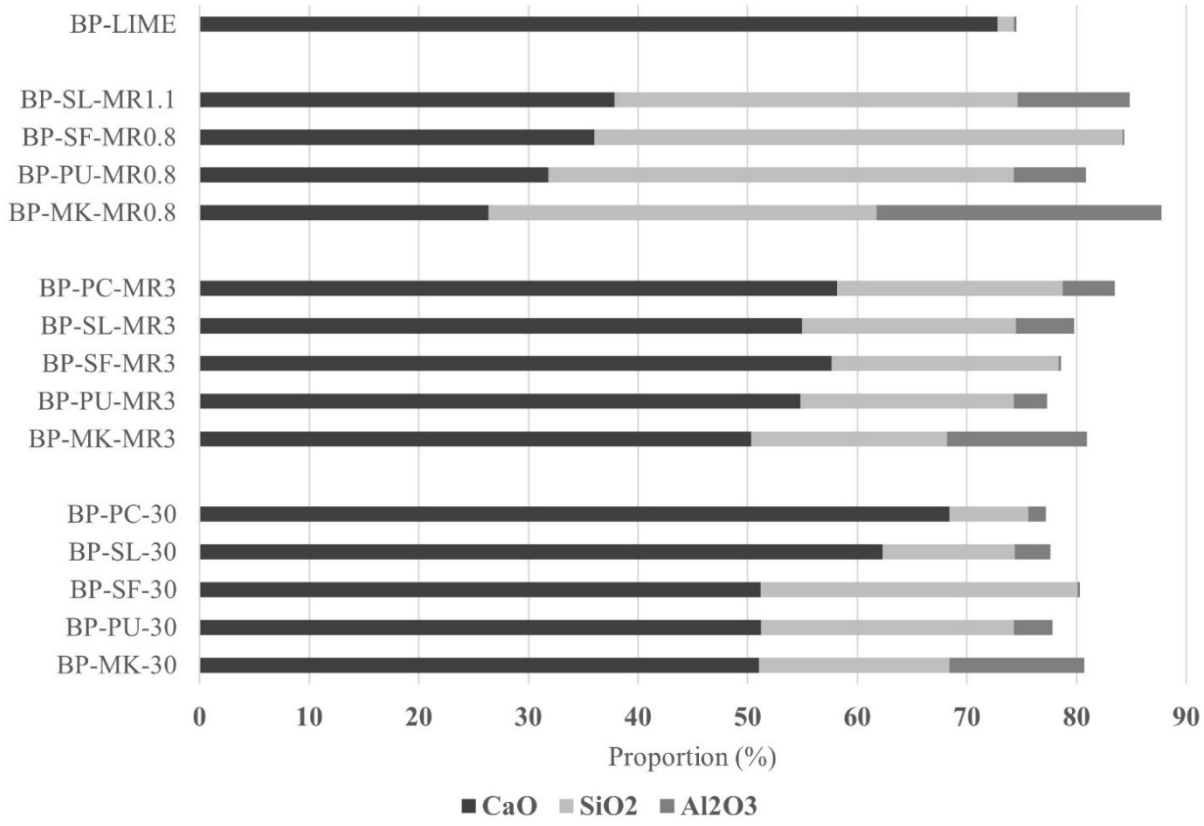

Figure 26- The main chemical composition of binder paste samples

In the molar ratio-based binders, the proportions of CaO and SiO_2 are fixed. However, the Al_2O_3 content still varies between binders. The amount of CaO in binders with a molar ratio of 3.0 is noticeably higher than in those with a molar ratio of 0.8. This difference may lead to a shortage of alkaline activators in binders with a lower molar ratio, resulting in reduced gel production and leaving the clays unused.

Apart from the primary chemical components, other elements in the binder can significantly influence its properties. For example, the high MgO content in slag binders (refer to Table 19) is noteworthy. MgO can contribute to delayed expansion and subsequent cracking in the binder paste over time. Therefore, a higher proportion of slag in the mix, which increases the MgO ratio, is associated with a greater occurrence of cracks in the binder paste samples.

4.2.3 Compressive Strength

The maximum compressive strength and corresponding coefficient of variation of the hempcrete mix designs with various binders are summarized in Table 26. These values are averages based on six specimens per mix design. Finely ground hemp hurd (specifications in Table 20 and Table 21) was used with a 1:1 binder-to-hemp ratio by weight and a target density of 190 kg/m³. The compressive strength values fall in the range of approximately 0.01 to 0.1 MPa. The coefficient of variation for compressive strength, ranging from 1.33% to 11.59%, is lower than the 4.2% to 41% reported in other studies (de Bruijn *et al.*, 2009; Mahmood *et al.*, 2024; Walker, 2013). This relatively lower variation is mainly due to the consistent density across all samples and the uniform distribution of finely ground hemp hurd particles.

Table 26 also presents the modulus of elasticity and its coefficient of variation, with values ranging from 0.31 to 4.91 MPa and coefficients of variation between 4.16% and 22.55%. These results indicate a relatively lower variation in Modulus of elasticity compared to the wider range reported in previous studies (de Bruijn *et al.*, 2009; Elfordy *et al.*, 2008), which can be attributed to the stability of the density (Mahmood *et al.*, 2024). However, the uniform hemp hurd particle size distribution resulted in a relatively even porosity arrangement throughout the samples, which can contribute to achieving more consistent values as well.

Table 26- Average values for hempcrete's compressive strength and modulus of elasticity with finely ground hemp hurd, target density of 190 kg/m^3, and 1:1 hemp-to-binder ratio by weight.

No.	Sample ID	σ (MPa)	CoV (%)	E (MPa)	CoV (%)
1	HC-MK-30	0.097	4.24	4.85	6.72
2	HC-PU-30	0.075	2.21	3.95	17.84
3	HC-SF-30	0.062	8.27	3.32	16.97
4	HC-SL-30	0.062	11.59	3.49	14.14
5	HC-PC-30	0.048	8.99	3.10	17.66
6	HC-MK-MR3	0.098	6.25	4.91	14.83
7	HC-PU-MR3	0.079	2.68	4.08	4.16
8	HC-SF-MR3	0.068	5.17	3.74	9.99
9	HC-SL-MR3	0.057	5.94	2.69	22.55
10	HC-PC-MR3	0.069	2.91	3.26	13.69
11	HC-MK-MR0.8	0.024	6.70	0.98	15.22
12	HC-PU-MR0.8	0.036	4.21	1.45	4.38
13	HC-SF-MR0.8	0.050	1.33	2.08	5.72
14	HC-SL-MR1.1	0.010	8.37	0.31	13.04
15	HC-Lime	0.048	5.00	2.23	18.20

σ=Ultimate compressive strength, CoV=Coefficient of variation, E=Modulus of elasticity

The elastic range of hempcrete varies significantly across studies (Walker, 2013). Unlike concrete, the binder is the most critical factor influencing the hempcrete modulus of elasticity (Nguyen *et al.*, 2009). Consequently, the binder-to-hemp hurd ratio plays the most important role in determining the modulus of elasticity. Figure 27 provides an insight into the comparison of the modulus of elasticity from different studies. Accordingly, a similar binder-to-hemp ratio of 1:1 by weight in Abdellatef *et al.* (2020), Mahmood *et al.* (2024), and the current study results in a marginal stiffness difference. On the other hand, the binder-to-hemp ratio of 5:1 to 3:1 in de Bruijn *et al.* (2009) and 2:1 in Elfordy *et al.* (2008) led to considerably different modulus of elasticity values compared to this study.

The low target density, due to the low binder-to-hemp ratio and low compaction, makes the compressive strength results lower than most previous studies, which report values between 0.10 and 0.85 MPa for densities ranging from 290 to 730 kg/m³ (Abdellatef *et al.*, 2020; de Bruijn *et al.*, 2009; Elfordy *et al.*, 2008; Sinka *et al.*, 2014; Walker, 2013). Additionally, when comparing these results with previous experiments, the differences in particle size should also be taken into consideration. Finer hemp hurd particles tend to result in lower mechanical properties (Arnaud & Gourlay, 2012). Accordingly, comparison of the results obtained in this study with those from previous research is not justifiable. Nonetheless, the findings meet expectations based on target density (Shea *et al.*, 2012) and are in line with hempcrete studies, with comparable densities and particle sizes. As an example, Mahmood *et al.* (2024) reported a mean compressive strength of 0.07 MPa and a modulus of elasticity of 3.27 MPa for hempcrete samples with a density of 200 kg/m³ and a similar hemp hurd particle size as used in the current study.

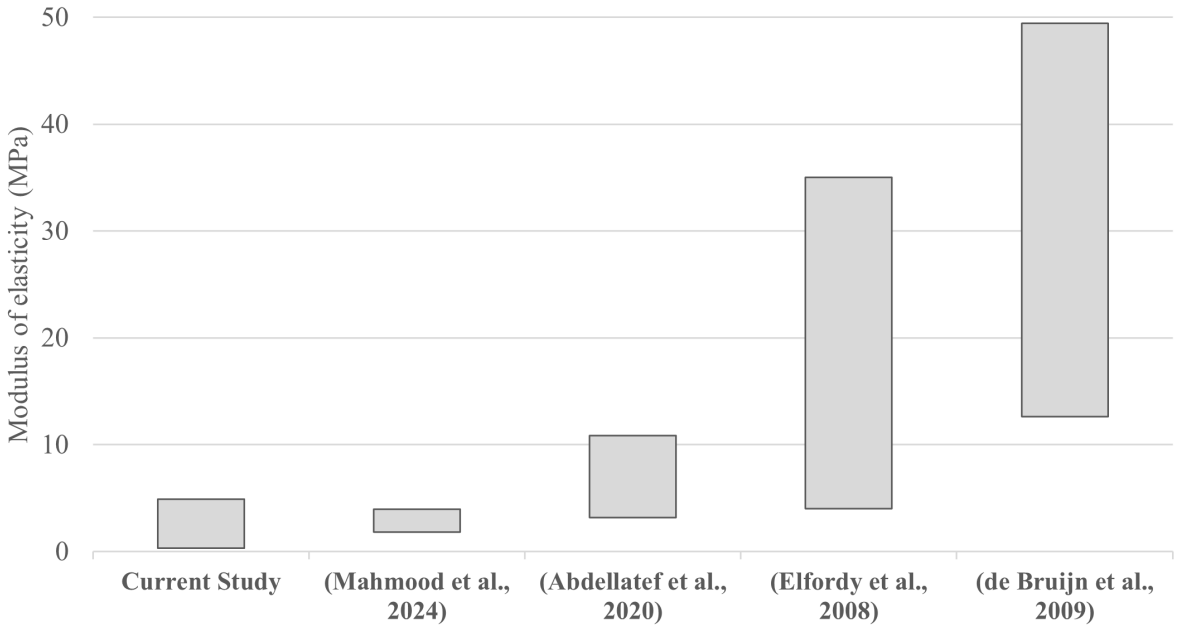

Figure 27- The modulus of elasticity comparison between studies

Furthermore, despite the low density achieved in the current study, the results fully satisfy the strength requirements for hempcrete as a building element capable of supporting its own weight, given its non-load-

bearing nature. To illustrate, the maximum compressive load applied per unit of plan area at the base of a 3-metre wall constructed with the target density hempcrete produced in this study is approximately 5.6 kPa (0.006 MPa). Therefore, even the lowest compressive strength values obtained in the current experiment are sufficient for the material's application in building assemblies.

4.2.3.1 Hemp Hurd Effect

4.2.3.1.1 Effect of Hemp Hurd Addition on Binder Pastes

Table 27 represents the compressive strength results of binder paste cubes along with their corresponding coefficients of variation. The results are based on the average of compression tests performed on six samples from the same batch. The compressive strength ranged from 0.86 MPa for the pumice-lime binder with a molar ratio of 0.8 (BP-PU-MR0.8) to 43.24 MPa for the 100% Portland cement binder paste with a molar ratio of 3 (BP-PC-MR3). The coefficient of variation ranged from 3.75% to 20.86%, with an average of 10.27%, which is consistent with values reported in previous studies (Daher *et al.*, 2022; Walker, 2013).

Comparing the compressive strength of binder pastes with that of hempcrete samples, the strength in hempcrete is significantly lower. Two main reasons have been identified in previous research. From one point of view, due to the large volume of hemp hurd in the mixture, the mechanical properties of hempcrete are predominantly influenced by the hemp hurd, which exhibits very low compressive strength relative to the binder (Murphy *et al.*, 2010). On the other hand, the soluble components of hemp have been found to retarding the binder hydration and considerably impact the mechanical properties of the specimens (Tale Ponga *et al.*, 2023; Walker, 2013; L. Wang *et al.*, 2021).

Based on the distinct trends in the mechanical properties of hempcrete samples compared to binder paste cubes, selecting binder pastes solely on the basis of the highest performance for use in hempcrete, as performed in a previous study (Walker, 2013), is unlikely to be a practical approach. The hempcrete and binder paste samples exhibited different behaviours under compression. The stress–strain curve for the binder paste samples began with a linear elastic deformation phase. As microcracks initiated, the curve

deviated from linearity at varying strain levels, depending on the binder composition, before reaching the ultimate stress. The maximum load for binder paste samples typically reached approximately 2- 3% of the total sample length, consistent with displacement values reported in previous studies (Daher *et al.*, 2022).

Table 27- Compressive strength and modulus of elasticity of binder paste cubes

No.	Sample ID	σ (MPa)	CoV (%)	E (MPa)	CoV (%)
1	BP-MK-30	1.93	9.39	218.7	33.05
2	BP-PU-30	1.73	8.26	163.3	13.58
3	BP-SF-30	3.23	4.20	111.7	20.75
4	BP-SL-30	6.81	15.72	538.3	9.81
5	BP-PC-30	5.34	12.28	816.5	8.67
6	BP-MK-MR3	1.96	14.28	195.9	46.60
7	BP-PU-MR3	2.29	10.22	229.8	13.84
8	BP-SF-MR3	1.46	10.59	133.6	36.14
9	BP-SL-MR3	8.21	5.60	453.5	40.48
10	BP-PC-MR3	43.24	9.48	-	-
11	BP-MK-MR0.8	0.94	3.75	90.7	12.82
12	BP-PU-MR0.8	0.86	6.28	89.1	18.21
13	BP-SF-MR0.8	0.92	20.86	71.0	21.37
14	BP-SL-MR1.1	0.89	11.28	268.2	30.09
15	BP-LIME	1.29	11.85	87.3	33.63

σ=Ultimate compressive strength, CoV=Coefficient of variation, E=Modulus of elasticity

Finely ground hemp hurd hempcrete specimens exhibited an initial linear deformation phase up to approximately 50% strain, during which the binder component bore the load. Beyond this phase, the curve showed significant deformation under nearly constant stress, primarily due to the contribution of hemp hurd particles after binder failure (Brzyski *et al.*, 2020). Upon reaching the ultimate stress, the sample lost its capacity to resist the applied load, leading to a marked increase in deformation. Consequently, the maximum load for hempcrete samples was observed at an average strain of approximately 5% of the total

sample length. Overall, hempcrete samples promoted greater plastic deformation, whereas the binder paste cubes demonstrated a more brittle behaviour (Murphy *et al.*, 2010).

The addition of SCMs to hydrated lime, either at a 30/70 ratio or according to a CaO/SiO_2 molar ratio of 3, increased the compressive strength of the binder paste samples (refer to Table 29- 1st row). This finding agrees with previous studies reporting that incorporating SCMs into hydrated lime enhances compressive strength due to the formation of additional hydration products (Daher *et al.*, 2022; Walker, 2013). However, binder pastes with a CaO/SiO_2 molar ratio of 0.8 sustained a significantly lower compressive load compared to the hydrated lime reference (Table 29- 2nd row). The reason can be attributed to the reduced calcium content in binders with a CaO/SiO_2 molar ratio of 0.8, which results in an insufficient amount of calcium acting as the alkaline activator to react with available clays. Consequently, a portion of the silica and alumina remains unreacted, leading to compromised structural integrity.

Regarding the SCM-to-lime binder pastes with a 30/70 proportion, pumice, metakaolin, and silica fume (pozzolans) exhibited lower compressive strength, whereas slag and Portland cement (hydraulic binders) achieved the highest strength. Pavía & Aly (2016) reported a sixfold improvement in the compressive strength of lime binder hempcrete when 30% of the binder was replaced with slag, similar to what was observed in this study. Compared with the hempcrete compressive strength results using the same binders (presented in Table 26), an opposite trend is identified. Binder pastes with metakaolin and pumice, which recorded the lowest compressive strength in the paste form, ranked highest in the hempcrete mixtures, while Portland cement exhibited the lowest compressive strength in the hempcrete 30/70 mix designs. It appears that the hemp hurd, acting as an active component, influences the reactions. The soluble components in hemp neutralize a substantial portion of the reaction by interfering with binder hydration (Tale Ponga *et al.*, 2023; Walker, 2013). Accordingly, the hemp hurd had the most pronounced effect on the hydration of hydraulic materials, with a relatively lower impact on pozzolanic materials. Furthermore, Walker (2013) stated that hemp hurd influences silica more than alumina hydration. Having a deeper investigation into hempcrete binders, the results of this study support the claimed theory. As an example, the hydration

interference in metakaolin and pumice with relatively high alumina content was less evident than silica fume with the highest portion of silica and a negligible portion of alumina.

In binder paste compositions with a CaO/SiO_2 molar ratio of 3, significant differences were observed among the binders (Table 28- 2nd row). Portland cement without the addition of lime (BP-PC-MR3), serving as the reference sample, exhibited the highest compressive strength among all binder pastes, with a statistically significant difference and a high T-score compared to slag at a molar ratio of 3 (Table 29- 3rd row). Nonetheless, the overall trend was similar to that observed in the 30/70 binders, with hydraulic binders achieving higher compressive strength than pozzolanic binders. Moreover, a reverse pattern was observed for MR3 binder pastes compared to the hempcrete samples, while Portland cement and slag produced the lowest compressive strength in hempcrete, metakaolin, pumice, and silica fume performed better. Similar to percentage-based samples, hemp hurd's soluble retardant characteristic affects the binders' hydraulicity (Tale Ponga *et al.*, 2023).

The variation in compressive strength for binder pastes with a molar ratio of 0.8 (and 1.1 for slag) was observed to be statistically insignificant compared to the lime binder with a p-value of 65% (Table 28- 3rd row). All compressive strength values in this group were lower than those of the reference hydrated lime (see Table 29- 2nd row). This category recorded the lowest strength for both binder pastes and hempcrete samples, indicating inferior mechanical properties relative to other groups. As noted earlier, the insufficient calcium content, serving as the alkaline activator, in binders with a molar ratio of 0.8, was the primary reason for the presence of unreacted clays.

Table 28- Statistical analysis of binder paste cubes compressive strength results- ANOVA

ANOVA	SS	df	MS	F	P-value	F crit
30/70 SCM/lime	117.17	4	29.29	88.82	2.12E-14	2.76
MR3 (MK, PU, SF)	2.10	2	1.05	20.07	5.75E-05	3.68
MR0.8 (+ SL-MR1.1)	0.02	3	0.01	0.56	0.65	3.10

Table 29-Statistical analysis of binder paste cubes' compressive strength results- T-test

Comparison between samples	T-score	P-value
BP-LIME VS BP-SF-MR3	1.90	0.04 (< 5%)
BP-MK-MR0.8 VS BP-LIME	5.43	0.0008 (< 5%)
BP-PC-MR3 VS BP-SL-MR3	20.79	2.38E-06 (<5%)

The modulus of elasticity and its corresponding coefficients of variation for the binder pastes are presented in Table 27 as well. The values ranged from 71 MPa for the silica fume-lime binder with a molar ratio of 0.8 to 816.5 MPa for the Portland cement-lime binder in the 30/70 proportion. Since the apparatus used for Portland cement binder with a molar ratio of 3 (100% PC) proceeded based on load per time, the modulus of elasticity could not be derived from the generated data. However, given its significantly higher compressive strength, the predicted modulus of elasticity for this binder is expected to be substantially higher as well.

As anticipated, the binder pastes exhibited considerably higher moduli of elasticity compared to their hempcrete counterparts, reflecting their notably greater stiffness. Both binder pastes and hempcrete samples showed the lowest stiffness in specimens with a molar ratio of 0.8. Interestingly, the 100% slag hempcrete with a molar ratio of 1.1, which demonstrated the lowest modulus of elasticity among hempcrete samples, still achieved a modulus of elasticity of 268.2 MPa, exceeding the average value for binder pastes. The differences between binder pastes and hempcrete samples followed a similar pattern to that observed in the compressive strength results. Specifically, the Portland cement and slag, which recorded the highest moduli of elasticity in binder pastes, corresponded to the lowest values in the hempcrete results. In contrast, metakaolin and pumice, characterized by low stiffness in the binder pastes, were associated with the highest modulus of elasticity in hempcrete samples. Since the modulus of elasticity trends closely followed the compressive strength data, the previously provided explanation regarding chemical composition and its effect on reaction products is also valid for interpreting modulus of elasticity behaviour.

The comparison of these results with other studies proved challenging due to the limited number of comparable experiments. Walker (2013) reported 28-day compressive strengths for binder pastes of 0.8 MPa for hydrated lime, 5.3 MPa for metakaolin-lime (30/70), and 5.4 MPa for slag-lime (30/70), with coefficients of variation ranging from approximately 10.6% to 13.1%. The corresponding compressive strengths and coefficients of variation for binder pastes in this study are presented in Table 30. Considering the differences in surface area reported in Walker's study, particularly for metakaolin, the observed differences in compressive strength are justifiable. To be specific, the metakaolin used in Walker's study, with a surface area of 18.33 m^2/g, is considerably more reactive than the equivalent material used here (2.6 m^2/g), using similar apparatus to determine the magnitudes. The differences in slag binder results between the two studies are insignificant when the coefficient of variation is taken into account. Regarding the lime binder, the author did not report the surface area. However, considering the differences in chemical composition between the employed hydrated limes in the two experiments, the observed variations are legitimate.

Table 30- The comparison of compressive strength results in binder pastes between the two studies

Experiment	Lime σ (MPa)	Lime CoV (%)	MK σ (MPa)	MK CoV (%)	SL σ (MPa)	SL CoV (%)
Current study	1.29	11.85	1.93	9.39	6.81	15.72
(Walker, 2013)	0.8	10.57	5.3	11.93	5.4	13.1

-σ= Compressive strength, CoV= Coefficient of variation, MK= Metakaolin, SL= Slag

In addition, Daher *et al.* (2022) investigated the effects of replacing a commercial binder comprising hydrated lime, hydraulic lime, pozzolan, and additives with 10% and 20% metakaolin in binder paste cylinders. The findings indicated that the inclusion of metakaolin enhanced the mechanical properties of the binder pastes, achieving coefficients of variation between 10% and 12%, and resulted in a modest improvement in the modulus of elasticity. A similar trend was observed for hempcrete samples prepared with comparable binder formulations. The findings of the current study are, therefore, in complete agreement with those reported in the referred experiment.

4.2.3.1.2 Effect of Hemp Hurd Particle Sizes on Hempcrete

The difference in particle size between as-received and finely ground hemp hurd in hempcrete contributes to variations in mechanical behaviour. To investigate this effect, two sets of specimens were prepared under identical procedures, curing conditions, mix design, and target density, with the only variable being the hemp hurd particle size. The average compressive strength and modulus of elasticity for six specimens in each group are summarized in Table 31. Additionally, the statistical analysis in Table 32 offers only a slight change in compressive strength but a significant difference in the modulus of elasticity values of samples.

Table 31- Sample specifications for mechanical properties investigation using different particle sizes

Sample ID	Hemp Particles	Density	σ (MPa)	E (MPa)
CHC-MK-30	As received	188.9	0.112	0.88
HC-MK-30	Finely ground	190.0	0.097	4.85

Table 32- Statistical analysis of mechanical properties results in hempcrete with as-received hemp hurd compared to the finely ground- T-test

Comparison between samples	T-score	P-value
HC-MK-30 VS CHC-MK-30 (Max compression)	-1.66	0.079 (> 5%)
HC-MK-30 VS CHC-MK-30 (Modulus of elasticity)	20.60	0.001 (< 5%)

The compressive strength test results indicated two distinct behaviours, as illustrated in Figure 28 and Figure 29, with challenging comparisons. The as-received hemp hurd hempcrete exhibited progressive ductile behaviour similar to previous observations (Brzyski *et al.*, 2020; Chabannes *et al.*, 2014; Walker, 2013). Initially, the tests showed a linear elastic response, followed by a plateau with considerable displacement accompanied by only a slight increase in load, and finally, a steep, continuous increase in load associated with the minimization of trapped air between particles. In the first stage, the compression load primarily affected the binder between the hemp particles, which demonstrated higher stiffness (Walker, 2013). Once the binder matrix failed, more ductile behaviour was observed as the stress was transferred to

the hemp particles, thereby allowing the load to continue (Murphy *et al.*, 2010). Visible cracks appeared before the plateau was reached, and the specimens experienced noticeable permanent deformation during the plateau stage. That is why the ultimate compressive strength for the as-received hemp hurd samples was defined at a deformation of 10% of the sample's total length in this study before the plateau was reached (see Figure 28). The final stage is characterized by significant damage to sample uniformity owing to the high deformation capacity of hemp hurd. While the intertwined hurd remained intact, not demonstrating any complete failure on the curve (Chabannes *et al.*, 2014), due to the aggregate interlock between the hemp particles. Notably, even at 65% sample length deformation, no major failure was observed on the graph (Figure 28).

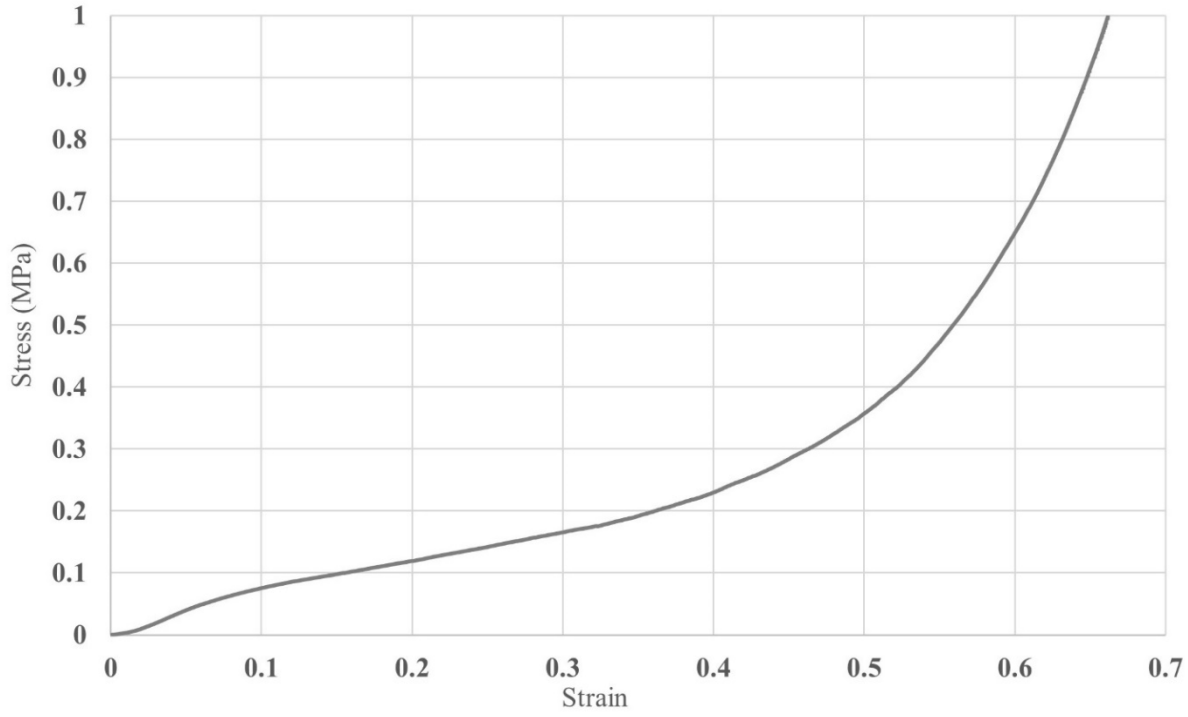

Figure 28- Stress-strain curve of the as-received hemp hurd sample

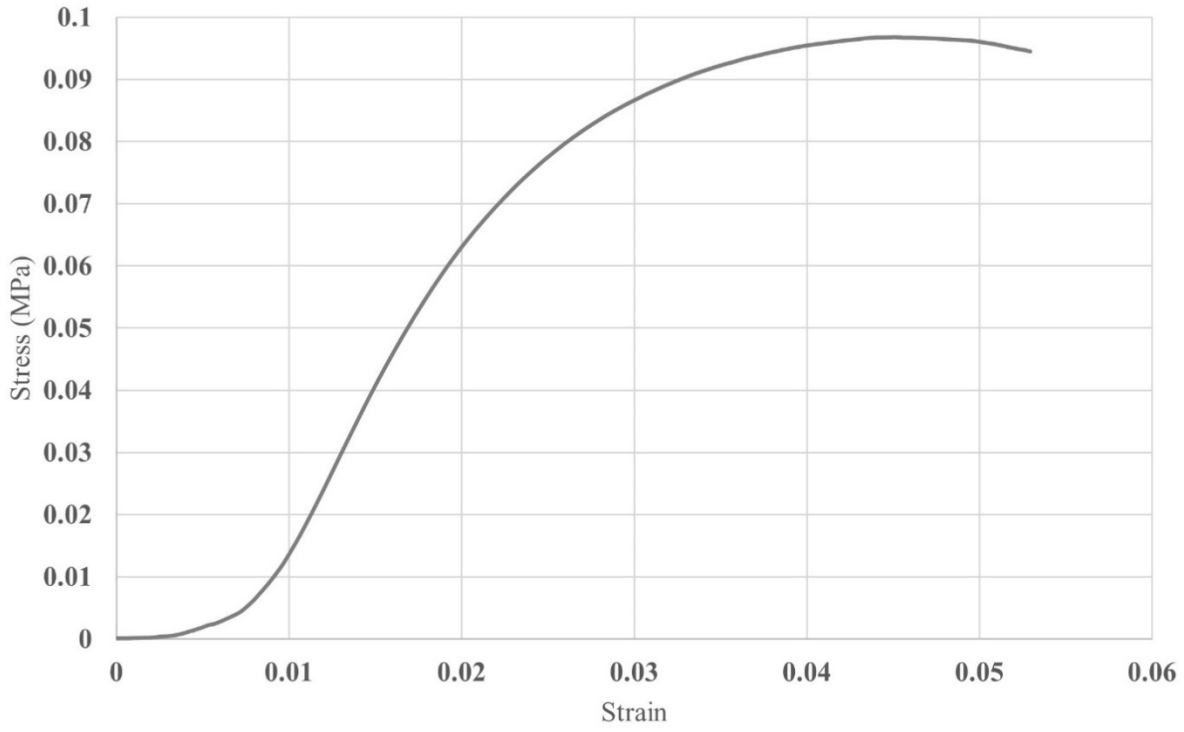

Figure 29- Stress-strain curve of the finely ground hemp hurd sample

In contrast, the compressive strength tests for specimens with ground hemp hurd began with an elastic response where the binder carried the load. However, once the binder failed, a marked increase in deformation was observed with minimal change in force until the ultimate stress was reached. The absence of an interlock between the smaller hemp particles led to early brittle failure. The interconnected pores throughout the samples caused the formation of full cracks, while no considerable deformation was observed. A declining force trend eventually accompanies this ultimate compressive load. Similar observations have been reported in previous studies (Mahmood *et al.*, 2024; Sinka *et al.*, 2014).

As shown in Figure 30(a), at the point of ultimate compressive strength, the finely ground hemp hurd sample exhibits a complete crack with minimal overall deformation (approximately 5% of the sample length). Since the compression test was not conducted under confinement, an indirect tensile force was also applied to the specimen. This lateral force prompted the sample to expand laterally rather than resist compression. Given

the low modulus of elasticity of the finely ground hemp hurd sample, this applied lateral force likely contributed to the complete cracking and premature failure of the specimen before additional compressive load could be sustained. Furthermore, the reduced particle size in finely ground hemp hurd hempcrete results in a higher specific surface area, which in turn leads to a lower degree of binder coverage and fewer bonds between the hemp particles (Arnaud & Gourlay, 2012).

In contrast, the as-received hemp hurd sample is capable of experiencing high deformation without reaching its ultimate compressive strength (Figure 30(b)). Owing to the inherent flexibility of hemp hurd, attributable to its porous nature, this behaviour is expected. The sample begins to disintegrate and experiences severe damage at approximately 16- 18% deformation of the total sample length, a finding that is consistent with previous studies (Brzyski *et al.*, 2020; Walker, 2013).

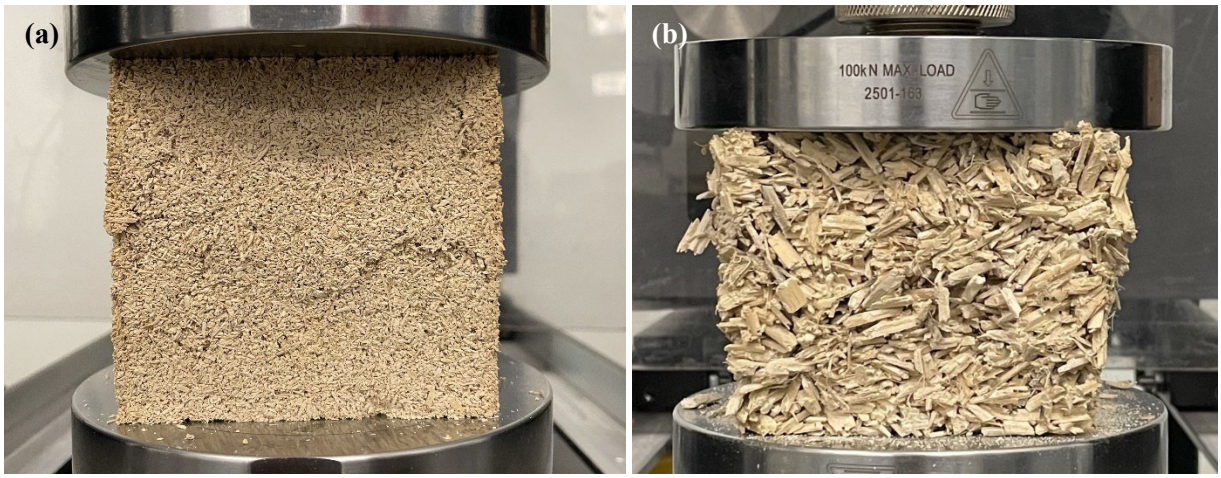

Figure 30- a) The crack in the finely ground hemp hurd hempcrete sample at failure during the compressive strength test, b) The significant deformation in the as-received hemp hurd hempcrete sample without major failure

The modulus of elasticity for both groups was calculated from the slope of the linear elastic region; however, the extent of this region differed between sample types. The average modulus of elasticity for as-received hemp hurd samples was 0.88 MPa, indicating a considerably lower value compared to the 4.85 MPa recorded for the finely ground samples. This finding corroborates earlier reports noting that the larger,

more ductile particles in hempcrete contribute to a more flexible behaviour compared to the brittle response of finely ground hemp hurd samples (Brzyski *et al.*, 2020).

Furthermore, the energy required to deform each group of samples was compared in this study as well. As illustrated in Figure 31, the as-received hemp hurd sample requires approximately 170 kJ of energy per unit of volume to achieve 65% deformation of its total length without complete failure, indicating that it did not reach its maximum capacity. By contrast, Figure 32 shows that only 3.35 kJ/m^3 is required to achieve maximum compression and complete failure in the finely ground hemp hurd sample. The ability of the as-received hemp hurd sample to absorb over 50 times more energy per unit volume before failure, compared to the finely ground sample, indicates its remarkably higher toughness.

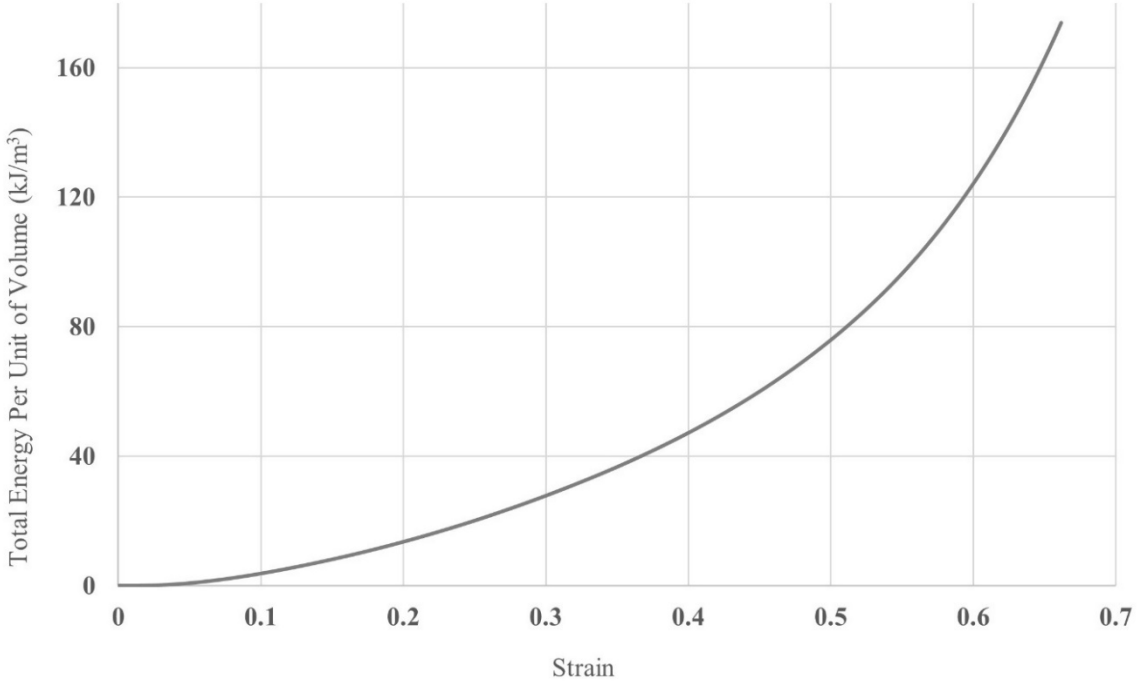

Figure 31- Total energy per unit of volume for the as-received hemp hurd sample as a function of strain

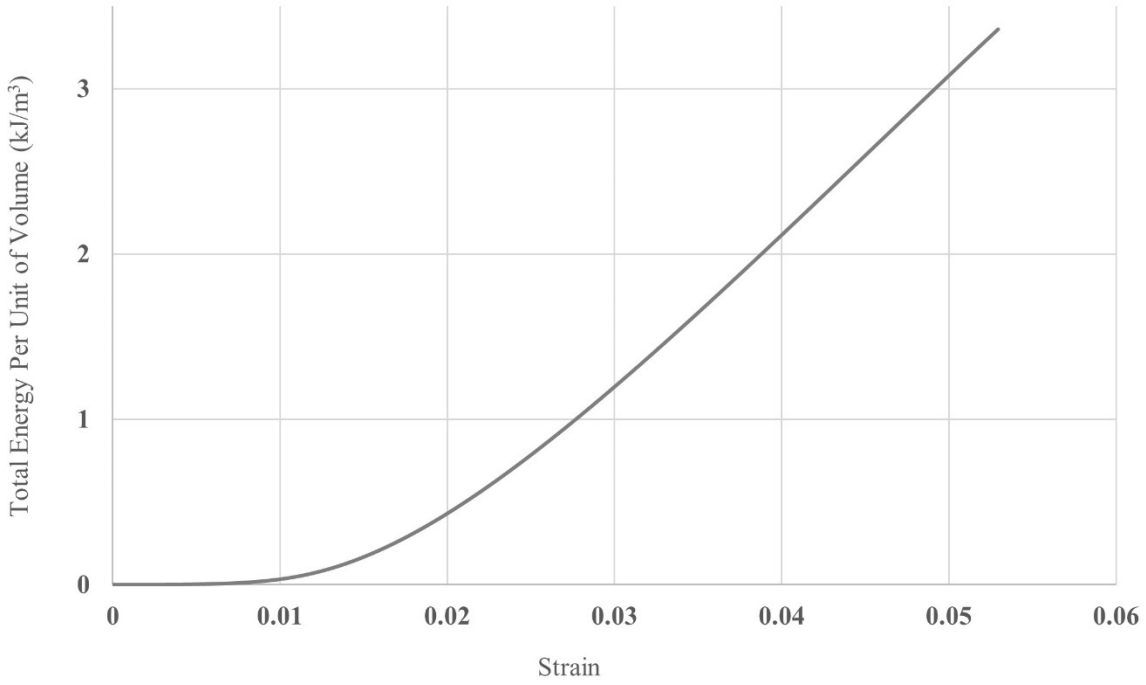

Figure 32- Total energy per unit of volume for the finely ground hemp hurd sample as a function of strain

A closer comparison of the energy required for deformation is provided in Figure 33. As can be perceived, the specimen containing as-received hemp particles required considerably less energy to deform under a given strain. To illustrate, approximately 3.1 kJ/m^3 is needed to produce a 5-mm deformation in a finely ground hemp hurd sample, whereas the as-received hemp hurd sample undergoes the same deformation with only 0.8 kJ/m^3 of energy. Moreover, given the same amount of energy of 2 kJ applied to a unit of volume, the as-received hemp hurd specimen deforms by approximately 7.4 mm, compared to only 3.9 mm for the finely ground sample, emphasizing the low stiffness of hempcrete made with as-received hemp hurd. Considering the as-received hempcrete's high toughness properties along with low stiffness, hempcrete incorporating as-received hemp hurd offers a sponge-like quality, which makes it a suitable candidate for applications in seismic areas.

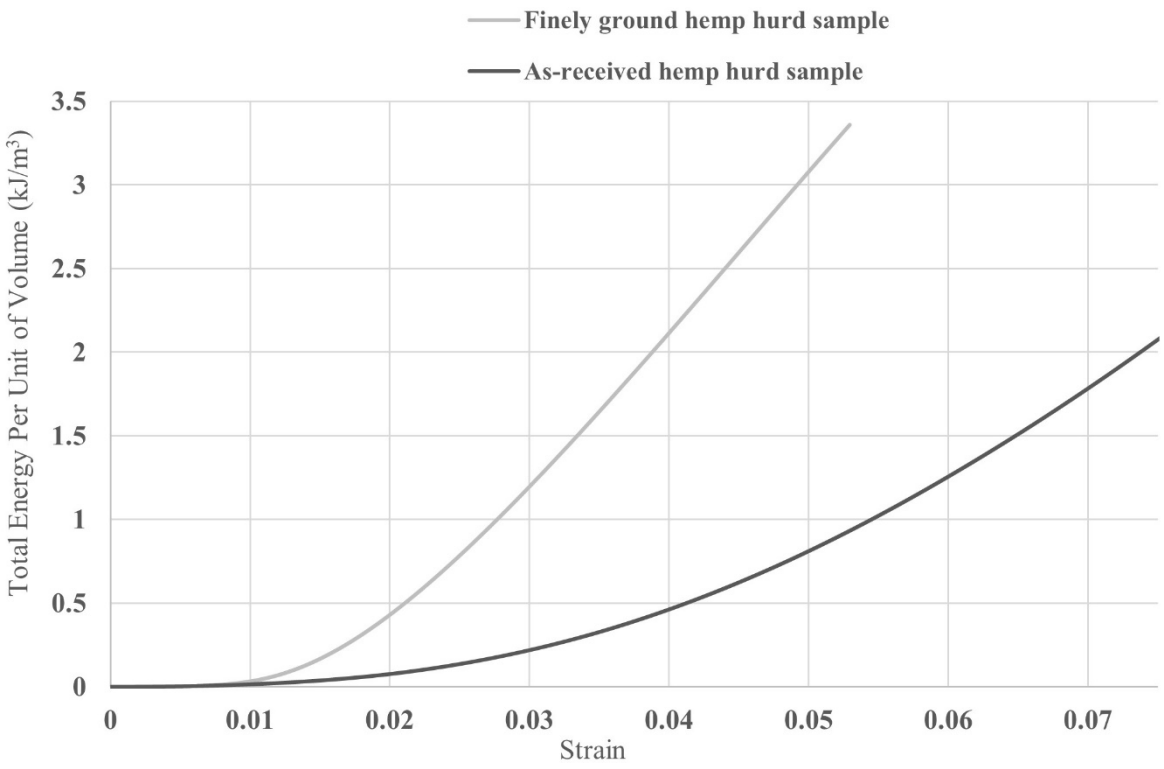

Figure 33- Energy per unit of volume comparison of samples based on strain

4.2.3.2 Binder's Effect

4.2.3.2.1 Comparison to Reference Sample

The addition of SCMs to hydrated lime has been reported to enhance the mechanical properties of hempcrete (Nguyen *et al.*, 2010). For example, replacing 20% of a commercial binder (including 75% hydrated lime) with metakaolin in hempcrete produced with a 1:3 binder-to-hemp by volume ratio increased the compressive strength from 0.29 to 0.42 MPa. However, because the density also increased from 420 to 445 kg/m³, it is difficult to isolate the influence of density from that of binder hydraulicity (Daher *et al.*, 2022). From a chemical composition standpoint, the hydraulicity and, consequently, the mechanical properties of hydrated lime, which is primarily composed of calcium, can be improved by incorporating clays rich in silica and alumina (Ra *et al.*, 2023; X. Wang *et al.*, 2024). Nevertheless, in hempcrete

formulations containing a higher ratio of hemp hurd, the differences in mechanical properties between hydrated lime and SCM-based binders are less pronounced (Murphy *et al.*, 2010).

Table 33 presents a statistical comparison between hempcrete produced with mix-designed binders and pure hydrated lime, thereby providing insights into the influence of SCMs in hempcrete binders. In hempcrete with a 30/70 SCM-to-hydrated lime ratio, the replacement of 30% lime with each SCM resulted in a notable increase in the clay content of the resulting binder, except in the case of Portland cement. The high silica content in Portland cement creates a binder composition that is very similar to that of hydrated lime (see Figure 26). That explains why the replacement of lime with Portland cement did not significantly affect the maximum compressive strength (p-value = 45%), even though the replacement of lime with all other SCMs in hempcrete led to considerable enhancement in compressive strength.

For hempcrete binders with a CaO/SiO_2 molar ratio of 3, all formulations exhibited significant improvements in compressive strength compared to the lime binder. The constant calcium-to-silica ratio produced a more consistent composition, although differences in alumina content resulted in varied compressive strength values. Furthermore, the HC-PC-MR3 binder, composed entirely of Portland cement, demonstrated higher compressive strength than the hydrated lime hempcrete. The absence of clay in the hydrated lime binder, in contrast to the balanced calcium-to-silica ratio of the Portland cement binder, likely accounts for the less desirable mechanical properties of lime-hempcrete.

Conversely, achieving hempcrete binders with a molar ratio of 0.8 led to a significant decline in compressive strength when hydrated lime was partially replaced with metakaolin or pumice. The use of 100% slag as a hempcrete binder (HC-SL-MR1.1) also yielded comparable results. It appears that, at a molar ratio of 0.8, the calcium content is insufficient for a complete reaction with the clay minerals, leaving some unreacted material between the hurd particles. During compression, the absence of adequate bonding in the unreacted binder can precipitate an early collapse. In contrast, hempcrete prepared with a 0.8 molar ratio binder that incorporated silica fume exhibited a slightly higher compressive strength, although the

difference was not statistically significant (see Table 33) when compared to lime-hempcrete. The primary distinction between silica fume and the other SCMs is the marked absence of alumina in silica fume. Accordingly, the observations from this study suggest that unreacted alumina has a more detrimental effect on the mechanical properties of hempcrete than silica. Nevertheless, further microscopic investigations are required to identify the specific reactions between each clay component and the calcium content.

Table 33- Statistical comparison between hempcrete mix designs and hydrated lime hempcrete

Comparison between samples	T-score	P-value
HC-MK-30 VS HC-LIME	25.14	3.36E-09
HC-PU-30 VS HC-LIME	22.57	1.56E-09
HC-SF-30 VS HC-LIME	5.84	0.0003
HC-SL-30 VS HC-LIME	4.34	0.0024
HC-PC-30 VS HC-LIME	-0.14	0.45 (>5%)
HC-MK-MR3 VS HC-LIME	18.55	1.64E-07
HC-PU-MR3 VS HC-LIME	23.18	2.52E-10
HC-SF-MR3 VS HC-LIME	11.36	6.14E-07
HC-SL-MR3 VS HC-LIME	5.22	0.0003
HC-PC-MR3 VS HC-LIME	16.13	8.68E-09
HC-MK-MR0.8 VS HC-LIME	-20.22	4.12E-09
HC-PU-MR0.8 VS HC-LIME	-10.80	2.39E-06
HC-SF-MR0.8 VS HC-LIME	1.57	0.084 (>5%)
HC-SL-MR1.1 VS HC-LIME	-37.04	1.29E-08

The modulus of elasticity reported in Table 26 follows a trend similar to that observed for compressive strength. Specifically, the modulus of elasticity of hempcrete was enhanced by replacing 30% of the lime with SCMs and by employing a CaO/SiO_2 molar ratio of 3. Similar observations have been made in previous studies that replaced a small portion of lime (or a commercial binder containing at least 70% hydrated lime) with SCMs (Daher *et al.*, 2022; Murphy *et al.*, 2010). However, consistent with compressive strength results

(Abdellatef *et al.*, 2020), the modulus of elasticity in hempcrete composed of binders with a molar ratio of 0.8 declined relative to that of lime-hempcrete.

4.2.3.2.2 30/70 SCMs-to-Hydrated Lime

Previous studies have demonstrated that the type of binder significantly influences the mechanical properties of hempcrete (Nguyen *et al.*, 2010). In this study, the compressive strength of hempcrete produced with 30/70 SCM-to-lime binders was compared to that of Portland cement-to-lime hempcrete, which served as the reference (presented in Table 26). As shown in Table 34, all four SCM-lime hempcrete formulations exhibited a significant improvement in compressive strength relative to the reference. The 30/70 PC-to-lime formulation contains only approximately 9% clay in total, owing to the low clay content of its components. In contrast, the clay content in the other 30/70 SCM-lime mix designs increased to approximately 30%, thereby enhancing the reactivity of the binder.

The differences in compressive strength among the various binder mix designs can be further explained by considering their chemical compositions. Accordingly, two factors should be taken into consideration: the total clay content and the Al_2O_3/SiO_2 proportions. The specimens containing metakaolin, pumice, and silica fume have around 30% clay content, which is substantially higher than that of the slag sample (approximately 15%), while the Portland cement hempcrete exhibits the lowest clay content at about 9%. Concurrently, the Al_2O_3/SiO_2 ratios differ among the samples; the metakaolin specimen has the highest ratio (0.71), followed by slag (0.27), Portland cement (0.22), and pumice (0.15), with the specimen containing silica fume having only 0.007.

Accordingly, the 30/70 metakaolin-lime hempcrete, with the highest clay content and the highest Al_2O_3/SiO_2 ratio, demonstrated the best compressive strength among all five mix designs. The pumice-based sample, having a similar clay content but a lower Al_2O_3/SiO_2 ratio, ranked second, while the specimen containing silica fume, despite its similarly high clay content, ranked third due to its very low alumina content. Although the slag and Portland cement specimens contain higher Al_2O_3/SiO_2 ratios than the pumice

sample, they exhibit lower compressive strengths because of their lower overall clay content. In particular, the Portland cement specimen recorded the lowest compressive strength, as both its clay content and Al_2O_3/SiO_2 ratio were lower than those of the slag hempcrete. Notably, the specimens containing silica fume and slag demonstrated similar compressive strength values (see Table 34). Even though the silica fume sample lacked alumina significantly, its higher clay content appears to compensate for the value difference. This observation aligns with Walker's study, which identified the high reactivity of binder components as the main contributor to the enhanced strength of hempcrete, despite its porosity and apparent density (Walker, 2013).

As illustrated in Figure 34, the trend in the modulus of elasticity aligns with the compressive strength results for the 30/70 SCM-lime binder hempcrete. However, based on the analysis provided in Table 34, the differences in modulus of elasticity among the hempcrete mix designs are statistically insignificant (with p-values greater than 5% and low t-scores). The high coefficients of variation in hempcrete modulus of elasticity (presented in Table 26), further indicates that the values among the different mix designs are relatively similar.

Table 34- Statistical comparison between the hempcrete, made with 30/70 SCM-to-hydrated lime binder

Comparison between samples	Compressive strength		Modulus of elasticity	
	T-score	P-value	T-score	P-value
HC-MK-30 VS HC-PU-30	12.13	2.95352E-06	1.99	0.07 (> 5%)
HC-PU-30 VS HC-SF-30	6.19	0.0004	1.21	0.15 (> 5%)
HC-SF-30 VS HC-SL-30	0.03	0.49 (> 5%)	-0.38	0.36 (> 5%)
HC-SL-30 VS HC-PC-30	4.00	0.002	0.90	0.21 (> 5%)

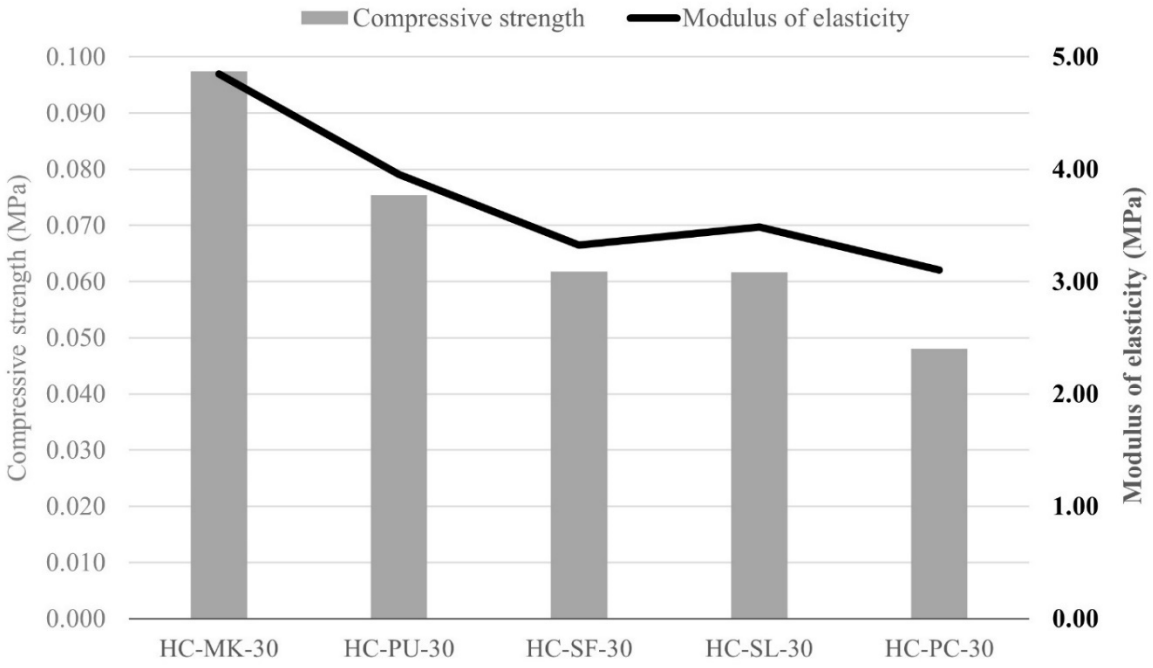

Figure 34- Compressive strength and modulus of elasticity comparison in hempcrete samples with 30/70 SCM-to-hydrated lime binder

4.2.3.2.3 Molar ratio of 3.0

As mentioned earlier, a CaO/SiO_2 molar ratio of 3 was used for the SCM-lime mix designs, equivalent to the ratio of 100% Portland cement. The compressive strength values, ranging from 0.098 to 0.057 MPa, cover a narrower range of results than those obtained with percentage-based binder compositions. By defining the calcium/silica molar ratio as the key factor influencing binder mechanical properties, as discussed in the literature review, a more homogeneous set of compressive strength results was achieved. Although only two main binder compositions could be controlled in the mixed design by fixing the calcium/silica ratio, the alumina/silica ratio was not held constant. However, other factors affect the mechanical properties of the binders and, subsequently, the hempcrete. Factors like the ratio of calcium/clay content can be examined and compared to the achieved outcome in this study.

Similar to the 30/70 SCM-lime hempcrete binders, the metakaolin-containing sample demonstrated the highest compressive strength among all MR3 mix designs. This superior performance can be attributed to

metakaolin's high clay content, elevated Al_2O_3/SiO_2 ratio, and the highest specific surface area among the SCMs, all of which contribute to its reactivity. Slag-lime hempcrete was expected to rank second due to its high clay and alumina contents and relatively high surface area after metakaolin. However, the high MgO content in the slag mixture appears to have weakened the structure, ultimately placing it last. The presence of MgO can induce internal stress through expansion and microcracking, as its hydration produces magnesium hydroxide ($Mg(OH)_2$), which then reacts with silica to form magnesium silicate hydrates (M-S-H) gel. This gel does not significantly contribute to overall strength and may consume silica that would otherwise form a strength-enhancing C-S-H gel.

Alternatively, the pumice-lime mix design, despite having one of the lowest clay contents and a low Al_2O_3/SiO_2 ratio, ranked second in compressive strength after metakaolin. The high K_2O and Na_2O content, totalling 7.5%, appears to act as an additional activator. They result in significantly higher compressive strength, as indicated in Table 35, when compared to slag and Portland cement mix designs with higher clay and alumina contents. Finally, the mixed composition comprising Portland cement and silica fume achieved similar maximum strength, with differences that were statistically insignificant based on Table 35. These results suggest that the higher clay and alumina content in the Portland cement binder had a comparable effect on strength as the higher surface area provided by the silica fume in the mix design.

As shown in Figure 35 and consistent with hempcrete produced using percentage-based binders, the modulus of elasticity trend in the molar ratio-based mix designs aligns with the compressive strength results. Hempcrete containing metakaolin achieved the highest modulus of elasticity, while the slag-based binder exhibited the lowest modulus of elasticity among all compositions. The overall high p-values and low t-values, ranging between 3% and 11%, as listed in Table 35, indicate that the variations in modulus of elasticity are not statistically significant.

In summary, comparing hempcrete produced with molar ratio-based binders is a more efficient approach than using percentage-based formulations. By maintaining a constant CaO/SiO_2 molar ratio, the comparison

became more controlled, allowing other compositional parameters such as alumina and magnesia contents to be more effectively evaluated. However, further studies are necessary to isolate the effects of other various factors in binders to determine their relative impact and to prioritize them accordingly.

Table 35- Statistical comparison between the hempcrete, using binders with a CaO/SiO_2 molar ratio of 3

Comparison between samples	Compressive strength		Modulus of elasticity	
	T-score	P-value	T-score	P-value
HC-MK-MR3 VS HC-PU-MR3	7.41	0.00016	1.91	0.10 (> 5%)
HC-PU-MR3 VS HC-PC-MR3	8.12	5.16E-06	2.98	0.03
HC-PC-MR3 VS HC-SF-MR3	0.53	0.30 (> 5%)	-1.42	0.11 (> 5%)
HC-SF-MR3 VS HC-SL-MR3	5.47	0.00014	2.19	0.08 (> 5%)

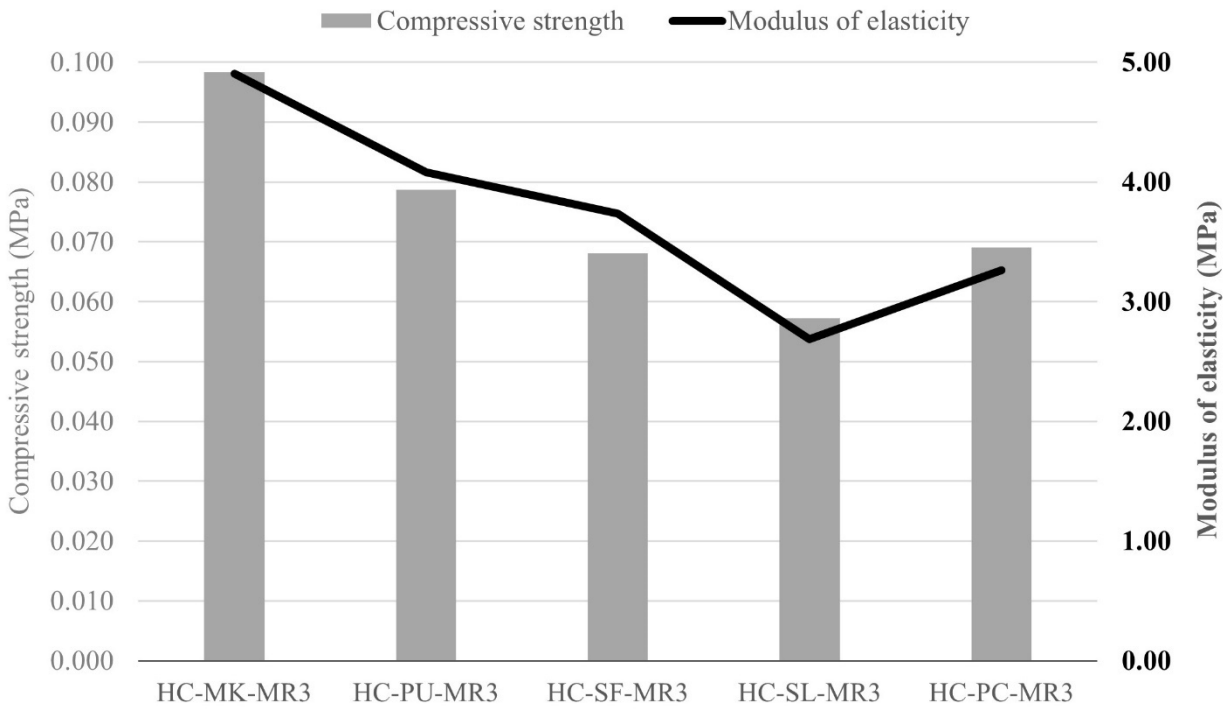

Figure 35- Compressive strength and modulus of elasticity comparison in hempcrete, using binders with a CaO/SiO_2 molar ratio of 3

4.2.3.2.4 Molar ratio of 0.8

The comparison between hempcrete produced with binders at a molar ratio of 0.8 and those at 3.0 indicates a considerable reduction in mechanical properties (see Table 36). This decrease can primarily be attributed to the lower alkaline activator content, specifically, the reduced availability of calcium to react with the clays. Based on the chemical composition of the three mix designs formulated at a 0.8 molar ratio, and as discussed previously, the calcium deficiency had a more pronounced negative impact on the alumina content than on silica (Table 36). Consequently, the silica fume-based binder, which contains negligible alumina, was affected the least, whereas the metakaolin-based binder, with the highest alumina content, suffered the most from the lack of activator. Although the hempcrete with a slag binder exhibited relatively similar mechanical properties, its unique molar ratio renders its composition, and thus its performance, not comparable with the 0.8 molar ratio binder hempcrete.

Similar to both previous categories, and as illustrated in Figure 36, the modulus of elasticity trends in the samples correlate with their compressive strength values. The p-values for the modulus of elasticity comparisons, ranging from 0.1% to 0.9% (Table 36), indicate that the differences among the MR0.8 groups are more statistically significant than those observed in the MR3 and percentage-based (30/70) samples. This finding suggests that the lack of a sufficient activator has a stronger effect on the decline in material modulus of elasticity than does the type of hydration gel produced. In addition, when handling, the 0.8 molar ratio hempcrete samples were observed to demonstrate noticeably lower structural integrity and stiffness compared to the other categories. This reduced stiffness was most evident in the metakaolin-based sample relative to the silica fume and pumice samples. However, the low stiffness and fragility observed in the slag specimens (HC-SL-MR1.1) were so severe that handling and supporting these samples became particularly challenging.

Table 36- Statistical comparison between the hempcrete, using binders with a CaO/SiO_2 molar ratio of 0.8 (and slag hempcrete with the molar ratio of 1.1)

Comparison between samples	Compressive strength		Modulus of elasticity	
	T-score	P-value	T-score	P-value
HC-MR3 VS HC-MR0.8	4.04	0.003	4.78	0.001
HC-SF-MR0.8 VS HC-PU-MR0.8	21.07	6.83382E-08	8.08	0.002
HC-PU-MR0.8 VS HC-MK-MR0.8	12.69	8.5931E-08	5.00	0.008
HC-MK-MR0.8 VS HC-SL-MR1.1	19.54	1.14812E-07	7.47	0.009

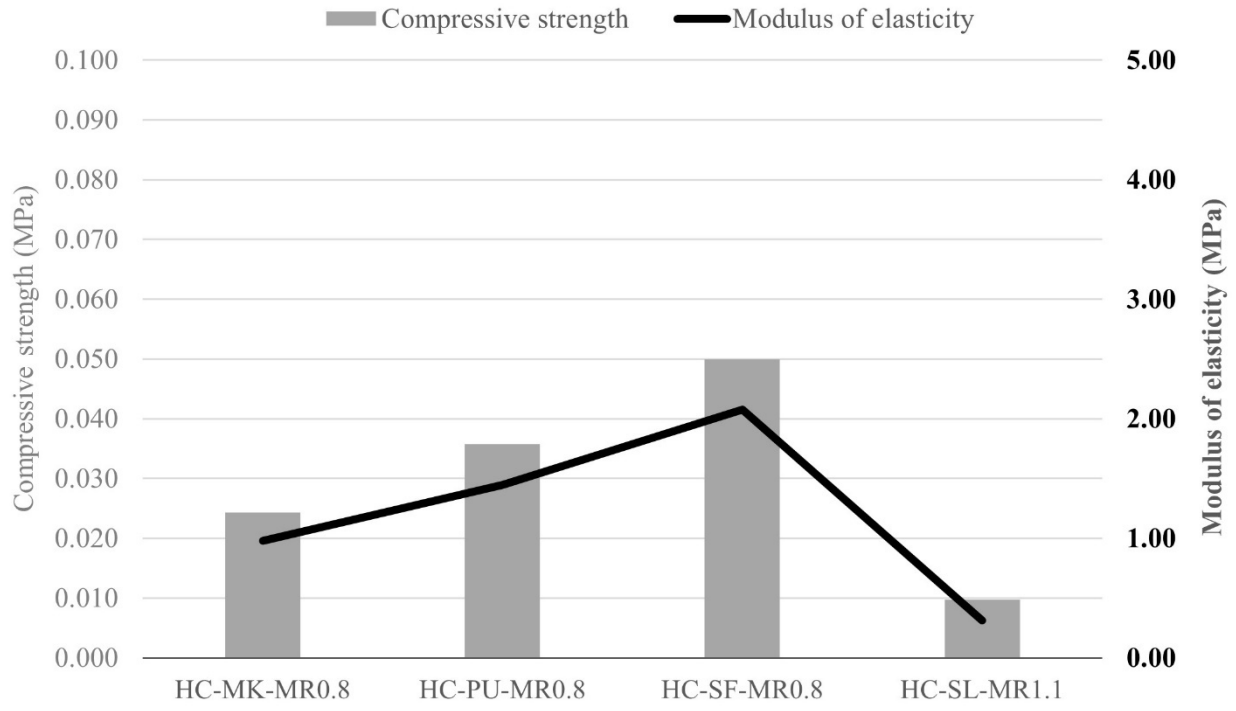

Figure 36- Compressive strength and modulus of elasticity comparison in hempcrete, using binders with a CaO/SiO_2 molar ratio of 0.8 (and slag hempcrete with a molar ratio of 1.1)

4.2.3.2.5 Different Proportion of an SCM

Figure 37 represents the trend of compressive strength values as a function of the SCM proportions in the binder pastes. The results for Portland cement, due to their significant difference from the other trends, have been disregarded. As demonstrated in Table 37, the introduction of SCMs increased the compressive

strength in all mix designs, regardless of the binder type. After reaching the peak compressive strength, further increases in the SCM proportion resulted in a reduction of the strength. However, the peak point varied depending on the binder type. Replacing hydrated lime with various proportions of slag produced the greatest improvement among the binders, with a peak occurring when approximately half of the lime was replaced by slag. Silica fume, on the other hand, appeared to yield minimal improvement when approximately 20% of the lime was replaced, with a significant peak at 30% replacement (see Table 37) and a decline at 50% replacement. Neither Metakaolin nor pumice produced a considerable improvement when replacing hydrated lime; both exhibited a slight peak at approximately 25- 30% replacement, followed by a decline. However, additional data points for SCM proportions in binder pastes are required to determine the optimum value for each SCM-to-lime mixture.

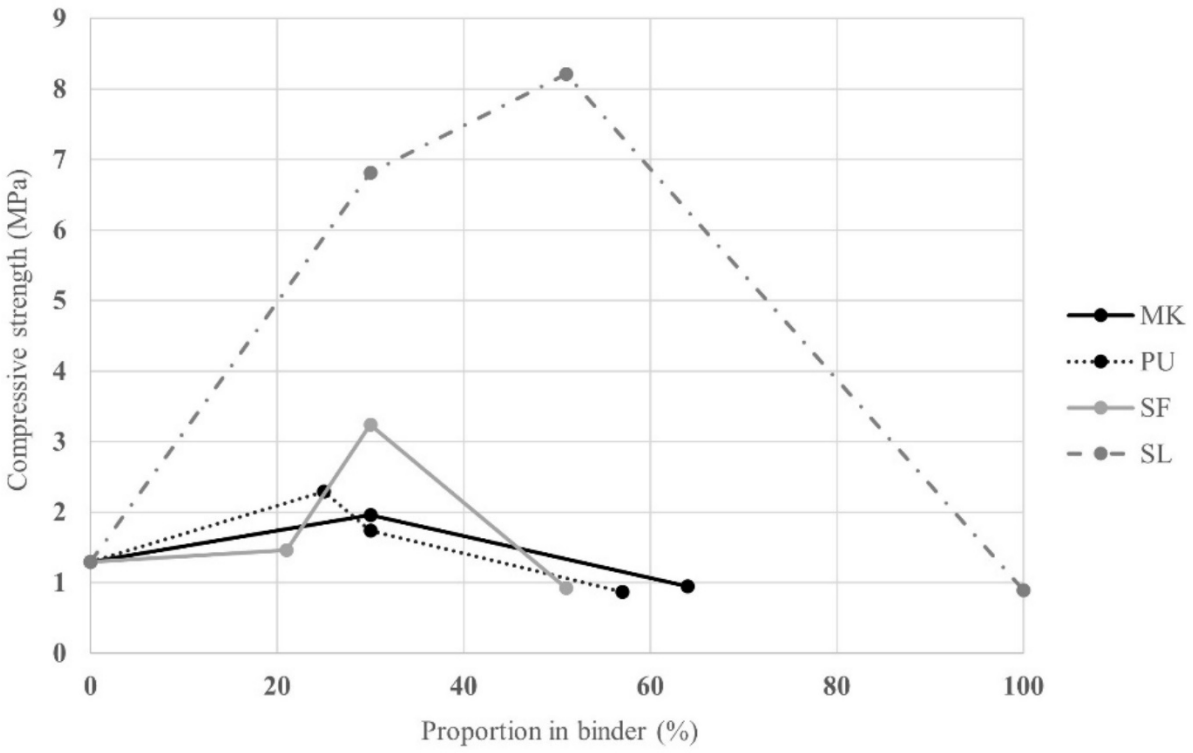

Figure 37- The compressive strength trend based on SCM proportions in binder pastes

As expected, the trend in the modulus of elasticity follows a pattern similar to that of compressive strength when considering SCM proportions in binder pastes, as illustrated in Figure 38. However, comparing the P-value and T-score ranges with the compressive strength results indicates less significant variations in the modulus of elasticity. Binders containing silica fume were the only exception; even though there was a considerable increase in compressive strength with approximately a 50% replacement of silica fume, the modulus of elasticity did not show a significant change (according to Table 37).

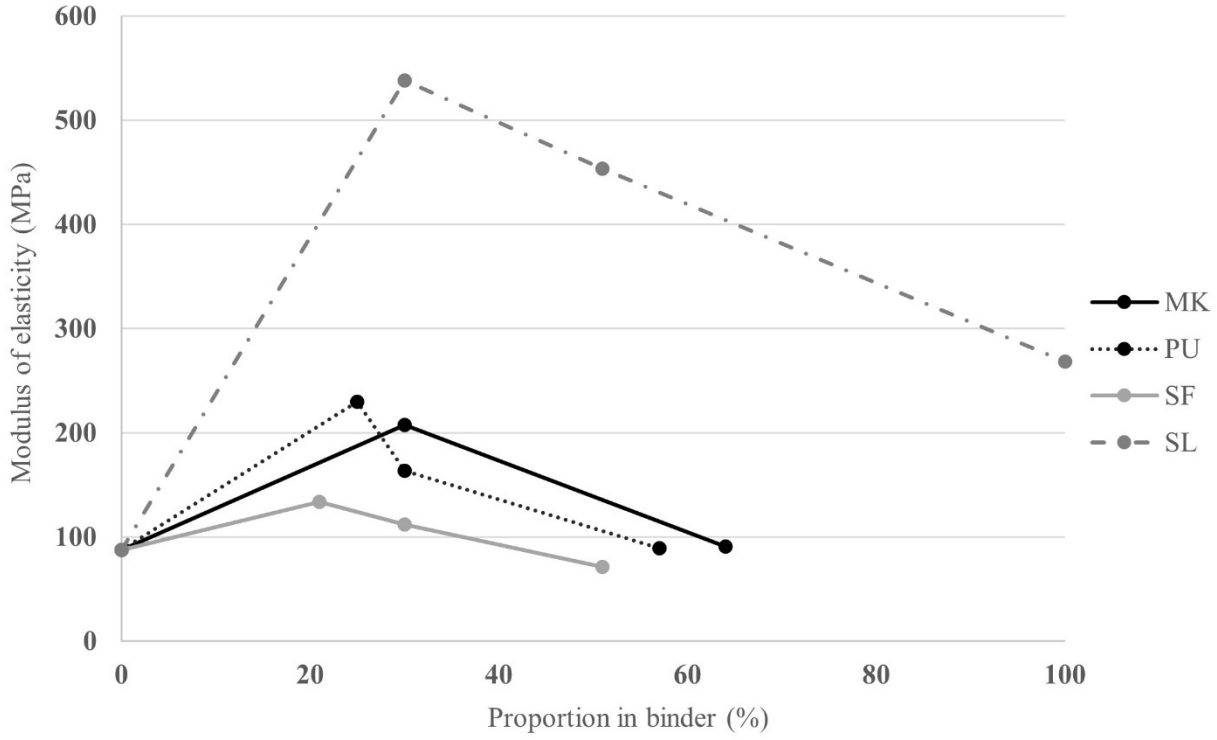

Figure 38- The modulus of elasticity trend based on SCM proportions in binder pastes

Table 37- Statistical comparison between different proportions of the SCMs in binders of binder paste samples

Comparison between samples	Compressive strength		Modulus of elasticity	
	T-score	P-value	T-score	P-value
BP-LIME VS BP-MK-30	-5.13	0.0004	-3.44	0.005
BP-MK-30 VS BP-MK-MR0.8	8.83	0.0002	3.73	0.007
BP-LIME VS BP-PU-MR3	-8.75	5.35E-06	-5.70	0.002

BP-PU-MR3 VS BP-PU-30	4.97	0.0005	2.76	0.035 (>5%)
BP-PU-30 VS BP-PU-MR0.8	13.91	4.31E-06	4.06	0.028
BP-LIME VS BP-SF-MR3	-1.90	0.043	-1.42	0.125 (>5%)
BP-SF-MR3 VS BP-SF-30	-21.10	6.36E-10	0.71	0.264 (>5%)
BP-SF-30 VS BP-SF-MR0.8	23.97	9.13E-10	2.54	0.042
BP-LIME VS BP-SL-30	-12.50	2.90E-05	-11.00	0.029
BP-SL-30 VS BP-SL-MR3	-2.94	0.011	0.75	0.265 (>5%)
BP-SL-MR3 VS BP-SL-MR1.1	38.09	1.18E-07	1.60	0.104 (>5%)
BP-LIME VS BP-PC-30	-14.73	3.07E-06	-13.79	0.023
BP-PC-30 VS BP-PC-MR3	-22.35	1.66E-06	-	-

Additionally, Figure 39 demonstrates the trend of SCM proportions in hempcrete binders. The behaviour observed in hempcrete binders is different from that in binder paste cubes, likely due to the interference of hemp hurd in the reactions, as mentioned previously. Similar to the binder pastes, the introduction of SCMs appears to significantly increase the mechanical properties, with Portland cement being the exception (see Table 38). Excluding Portland cement, the SCMs reached their peak at approximately 20- 30% proportions in the hempcrete binders. Metakaolin and pumice, which produced the smallest variations in compressive strength when added to the binder pastes, exhibited the most significant changes when their proportions were increased in the hempcrete binder. Silica fume was the only SCM whose mechanical behaviour was not notably affected by the hemp hurd. Conversely, the slag binder, responsible for the most variation in compressive strength in the binder pastes, exhibited a slight increase in compressive strength when partially introduced and a significant decline when fully replacing the binder. Additionally, the alteration in the maximum strength value of hempcrete when lime was replaced by Portland cement was lower than that observed for other SCMs. Notably, Portland cement was the only binder that, when its proportion was increased in the hempcrete binder, increased in compressive strength. The underlying reasons for the behaviour of each material are discussed in detail in previous sections. As illustrated in Figure 40 and discussed previously, the modulus of elasticity follows a similar pattern to that observed for compressive strength, although the changes are less pronounced.

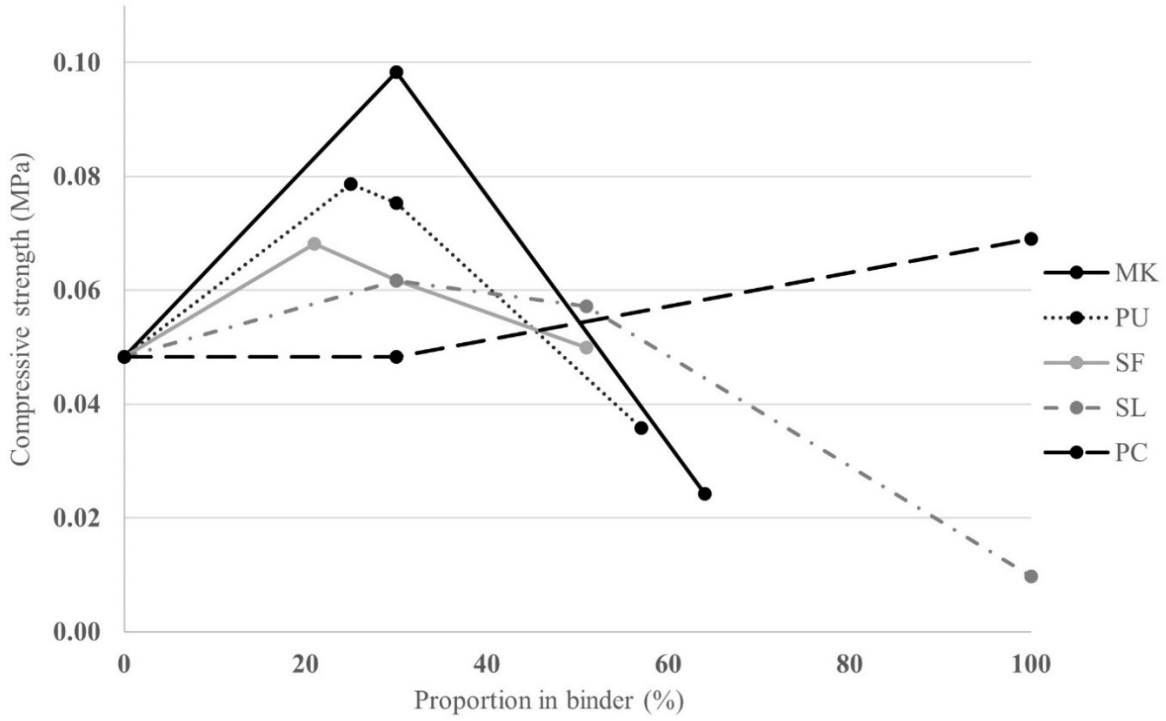

Figure 39- The compressive strength trend based on SCM proportions in hempcrete samples

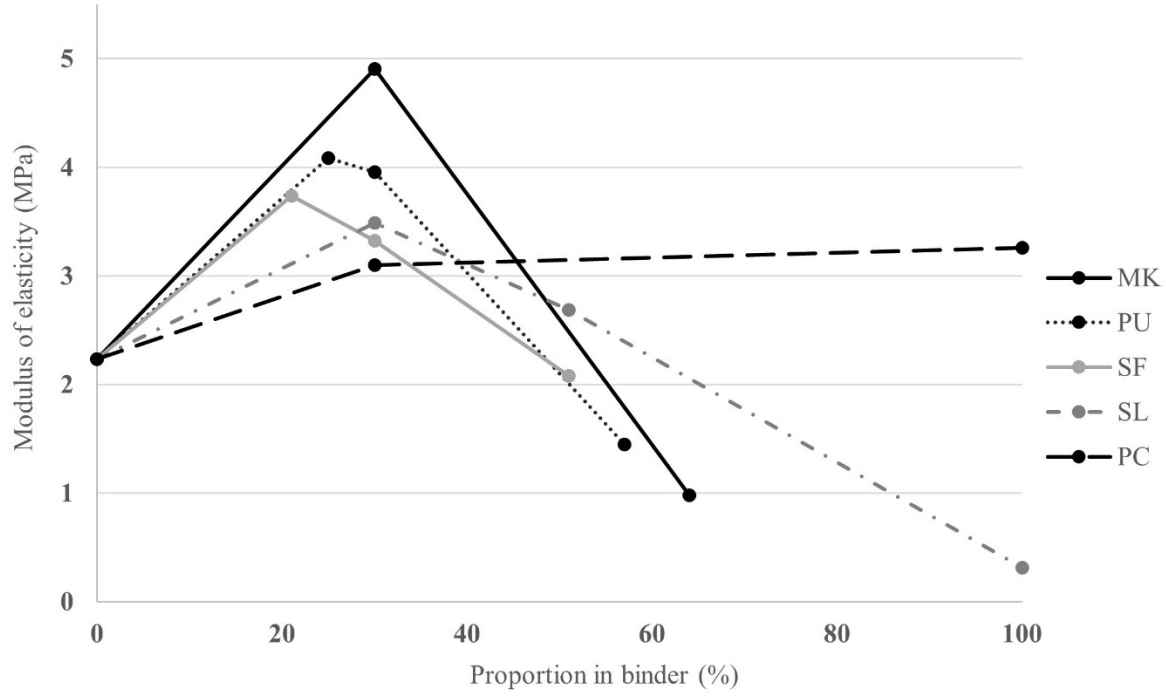

Figure 40- The modulus of elasticity trend based on SCM proportions in hempcrete samples

Table 38- Statistical comparison between different proportions of the SCMs in binders of hempcrete samples

Comparison between samples	Compressive strength		Modulus of elasticity	
	T-score	P-value	T-score	P-value
HC-LIME VS HC-MK-30	-18.55	1.64E-07	-5.26	0.007
HC-MK-30 VS HC-MK-MR0.8	28.52	6.15E-08	9.16	0.006
HC-LIME VS HC-PU-MR3	-23.18	2.52E-10	-6.10	0.052 (>5%)
HC-PU-MR3 VS HC-PU-30	3.02	0.007	0.31	0.394 (>5%)
HC-PU-30 VS HC-PU-MR0.8	43.17	5.34E-13	6.13	0.013
HC-LIME VS HC-SF-MR3	-11.36	6.14E-07	-4.19	0.026
HC-SF-MR3 VS HC-SF-30	2.50	0.017	1.06	0.183 (>5%)
HC-SF-30 VS HC-SF-MR0.8	5.64	0.001	3.74	0.032
HC-LIME VS HC-SL-30	-4.34	0.002	-3.10	0.027
HC-SL-30 VS HC-SL-MR3	1.39	0.104 (>5%)	1.55	0.130 (>5%)
HC-SL-MR3 VS HC-SL-MR1.1	33.27	2.46E-08	5.53	0.057 (>5%)
HC-LIME VS HC-PC-30	0.14	0.448 (>5%)	-2.04	0.067 (>5%)
HC-PC-30 VS HC-PC-MR3	-10.79	6.48E-06	-0.39	0.359 (>5%)

Similar observations have been made in previous literature. Walker (2013) stated that it had been repeatedly proven that a binder with high hydraulic behaviour (such as Portland cement) is not well suited for pairing with hemp hurd. However, the findings in this study do not entirely confirm the assumption that higher proportions of SCMs in hempcrete binders lead to improvements in the mechanical strength of the material, as stated in previous studies (Nguyen *et al.*, 2010). Alternatively, the trend revealed in this research is consistent with studies that indicate increasing the SCM proportion in the binder results in a non-linear response in the mechanical properties of hempcrete (Abdellatef *et al.*, 2020; Khan, 2020). An aligned behaviour in compressive strength and modulus of elasticity, as reported in this study, was observed in previous literature as well (Abdellatef *et al.*, 2020). Although the modulus of elasticity has been attributed to hempcrete density (Mahmood *et al.*, 2024), by stabilizing the density in this study, the relationship between compressive strength and modulus of elasticity becomes more evident.

4.2.4 Thermal Properties

Table 39 presents the thermal conductivity, thermal resistance, and specific heat capacity values of hempcrete fabricated using finely ground hemp hurd with a 1:1 hemp-to-binder ratio, targeting a density of 190 kg/m³ for all samples. Six distinct samples were tested in a heat flow meter for thermal conductivity and heat capacity within separate procedures. Tests were repeated on randomly selected samples to ensure both accuracy and precision. The measured thermal conductivity ranged from 0.0490 to 0.0548 W/m·K, with an average coefficient of variation of 1.58%. Similarly, the specific heat capacity ranged from 902 to 1005 J/kg·K, with an average coefficient of variation of 1.29%. This low variability in both thermal properties contrasts with the broader ranges reported in previous studies. The fine particle size of the hemp hurd likely minimized distribution variability among samples, leading to a considerably narrower range of results. Furthermore, the consistent density, as shown in Table 25, contributed to the low coefficients of variation in the thermal performance of hempcrete, in contrast to the higher values reported in other studies (Dhakal *et al.*, 2017; Walker & Pavía, 2014b).

Table 39- Average values for hempcrete's thermal conductivity, specific heat capacity, and thermal resistance with finely ground hemp hurd, target density of 190 kg/m^3, and 1:1 hemp-to-binder ratio by weight

No.	Sample ID	λ (W/m.K)	CoV (%)	c (J/kg.K)	CoV (%)	R-value (ft².°F.h/BTU)
1	HC-MK-30	0.0536	1.20	958	2.73	5.08
2	HC-PU-30	0.0537	1.08	951	1.48	5.07
3	HC-SF-30	0.0539	1.01	953	1.15	4.96
4	HC-SL-30	0.0542	2.42	938	0.46	5.02
5	HC-PC-30	0.0536	3.64	964	1.20	5.08
6	HC-MK-MR3	0.0536	1.11	951	0.97	5.08
7	HC-PU-MR3	0.0537	1.73	973	1.17	5.07
8	HC-SF-MR3	0.0541	0.80	966	1.40	5.03
9	HC-SL-MR3	0.0528	1.72	931	1.39	5.16
10	HC-PC-MR3	0.0529	2.47	932	2.51	5.15
11	HC-MK-MR0.8	0.0536	0.89	909	1.39	5.03
12	HC-PU-MR0.8	0.0535	0.71	939	0.96	5.04

13	HC-SF-MR0.8	0.0535	1.41	902	1.34	5.04
14	HC-SL-MR1.1	0.0490	2.59	908	0.48	5.33
15	HC-Lime	0.0548	0.93	1005	0.68	4.93

λ=Thermal conductivity, CoV=Coefficient of variation, c=Specific heat capacity, R-value=Thermal resistance

4.2.4.1 Binder Effect

Considering the thermal conductivity values of hempcrete, as shown in Table 40, a significant variation is observed in the overall results. However, within each binder category, whether based on percentage, a molar ratio of 3 or 0.8, no significant alterations were noted. In binder compositions incorporating SCMs, significant changes in thermal conductivity were observed when varying the SCM-to-lime proportion, with the exception of Portland cement hempcrete.

Table 40- Statistical analysis of thermal conductivity results for different categories of hempcrete- ANOVA

Group of samples	SS	df	MS	F	P-value	F crit
Total results	0.0001	14	9.98E-06	11.27	2.46E-13	1.83
30/70 SCM/lime	1.60E-06	4	3.99E-07	0.30	0.87	2.76
With a molar ratio of 3	7.31E-06	4	1.83E-06	2.32	0.08	2.76
With a molar ratio of 0.8	6.41E-08	2	3.20E-08	0.11	0.90	3.68
Containing Metakaolin	5.71E-06	2	2.86E-06	9.53	0.001	3.47
Containing pumice	5.73E-06	3	1.91E-06	4.75	0.012	3.10
Containing silica fume	4.42E-06	3	1.47E-06	4.67	0.012	3.10
Containing slag	0.0001	3	4.00E-05	36.17	2.86E-08	3.10
Containing Portland cement	1.03E-05	2	5.15E-06	2.67	0.10	3.68

Investigating in greater detail and based on the trend in Figure 41 as well as the data in Table 41, the initial replacement of hydrated lime with metakaolin, pumice, or silica fume appeared to be influential in decreasing thermal conductivity. However, with further increases in the SCMs proportion in hempcrete binders, the result did not experience a significant change. On the other hand, the introduction of slag and Portland cement slightly reduced thermal conductivity compared to lime hempcrete. Notably, increasing the slag content in the binder resulted in a significant decline in thermal conductivity, with the 100% slag

binder achieving the lowest values. In contrast, Portland cement-containing binders did not exhibit a significant decline, likely due to a relatively higher coefficient of variation in the results compared to other samples.

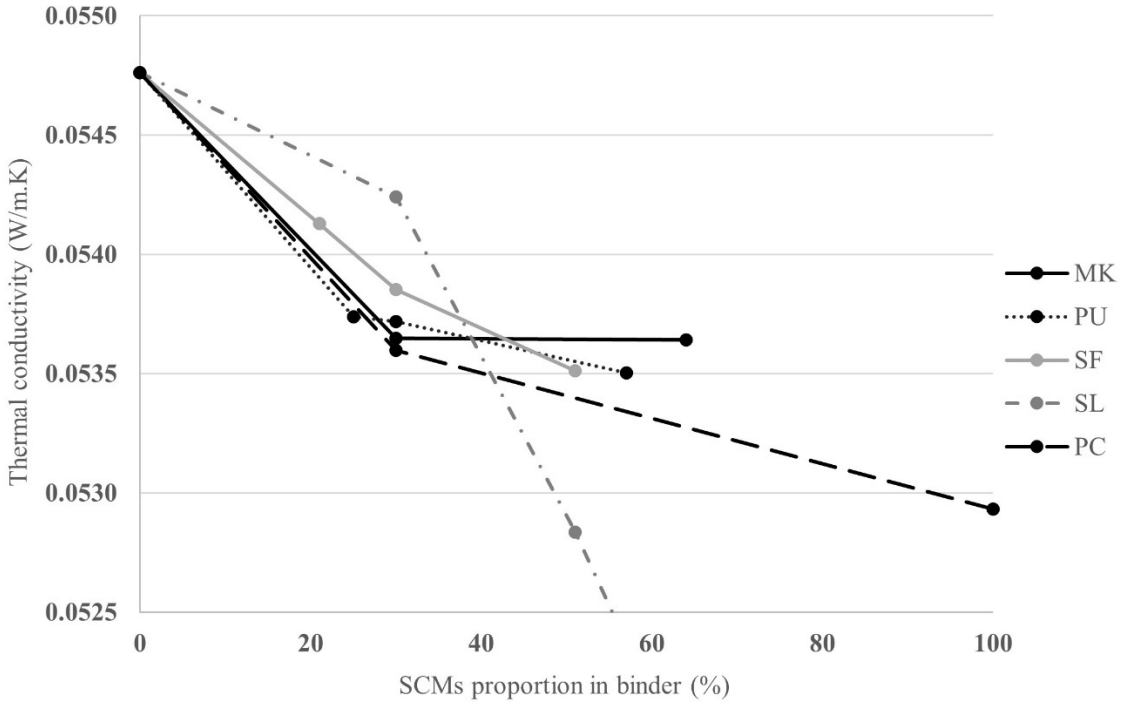

Figure 41- Thermal conductivity trend in hempcrete with the same SCM used in the binder composition

Table 41- Statistical analysis for thermal conductivity and specific heat capacity results for finely ground hemp hurd hempcrete

Comparison between samples	Thermal conductivity		Specific heat capacity	
	T-score	P-value	T-score	P-value
HC-LIME VS HC-MK-30	4.19	0.0006	8.25	2.95008E-07
HC-MK-30 VS HC-MK-MR0.8	-0.04	0.48 (> 5%)	6.06	1.47413E-05
HC-LIME VS HC-PU-MR3	2.36	0.02	5.85	0.0002
HC-PU-MR3 VS HC-PU-30	0.04	0.48 (> 5%)	3.00	0.007
HC-PU-30 VS HC-PU-MR0.8	0.76	0.23 (> 5%)	1.74	0.060
HC-LIME VS HC-SF-MR3	2.31	0.02	6.35	0.0002

HC-SF-MR3 VS HC-SF-30	0.98	0.18 (> 5%)	1.83	0.049
HC-SF-30 VS HC-SF-MR0.8	0.65	0.27 (> 5%)	7.65	8.64564E-06
HC-LIME VS HC-SL-30	0.91	0.20 (> 5%)	20.41	1.73741E-08
HC-SL-30 VS HC-SL-MR3	2.15	0.03	1.17	0.14
HC-SL-MR3 VS HC-SL-MR1.1	5.95	0.0001	4.14	0.003
HC-LIME VS HC-PC-30	1.41	0.10 (> 5%)	7.58	3.22389E-05
HC-PC-30 VS HC-PC-MR3	0.70	0.25 (> 5%)	3.02	0.010

Density has been identified as the most influential contributor to the thermal conductivity of hempcrete (Dhakal *et al.*, 2017; Elfordy *et al.*, 2008; Mahmood *et al.*, 2024) and, in some cases, as the sole factor affecting its thermal properties (Abdellatef *et al.*, 2020). In the present study, minimizing the influence of density provided an opportunity to focus on other factors that may impact thermal conductivity. Since all samples maintained the same target density and exhibited very low coefficients of variation (Table 25), the results suggest a regressive trend in thermal conductivity with increasing SCM proportions in the binder, which is consistent with previous literature (Abdellatef *et al.*, 2020; Walker & Pavía, 2014b). Increasing the SCM content enhances the binder's hydraulicity, which in turn reduces the thermal conductivity of hempcrete. The influence of binder hydraulicity appears to be more evident in such behaviour than that of other factors (Walker & Pavía, 2014b).

Previous studies have reported an insignificant impact of binder type on the thermal conductivity of hempcrete (Nguyen *et al.*, 2010; Walker & Pavía, 2014b). This observation is further supported by the present study, which features a very narrow density range and minimizes the effect of hemp hurd particle size distribution. In contrast, the study by Al-Tamimi *et al.* (2024) reported a wide range of densities, making it unclear whether the differences in thermal conductivity with various SCMs were due to binder variations or density variations. By maintaining a constant density, our findings indicate that the differences observed in that study were primarily attributable to density variations rather than to the SCM type.

Figure 42 compares the results of this study with those reported in previous literature. Thermal conductivity values ranging from 0.055 to 0.180 W/m·K have been reported for hempcrete densities between 140 and 627 kg/m³ (Abdellatef *et al.*, 2020; Al-Tamimi *et al.*, 2024; Brzyski *et al.*, 2020; Dhakal *et al.*, 2017; Mahmood *et al.*, 2024; Walker & Pavía, 2014b). The relatively lower thermal conductivity observed in this study, indicative of improved thermal resistance, can primarily be attributed to the very low target density of the hempcrete samples. In addition, the fine particle size of hemp shives may have contributed to the reduction in thermal conductivity, as noted in previous observations (Mahmood *et al.*, 2024). However, its impact on the significantly low coefficient of variation in results, as discussed before, is more evident. Overall, the results of this study are in complete agreement with those of previous studies that investigated a similar density range (Mahmood *et al.*, 2024).

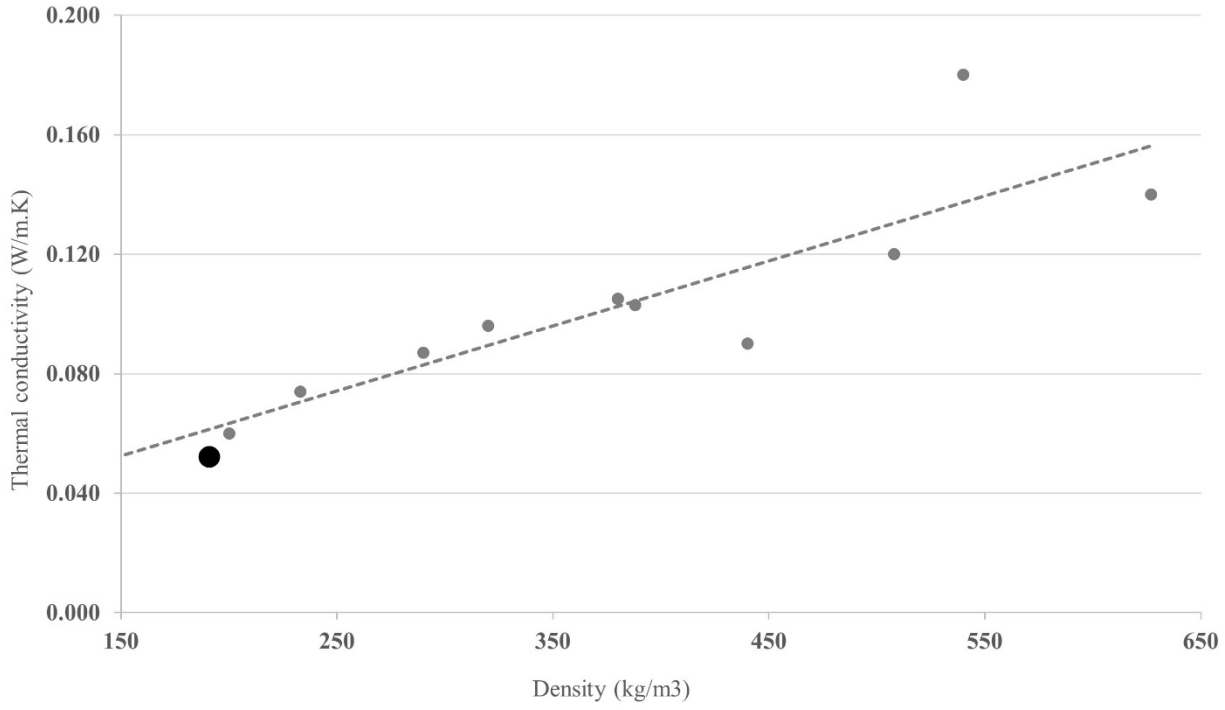

Figure 42- The comparison of thermal conductivity results of this study (bold point) with previous studies (Abdellatef *et al.*, 2020; Al-Tamimi *et al.*, 2024; Brzyski *et al.*, 2020; Dhakal *et al.*, 2017; Mahmood *et al.*, 2024; Walker & Pavía, 2014b)

The specific heat capacity results of the hempcrete samples were compared, analyzed, and summarized in Table 42. The results indicate that hempcrete with percentage-based binders did not exhibit significant variation, while hempcrete with molar ratio-based binders showed considerable variability among samples. Furthermore, varying the SCM-to-lime ratios within each SCM category resulted in significant changes in specific heat capacity values. Replacing hydrated lime with any SCM led to a statistically significant decline in specific heat capacity, as evidenced in Figure 43 (and Table 41). Increasing the SCM content in the binder further decreased the specific heat capacity as well.

Table 42- Statistical analysis of specific heat capacity results for different categories of hempcrete- ANOVA

Group of samples	SS	df	MS	F	P-value	F crit
Total results	63056.1	14	4504.0	24.84	1.45E-22	1.83
30/70 SCM/lime	2242.3	4	560.6	2.43	0.07	2.76
With a molar ratio of 3	8947.7	4	2236.9	10.04	5.47E-05	2.76
With a molar ratio of 0.8	4802.8	2	2401.4	18.69	8.46E-05	3.68
Containing Metakaolin	28075.3	2	14037.6	58.55	2.58E-09	3.47
Containing pumice	15076.2	3	5025.4	44.04	5.36E-09	3.10
Containing silica fume	32744.5	3	10914.8	87.90	1.08E-11	3.10
Containing slag	31324.1	3	10441.4	166.29	2.63E-14	3.10
Containing Portland cement	16367.4	2	8183.7	33.71	2.82E-06	3.68

As with thermal conductivity, density has been proven to exert a major influence on specific heat capacity (Mahmood *et al.*, 2024). The similar specific heat capacity values observed in binders with comparable SCM-to-lime ratios suggested that, after density, the proportion of SCM (serving as the hydraulic component of the binder regardless of the SCM type) was the primary factor determining the specific heat capacity of hempcrete. Previous studies have similarly reported no apparent effect of binder type on specific heat capacity. Abdellatef *et al.* (2020) observed a comparable decreasing trend when an SCM was added to the binder, whereas Walker & Pavía (2014b) reported an increasing trend with enhanced binder hydraulicity.

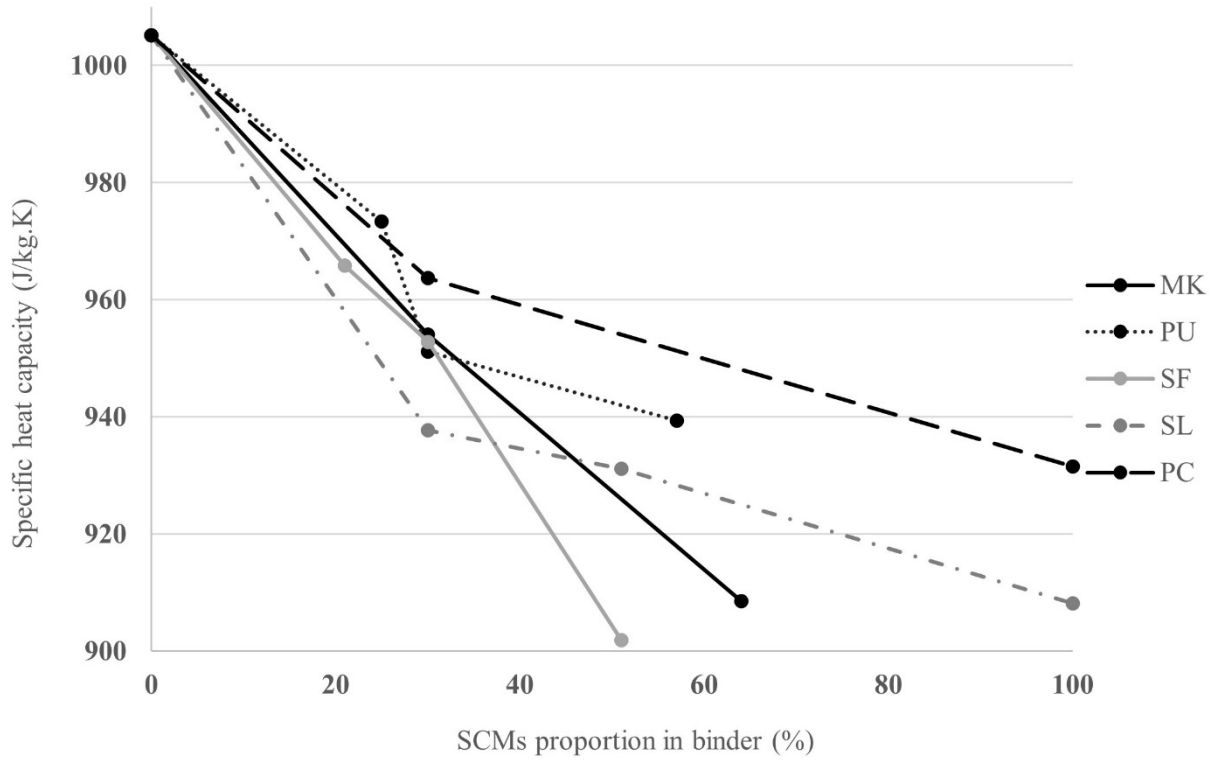

Figure 43- Specific heat capacity trend in hempcrete with the same SCM used in the binder composition

In addition, Figure 44 depicts the comparison of the range of specific heat capacity values achieved in previous studies with those obtained in the current experiment. For densities between 140 and 627 kg/m³, reported values ranged from 680 to 2025 J/kg·K (Abdellatef *et al.*, 2020; Al-Tamimi *et al.*, 2024; Brzyski *et al.*, 2020; Mahmood *et al.*, 2024; Walker & Pavía, 2014b). Similar to thermal conductivity, the relatively low range of results in this study is attributed to the low density of the samples. However, as shown in Figure 44, the results are in line with the previous observations. Although low-density hempcrete offers enhanced thermal resistance, it also exhibits a considerably lower heat capacity.

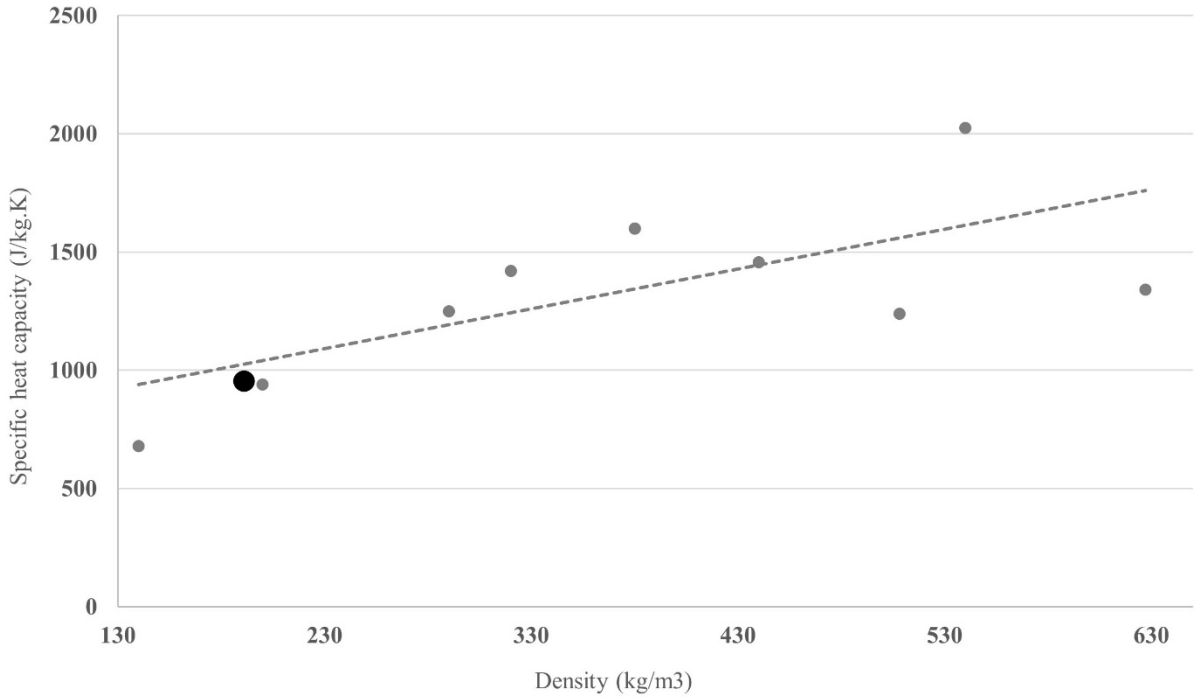

Figure 44- The comparison of specific heat capacity results of this study (bold point) with previous studies (Abdellatef *et al.*, 2020; Al-Tamimi *et al.*, 2024; Brzyski *et al.*, 2020; Mahmood *et al.*, 2024; Walker & Pavía, 2014b)

4.2.4.2 Hemp Hurd Effect

The thermal property values for hempcrete produced with a binder consisting of 30% metakaolin and 70% lime, using as-received hemp hurd, are outlined in Table 43. These values are compared to those for parallel hempcrete samples created with finely ground hemp hurd. The results indicate a significant improvement in the thermal resistance of the finely ground hempcrete samples, as shown in Table 44. The more uniform distribution of finely ground hemp hurd allows for a higher proportion of hemp hurd within the sample compared to as-received, larger particles. Given that the thermal conductivity of hemp hurd is considerably low, the increased ratio of hemp hurd in the finely ground samples results in lower overall thermal conductivity. Even though larger particles tend to increase porosity, which can partially compensate for the difference in thermal conductivity, the substantially higher proportion of hemp hurd in the finely ground

hempcrete still leads to a significantly lower thermal conductivity compared to the as-received hempcrete (Al-Tamimi & Bindiganavile, 2024).

According to Table 43, the specific heat capacity of the finely ground hempcrete samples was higher than that of the as-received samples. This difference is attributed to the more consistent distribution of hemp hurd in the finely ground mixture, resulting in a more solid structure. However, the observed difference in specific heat capacity was not statistically significant, as supported by the analysis presented in Table 44. Overall, consistent with previous studies (Brzyski *et al.*, 2020), the thermal properties of hempcrete appear to be less sensitive to variations in hemp hurd particle size compared to its mechanical properties.

Table 43- Average thermal conductivity and specific heat capacity value for hempcrete with as-received and finely ground hemp hurd, target density of 190 kg/m^3, and 1:1 hemp-to-binder ratio by weight

Sample ID	Particles	λ (W/m.K)	CoV (%)	c (J/kg.K)	CoV (%)
CHC-MK-30	As received	0.0592	0.92	935	2.24
HC-MK-30	Fine	0.0536	1.20	958	2.73

Table 44- Statistical analysis for thermal conductivity and specific heat capacity results in hempcrete with finely ground compared to as-received hemp hurd

Comparison between samples	Thermal conductivity		Specific heat capacity	
	T-score	P-value	T-score	P-value
CHC-MK-30 VS HC-MK-30	-19.77	3.03E-10	1.63	0.07

As summarized in Table 45, the thermal conductivity results for binder pastes ranged from 0.184 W/m·K for the binder with the highest proportion of metakaolin to 0.592 W/m·K for the 100% Portland cement binder. These results agree with the findings of the only comparable study available in the literature, considering both density and thermal conductivity (Nguyen *et al.*, 2010). When comparing the thermal properties of the binder pastes with their equivalent hempcrete samples, it is evident that the hemp hurd predominantly influences the results. As demonstrated in Table 46, significant variation was observed in all categories, whether based on molar ratio, percentage-based composition, or the specific SCM used. In

contrast, the thermal conductivity of the hempcrete samples (as presented in Table 39) is primarily determined by the high proportion of hemp hurd, resulting in relatively consistent results across different formulations.

Considering the specific heat capacity results listed in Table 45, values range from 759 to 1063 J/kg·K for binder pastes corresponding to metakaolin with a 0.8 molar ratio and hydrated lime, respectively. Although the low density of hempcrete is generally associated with low heat capacity, the relatively high heat capacity of hemp hurd compensates for this, resulting in overall heat capacity values similar to those of the binder pastes (see Table 39). However, the spread of specific heat capacity values in hempcrete is much narrower than that observed for binder pastes, as demonstrated in Table 47, with less significant variability.

Table 45- Average thermal conductivity, specific heat capacity, and thermal resistance value for binder paste cubes

No.	Sample ID	λ (W/m.K)	CoV (%)	c (J/kg.K)	CoV (%)	R-value (ft².°F.h/BTU)
1	BP-MK-30	0.240	2.77	945	4.20	1.16
2	BP-PU-30	0.286	2.06	929	2.39	0.99
3	BP-SF-30	0.266	2.66	910	1.58	1.07
4	BP-SL-30	0.363	1.37	914	3.02	0.78
5	BP-PC-30	0.370	1.00	917	5.57	0.77
6	BP-MK-MR3	0.282	1.82	963	2.29	0.99
7	BP-PU-MR3	0.376	1.55	979	1.54	0.74
8	BP-SF-MR3	0.222	1.99	849	2.31	1.25
9	BP-SL-MR3	0.380	1.23	816	6.47	0.75
10	BP-PC-MR3	0.592	1.58	886	3.58	0.48
11	BP-MK-MR0.8	0.184	4.30	759	4.96	1.48
12	BP-PU-MR0.8	0.251	2.78	850	3.52	1.11
13	BP-SF-MR0.8	0.195	5.37	760	2.88	1.45
14	BP-SL-MR1.1	0.328	3.76	916	2.36	0.85
15	BP-LIME	0.355	1.58	1063	3.44	0.78

λ=Thermal conductivity, CoV=Coefficient of variation, c=Specific heat capacity, R-value=Thermal resistance

Table 46- Statistical analysis of thermal conductivity results for different categories of binder pastes- ANOVA

Group of samples	SS	df	MS	F	P-value	F crit
Total results	0.88	14	0.06	1232	1.51E-82	1.83
30/70 SCM/lime	0.08	4	0.02	614	1.49E-24	2.76
With a molar ratio of 3	0.48	4	0.12	3139	2.28E-33	2.76
With a molar ratio of 0.8	0.02	2	0.01	102	1.83E-09	3.68
Containing Metakaolin	0.09	2	0.05	988	1.20E-16	3.68
Containing pumice	0.06	3	0.02	556	2.00E-19	3.10
Containing silica fume	0.09	3	0.03	559	1.92E-19	3.10
Containing slag	0.01	3	0.003	49	2.31E-09	3.10
Containing Portland cement	0.21	2	0.11	2394	1.62E-19	3.68

Table 47- Statistical analysis of specific heat capacity results for different categories of binder pastes- ANOVA

Group of samples	SS	df	MS	F	P-value	F crit
Total results	552274	14	39448	39.10	1.07E-28	1.83
30/70 SCM/lime	4875	4	1219	1.08	0.39 (> 5%)	2.76
With a molar ratio of 3	120727	4	30182	30.89	2.41E-09	2.76
With a molar ratio of 0.8	32829	2	16414	17.61	0.0001	3.68
Containing Metakaolin	281304	2	140652	97.37	2.56E-09	3.68
Containing pumice	143426	3	47809	64.73	1.78E-10	3.10
Containing silica fume	292880	3	97627	162.04	3.37E-14	3.10
Containing slag	187066	3	62355	46.63	3.27E-09	3.10
Containing Portland cement	107767	2	53884	32.66	3.42E-06	3.68

Comparing the thermal conductivity results of binder pastes with their characterizations, the results can primarily be attributed to dry density. The dry density reflects the sample's porosity and is thus a key factor in determining thermal conductivity. Although other factors, such as surface area or binder hydraulicity, may also impact thermal conductivity, none appears to be as governing as dry density.

In contrast, no relationship was found between the specific heat capacity of binder pastes and their dry density. Instead, the SCM component, which determines the hydraulicity of the material, appeared to have a direct influence on specific heat capacity. The hydrated lime without any SCM addition exhibited the highest specific heat capacity, while the incorporation of SCMs resulted in a decline in value. Furthermore, Figure 45 (and the corresponding statistics in Table 47) indicates that, when replacing 30% of lime with SCMs, the type of SCM does not significantly influence the specific heat capacity. However, an increase in the overall SCM content in the binder was observed to have a notable impact on the specific heat capacity of the samples.

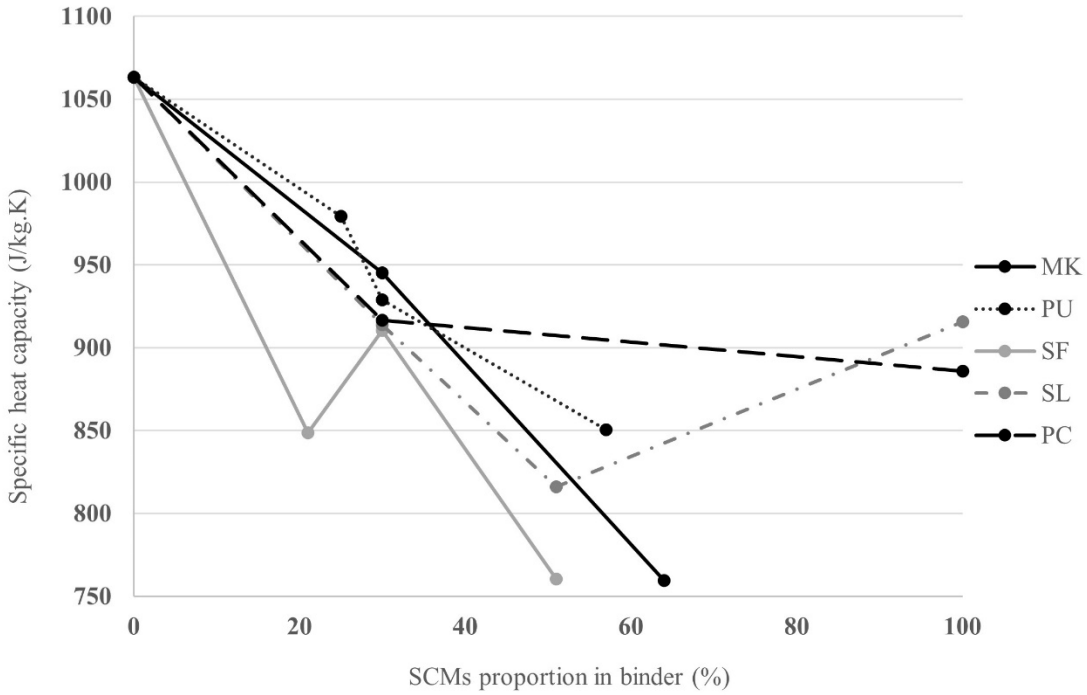

Figure 45- Specific heat capacity trend in binder pastes with the same SCM used in the composition

4.2.5 Water Vapour Permeability

The dominant effect of hemp hurd on hempcrete properties has been discussed several times in this study, and water vapour permeability is no exception. Consequently, the influence of binder type and composition on hempcrete's water vapour permeability appears less evident. However, the overall permeability of the

binder should be in line with that of the hemp hurd (Walker & Pavía, 2014b). Given that hemp hurd exhibits high permeability, a permeable binder can offer a consistent water vapour permeability behaviour in hempcrete. In this study, the water vapour permeability of the binder samples was evaluated independently of the hemp hurd. By eliminating the dominant effect of the hemp hurd, a more efficient comparison of binders was achieved, facilitating the identification of the most compatible binder for hempcrete. The particle size of the hemp hurd has been observed to have the least influence on the water vapour permeability of hempcrete (Brzyski *et al.*, 2020), which further underscores the binder's role as the key contributor.

Table 48 presents the water vapour permeability and the water vapour diffusion resistance factor, with results averaged over five distinct samples for each mix design. The water vapour diffusion resistance factor ranged from 3.5 for the mixture containing metakaolin and hydrated lime in a 64/36 proportion to 19.83 for the Portland cement binder paste. Similarly, the water vapour permeability values ranged from 1.03×10^{-11} to 5.79×10^{-11} kg/m.s.Pa for these mixed designs. There are not many studies comparing the results. However, the achieved water vapour permeability is in the same range as that reported in previous research (Issaadi *et al.*, 2015), although with a slightly higher magnitude. The permeability of binder materials is influenced by several factors, including component composition, porosity, and age (Alderete *et al.*, 2018; Issaadi *et al.*, 2015). Consequently, meaningful comparisons between binders are challenging unless these factors can be quantitatively accounted for. Furthermore, the coefficient of variation in this study ranged from 0.18% to 8.61% (as shown in Table 48), with an average of 2.39%, indicating a relatively low variability in the results.

The trend in the water vapour diffusion resistance factor is illustrated in Figure 46 as a function of the SCM proportion in the binder composition. As observed, the addition of metakaolin, pumice, and silica fume to the lime binder resulted in a slight reduction in the water vapour diffusion resistance factor. Alternatively, incorporating slag and Portland cement into the lime-based binder produced a significant increase in the resistance factor, with Portland cement exhibiting the highest increase. In other words, the inclusion of

pozzolanic materials in binders enhances water vapour permeability compared to hydrated lime, whereas hydraulic components tend to reduce permeability. However, the declining effect of hydraulic components is more pronounced than the enhancing effect of pozzolans in permeability (as shown in Table 49). The porosity of the binder pastes is identified as the most critical factor affecting water vapour permeability (Alderete *et al.*, 2018). Accordingly, the slag- and Portland cement-containing binders, which exhibited the highest apparent densities among all binders (shown in Table 23), also demonstrated the highest water vapour diffusion resistance factors.

Table 48- Average values for binder pastes' water vapour permeability and water vapour diffusion resistance factor

No.	Sample ID	WVP (kg/m.s.Pa)	CoV (%)	μ	CoV (%)
1	BP-MK-30	5.43E-11	2.10	3.73	2.04
2	BP-PU-30	5.12E-11	1.68	3.95	1.64
3	BP-SF-30	5.17E-11	4.36	3.92	4.64
4	BP-SL-30	4.03E-11	0.18	5.02	0.18
5	BP-PC-30	4.18E-11	0.88	4.85	0.87
6	BP-MK-MR3	5.46E-11	0.23	3.71	0.23
7	BP-PU-MR3	5.05E-11	0.77	4.01	0.78
8	BP-SF-MR3	5.11E-11	3.19	3.96	3.05
9	BP-SL-MR3	2.56E-11	0.22	7.92	0.23
10	BP-PC-MR3	1.03E-11	7.29	19.83	8.13
11	BP-MK-MR0.8	5.79E-11	1.28	3.50	1.20
12	BP-PU-MR0.8	5.12E-11	1.80	3.96	1.84
13	BP-SF-MR0.8	5.40E-11	1.73	3.75	1.69
14	BP-SL-MR1.1	1.97E-11	8.61	10.31	7.68
15	BP-LIME	4.75E-11	1.56	4.27	1.60

WVP=Water vapour permeability, CoV=Coefficient of variation, μ=water vapour diffusion resistance factor

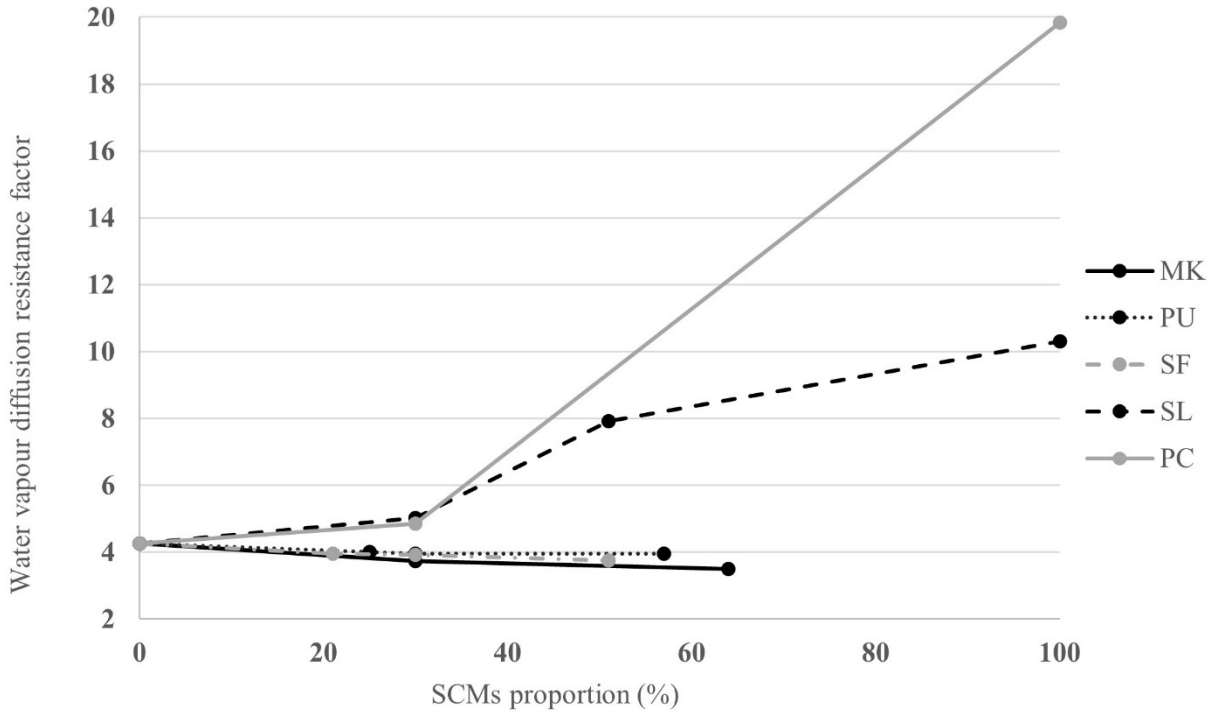

Figure 46- Water vapour diffusion resistance factor in binder pastes with the same SCM used in composition

Table 49- Statistical analysis of water vapour diffusion resistance factor for binders with the same SCM used in composition- ANOVA

Group of samples	SS	df	MS	F	P-value	F crit
Containing Metakaolin	0.48	2	0.24	19.59	0.019	9.55
Containing pumice	0.13	3	0.04	27.21	0.004	6.59
Containing silica fume	0.28	3	0.09	16.94	0.010	6.59
Containing slag	46.28	3	15.43	333.77	2.96E-05	6.59
Containing Portland cement	311.37	2	155.68	179.39	0.001	9.55

The results of this study appear to be in line with previous findings. As an example, Alderete *et al.* (2018) revealed that pozzolanic binders exhibit greater permeability than those containing slag. A similar report has been made by Walker (2013), indicating that metakaolin-based binders demonstrate higher water vapour permeability compared to slag-containing binders. In addition, Issaadi *et al.* (2015) found that partially replacing Portland cement with slag increases the permeability of binder pastes, further confirming

the present study's outcomes. Based on these observations, the higher permeability observed with metakaolin, pumice, and silica fume, as compared to slag and Portland cement, suggests that these materials are more suitable as binder components for achieving a more permeable binder and, consequently, a more consistent permeability profile in hempcrete.

Chapter 5

Conclusion, Limitations, and Future Research

5.1 Conclusion

This study aimed to introduce a more effective comparison of hempcrete components that have been less extensively examined, such as binder composition, through experimental research. To accomplish this, the most influential parameters in hempcrete characterization, namely, density and variations in hemp hurd particle size, were isolated. Hempcrete specimens were prepared using standardized, finely ground hemp hurd. The lightweight samples were developed with a relatively low target density of 190 kg/m^3 to maximize insulation performance. They were also produced with a relatively high hemp hurd-to-binder ratio (1:1 by weight), using locally available ingredients in Canada to minimize environmental impact.

In this context, hempcrete mix designs were developed using hydrated lime partially replaced by four different SCMs, aiming to enhance mechanical properties: metakaolin, pumice, silica fume, and slag. The results were compared with those of a similar mixture incorporating Portland cement as the most commonly used SCM, as well as a reference hempcrete composed solely of a hydrated lime binder. The replacement of hydrated lime with SCMs in hempcrete binders resulted in improved mechanical properties of the specimens, regardless of the SCM type. However, after reaching an optimal value, further increases in SCM content led to a decline in strength. This reduction was attributed to the insufficient availability of alkaline activators to fully react with the clay content. Binders incorporating pozzolanic SCMs exhibited higher compressive strength than those with hydraulic SCMs, with metakaolin ranked highest and slag ranked lowest. Nevertheless, all SCMs outperformed the reference SCM, Portland cement. Furthermore, hempcrete samples exhibited similar modulus of elasticity values across binders containing equal amounts of SCM, irrespective of SCM type. This indicates that while different SCMs in the binder composition of hempcrete result in varying compressive strength values, the modulus of elasticity remains independent of SCM type.

SCM content was also found to be influential in the hygrothermal properties of hempcrete. An increase in the SCM proportion in the binder resulted in a reduction in the thermal conductivity and heat capacity of the material. This trend was recorded regardless of the SCM type. In contrast, water vapour permeability was shown to be dependent on the specific SCM content in the hempcrete binder. Pozzolanic SCMs were identified as more suitable components, since they slightly enhanced the permeability of hydrated lime, whereas hydraulic SCMs significantly reduced it. Among the pozzolanic materials, metakaolin exhibited the highest permeability and was therefore identified as the most compatible SCM for hempcrete applications. These results suggest that the selection of an SCM for the binder should be based on the prioritized performance criteria. For instance, while metakaolin exhibited the best performance in both compressive strength and water vapour permeability, silica fume, as an industrial byproduct, may represent a more environmentally sustainable choice for hempcrete intended primarily for thermal insulation purposes.

In addition, the binder mix design was based on a novel approach using the binders' CaO/SiO_2 molar ratio. Accordingly, hempcrete binders with a CaO/SiO_2 molar ratio of 3 were developed and compared with binders having a molar ratio of 0.8, as well as with conventional percentage-based binders consisting of 70% hydrated lime and 30% SCM. By standardizing the most dominant molar ratio as the key factor in mechanical performance, the initial assumption was that this strategy would equalize compressive strength across all samples, thereby allowing for a concentration on the hygrothermal properties comparison. However, while the CaO/SiO_2 molar ratio was shown to influence mechanical properties, it was not the sole determining factor. Other variables, such as the alkaline activator-to-clay content ratio, binder surface area, and the molar ratios of additional chemical components, were also found to affect the mechanical strength of hempcrete. Despite this, hempcrete incorporating molar ratio-based binders demonstrated more consistent results than those made with conventional percentage-based binders. Furthermore, binders with a CaO/SiO_2 molar ratio of 3 produced hempcrete with superior mechanical properties compared to those with a ratio of 0.8, primarily due to the proportion of alkaline activator relative to clay content.

The specimens were also compared to their corresponding binder pastes, prepared without the addition of hemp hurd, to investigate the influence of bio-aggregate on binder properties. Comparing the compressive strength, a considerable reduction in strength was observed. This decrease was attributed to the dominant influence of the bio-aggregate, which possesses low mechanical strength, as well as the presence of soluble components in the hemp hurd that interfered with binder hydration. However, these soluble components were found to affect binders containing hydraulic SCMs with greater impact than those with pozzolanic characteristics, which further justifies the superior compressive behaviour of pozzolanic binders in hempcrete.

Furthermore, finely ground hemp hurd hempcrete was compared with conventional, as-received hemp hurd hempcrete to further examine the effect of hemp hurd particle size distribution. The hempcrete specimens containing finely ground hemp hurd exhibited slightly lower compressive strength than those prepared with as-received hemp particles. However, they demonstrated a more brittle behaviour, with a considerably higher modulus of elasticity compared to the more flexible behaviour of conventional hempcrete. The combination of low stiffness and high toughness in hempcrete incorporating as-received hemp hurd makes it a more suitable candidate for applications in earthquake-prone areas. Alternatively, hempcrete with finely ground hemp hurd showed superior thermal resistance and heat capacity. Accordingly, it is a more appropriate candidate for use as an insulation material due to the higher proportion of hemp hurd and the smaller volume of voids. Overall, whether fine or coarse hemp hurd particles are preferred depends on the intended application and the required performance characteristics.

5.2 Limitations and Recommendations for Future Work

This research offered insight into a novel approach for enabling more effective comparisons of hempcrete binder mix designs. However, further investigation is necessary to validate and expand upon these findings. The limitations of this study, which highlight opportunities for further research, are outlined as follows:

- By stabilizing the density, other variables such as the degree of compaction varied due to differences in binder components' densities. To address this issue, manual compaction was preferred over a standardized procedure. Future studies could focus on standardizing the compaction level to produce an equivalent void fraction in the specimens and compare the results accordingly.
- The specifications of the materials used in this study differed in several cases from those employed in previous research, leading to variations in the results. Future studies may prepare equivalent materials used in earlier work to enable direct comparison of outcomes.
- Although the use of finely ground hemp hurd contributed to more consistent results due to its reduced influence as a variable, the particle size was not optimized. Future research can focus on optimizing hemp hurd particle size to balance thermal insulation and mechanical performance.
- The effects of the studied parameters on hempcrete with higher target densities remain unexplored. In particular, the performance of molar ratio-based binders in higher-density hempcrete should be investigated.
- Further research is recommended to determine the optimal CaO/SiO_2 molar ratio for hempcrete binders. Additional chemical composition proportions, such as Al_2O_3/SiO_2 molar ratio and the proportion of alkaline activator relative to clay content, may also be taken into consideration for their influence on binder performance.
- A broader range of SCM proportions should be tested in hempcrete binders to more precisely characterize the behaviour of each combination across various properties.
- A detailed microstructural analysis of the chemical reactions between hempcrete components was beyond the scope of this study. However, future investigations are encouraged to explore these interactions to enhance understanding of material compatibility. Particular attention could be given to the effects of soluble compounds on SCMs and hydrated lime, as well as overall binder reactivity.
- Future studies may consider curing specimens under specific environmental conditions tailored to each binder type. This could enhance the hydration reactions and improve mechanical performance.

- Additional tests on the prepared specimens, such as flexural strength, moisture buffering capacity, acoustic performance, and fire resistance, are recommended to further assess material properties.
- A combination of different particle size measurement techniques is suggested to achieve a more precise determination of binder component particle sizes, due to the high margin of error associated with the laser diffraction method.
- Finally, a life cycle analysis of the hempcrete formulations should be conducted to evaluate the carbon footprint and environmental impact of the produced materials.

References

Abdellatef, Y., Khan, M. A., Khan, A., Alam, M. I., & Kavgic, M. (2020). Mechanical, Thermal, and Moisture Buffering Properties of Novel Insulating Hemp-Lime Composite Building Materials. Materials, 13(21), Article 21. https://doi.org/10.3390/ma13215000

Advanced Cement Technologies. (2025, January). Metakaolin. https://www.metakaolin.com/metakaolin/

Ahmad, M. R., Pan, Y., & Chen, B. (2021). Physical and mechanical properties of sustainable vegetal concrete exposed to extreme weather conditions. Construction and Building Materials, 287, 123024. https://doi.org/10.1016/j.conbuildmat.2021.123024

Ahmed, A. T. M. F., Islam, M. Z., Mahmud, M. S., Sarker, M. E., & Islam, M. R. (2022). Hemp as a potential raw material toward a sustainable world: A review. Heliyon, 8(1), e08753. https://doi.org/10.1016/j.heliyon.2022.e08753

Albidah, A. S. (2021). Effect of partial replacement of geopolymer binder materials on the fresh and mechanical properties: A review. Ceramics International, 47(11), 14923–14943. https://doi.org/10.1016/j.ceramint.2021.02.127

Alderete, N., Zaccardi, Y. A. V., Maio, A. A. D., & Belie, N. D. (2018). Isothermal water vapour permeability of concrete with different supplementary cementitious materials. Materiales de Construcción, 68(330), Article 330. https://doi.org/10.3989/mc.2018.02517

Almalkawi, A. T., Hamadna, S., & Soroushian, P. (2017). One-part alkali activated cement based volcanic pumice. Construction and Building Materials, 152, 367–374. https://doi.org/10.1016/j.conbuildmat.2017.06.139

Al-Tamimi, A., & Bindiganavile, V. (2024). Optimizing Mixture Components, Shiv Size and Content in Hempcrete for Thermal Capacitance. In N. Banthia, S. Soleimani-Dashtaki, & S. Mindess (Eds.), Smart & Sustainable Infrastructure: Building a Greener Tomorrow (pp. 641–649). Springer Nature Switzerland. https://doi.org/10.1007/978-3-031-53389-1_58

Al-Tamimi, A. S., Qasem, N. A. A., & Bindiganavile, V. (2024). Thermal performance evaluation of hempcrete masonry walls for energy storage in cold weather. Applied Thermal Engineering, 248, 123304. https://doi.org/10.1016/j.applthermaleng.2024.123304

Amziane, S., & Sonebi, M. (2016). Overview on Biobased Building Material made with plant aggregate. RILEM Technical Letters, 1, 31–38. https://doi.org/10.21809/rilemtechlett.2016.9

Ardanuy, M., Claramunt, J., & Toledo Filho, R. D. (2015). Cellulosic fiber reinforced cement-based composites: A review of recent research. Construction and Building Materials, 79, 115–128. https://doi.org/10.1016/j.conbuildmat.2015.01.035

Arehart, J. H., Nelson, W. S., & Srubar, W. V. (2020). On the theoretical carbon storage and carbon sequestration potential of hempcrete. Journal of Cleaner Production, 266, 121846. https://doi.org/10.1016/j.jclepro.2020.121846

Arnaud, L., & Gourlay, E. (2012). Experimental study of parameters influencing mechanical properties of hemp concretes. Construction and Building Materials, 28(1), 50–56. https://doi.org/10.1016/j.conbuildmat.2011.07.052

Arrigoni, A., Pelosato, R., Melià, P., Ruggieri, G., Sabbadini, S., & Dotelli, G. (2017). Life cycle assessment of natural building materials: The role of carbonation, mixture components and transport in the environmental impacts of hempcrete blocks. Journal of Cleaner Production, 149, 1051–1061. https://doi.org/10.1016/j.jclepro.2017.02.161

Asghari, N., & Memari, A. M. (2024). State of the Art Review of Attributes and Mechanical Properties of Hempcrete. Biomass, 4(1), Article 1. https://doi.org/10.3390/biomass4010004

ASTM C109/C109M − 21, Standard Test Method for Compressive Strength of Hydraulic Cement Mortars (Using 2-in. Or [50 mm] Cube Specimens). (2021). ASTM Standard.

ASTM C143/C143M− 20, Standard Test Method for Slump of Hydraulic Cement Concrete. (2020). ASTM International.

ASTM C150/C150M − 24 Standard Specification for Portland Cement. (2024). ASTM International.

ASTM C469/C469M-22, Standard Test Method for Static Modulus of Elasticity and Poisson's Ratio of Concrete in Compression. (2022). ASTM International.

ASTM C518- 21, Standard Test Method for Steady-State Thermal Transmission Properties by Means of the Heat Flow Meter Apparatus. (2021). ASTM International. https://compass.astm.org/document/?contentCode=ASTM%7CC0518-21%7Cen-US&proxycl=https%3A%2F%2Fsecure.astm.org&fromLogin=true

ASTM C618 − 23, Standard Specification for Coal Ash and Raw or Calcined Natural Pozzolan for Use in Concrete. (2023). ASTM Standard.

ASTM C989/C989M-24, Standard Specification for Slag Cement for Use in Concrete and Mortars. (2024). ASTM International.

ASTM E96/E96M-24, Standard Test Methods for Gravimetric Determination of Water Vapor Transmission Rate of Materials. (2024). ASTM International.

Awwad, E., Hamad, B., Mabsout, M., & Khatib, H. (2014). Structural Behavior of Simply Supported Beams Cast with Hemp-Reinforced Concrete. Structural Journal, 111(6), 1307–1316. https://doi.org/10.14359/51687032

Barbhuiya, S., & Bhusan Das, B. (2022). A comprehensive review on the use of hemp in concrete. Construction and Building Materials, 341, 127857. https://doi.org/10.1016/j.conbuildmat.2022.127857

Barbieri, V., Lassinantti Gualtieri, M., & Siligardi, C. (2020). Wheat husk: A renewable resource for bio-based building materials. Construction and Building Materials, 251, 118909. https://doi.org/10.1016/j.conbuildmat.2020.118909

Bendouma, M., Fortin, P., Perraton, D., & Ouellet-Plamondon, C. (2023). Binder Formulation and Properties of Hemp Concrete. In S. Amziane, I. Merta, & J. Page (Eds.), Bio-Based Building Materials (pp. 442–449). Springer Nature Switzerland.

Benmahiddine, F., Bennai, F., Cherif, R., Belarbi, R., Tahakourt, A., & Abahri, K. (2020). Experimental investigation on the influence of immersion/drying cycles on the hygrothermal and mechanical properties of hemp concrete. Journal of Building Engineering, 32, 101758. https://doi.org/10.1016/j.jobe.2020.101758

Benmahiddine, F., Cherif, R., Bennai, F., Belarbi, R., Tahakourt, A., & Abahri, K. (2020). Effect of flax shives content and size on the hygrothermal and mechanical properties of flax concrete. Construction and Building Materials, 262, 120077. https://doi.org/10.1016/j.conbuildmat.2020.120077

Bennai, F., El Hachem, C., Abahri, K., & Belarbi, R. (2018). Microscopic hydric characterization of hemp concrete by X-ray microtomography and digital volume correlation. Construction and Building Materials, 188, 983–994. https://doi.org/10.1016/j.conbuildmat.2018.08.198

Boulic, P., Allegret, S., & Arnaud, L. (2013). Hemp Industrial Production and Uses. CAB International.

Bp Statistical Review of World Energy (71 edition; p. 58). (2022). bp. www.bp.com

Brzyski, P. (2018). The effect of pozzolan addition on the physical and mechanical properties of lime mortar. E3S Web of Conferences, 49, 00009. https://doi.org/10.1051/e3sconf/20184900009

Brzyski, P., Gładecki, M., Rumińska, M., Pietrak, K., Kubiś, M., & Łapka, P. (2020). Influence of Hemp Shives Size on Hygro-Thermal and Mechanical Properties of a Hemp-Lime Composite. Materials, 13(23), Article 23. https://doi.org/10.3390/ma13235383

Building Materials and the Climate: Constructing a New Future. (2023). United Nations Environment Programme. https://wedocs.unep.org/xmlui/handle/20.500.11822/43293

Bumanis, G., Vitola, L., Pundiene, I., Sinka, M., & Bajare, D. (2020). Gypsum, Geopolymers, and Starch—Alternative Binders for Bio-Based Building Materials: A Review and Life-Cycle Assessment. Sustainability, 12(14), Article 14. https://doi.org/10.3390/su12145666

Cabeza, L. F., Boquera, L., Chàfer, M., & Vérez, D. (2021). Embodied energy and embodied carbon of structural building materials: Worldwide progress and barriers through literature map analysis. Energy and Buildings, 231, 110612. https://doi.org/10.1016/j.enbuild.2020.110612

Canadian Commission on Building and Fire Codes. (2022). National Building Code of Canada 2020 (Fifteenth edition 2020.). Canadian Commission on Building and Fire Codes,.

Carbon Dioxide Concentration | NASA Global Climate Change. (2024). Climate Change: Vital Signs of the Planet. https://climate.nasa.gov/vital-signs/carbon-dioxide?intent=111

Chabannes, M., Bénézet, J.-C., Clerc, L., & Garcia-Diaz, E. (2014). Use of raw rice husk as natural aggregate in a lightweight insulating concrete: An innovative application. Construction and Building Materials, 70, 428–438. https://doi.org/10.1016/j.conbuildmat.2014.07.025

Chau, K., Fleck, R., Irga, P. J., Torpy, F. R., Wilkinson, S. J., & Castel, A. (2023). Hempcrete as a substrate for fungal growth under high humidity and variable temperature conditions. Construction and Building Materials, 398, 132373. https://doi.org/10.1016/j.conbuildmat.2023.132373

Chellapandian, M., Arunachelam, N., Maheswaran, J., & Kumar, N. P. (2024). Shear behavior of low-cost and sustainable bio-fiber based engineered cementitious composite beams –experimental and theoretical studies. Journal of Building Engineering, 84, 108497. https://doi.org/10.1016/j.jobe.2024.108497

Ciment Quebec. (2024). Portland Cement. https://www.cimentquebec.com/en-can/cement/product-line/portland-cement/

Climate Change—NASA Science. (2024). https://science.nasa.gov/climate-change/

Collet, F., Bart, M., Serres, L., & Miriel, J. (2008). Porous structure and water vapour sorption of hemp-based materials. Construction and Building Materials, 22(6), 1271–1280. https://doi.org/10.1016/j.conbuildmat.2007.01.018

Collet, F., Chamoin, J., Pretot, S., & Lanos, C. (2013). Comparison of the hygric behaviour of three hemp concretes. Energy and Buildings, 62, 294–303. https://doi.org/10.1016/j.enbuild.2013.03.010

Costantine, G., Maalouf, C., Moussa, T., & Polidori, G. (2018). Experimental and numerical investigations of thermal performance of a Hemp Lime external building insulation. Building and Environment, 131, 140–153. https://doi.org/10.1016/j.buildenv.2017.12.037

Daher, S., Benazzouk, A., Hamed, H., & Langlet, T. (2022). Performance Improved of a Lime and Hemp-Based Concrete through the Addition of Metakaolin. Fluid Dynamics & Materials Processing, 19(5), 1091–1113. https://doi.org/10.32604/fdmp.2023.020348

de Bruijn, P. B., Jeppsson, K.-H., Sandin, K., & Nilsson, C. (2009). Mechanical properties of lime–hemp concrete containing shives and fibres. Biosystems Engineering, 103(4), 474–479. https://doi.org/10.1016/j.biosystemseng.2009.02.005

de Bruijn, P., & Johansson, P. (2013). Moisture fixation and thermal properties of lime–hemp concrete. Construction and Building Materials, 47, 1235–1242. https://doi.org/10.1016/j.conbuildmat.2013.06.006

Delhomme, F., Castel, A., Almeida, A., Jiang, C., Moreau, D., Gan, Y., Wang, X., & Wilkinson, S. (2022). Mechanical, Acoustic and Thermal Performances of Australian Hempcretes. In C. Ha-Minh, A. M. Tang, T. Q. Bui, X. H. Vu, & D. V. K. Huynh (Eds.), CIGOS 2021, Emerging Technologies and Applications for Green Infrastructure (pp. 753–761). Springer Nature. https://doi.org/10.1007/978-981-16-7160-9_76

Dhakal, U., Berardi, U., Gorgolewski, M., & Richman, R. (2017). Hygrothermal performance of hempcrete for Ontario (Canada) buildings. Journal of Cleaner Production, 142, 3655–3664. https://doi.org/10.1016/j.jclepro.2016.10.102

Elfordy, S., Lucas, F., Tancret, F., Scudeller, Y., & Goudet, L. (2008). Mechanical and thermal properties of lime and hemp concrete ("hempcrete") manufactured by a projection process. Construction and Building Materials, 22(10), 2116–2123. https://doi.org/10.1016/j.conbuildmat.2007.07.016

Elzeadani, M., Bompa, D. V., & Elghazouli, A. Y. (2022). One part alkali activated materials: A state-of-the-art review. Journal of Building Engineering, 57, 104871. https://doi.org/10.1016/j.jobe.2022.104871

Evrard, A. (2008). Transient hygrothermal behaviour of Lime-Hemp Materials. Ecole Polytechnique de Louvai.

Evrard, A., & De Herde, A. (2010). Hygrothermal Performance of Lime-Hemp Wall Assemblies. Journal of Building Physics, 34(1), 5–25. https://doi.org/10.1177/1744259109355730

Garcia-Lodeiro, I., Palomo, A., & Fernández-Jiménez, A. (2015a). An overview of the chemistry of alkali-activated cement-based binders. In Handbook of Alkali-activated Cements, Mortars and Concretes (pp. 19–47).

Garcia-Lodeiro, I., Palomo, A., & Fernández-Jiménez, A. (2015b). Crucial insights on the mix design of alkali-activated cement-based binders. In Handbook of Alkali-activated Cements, Mortars and Concretes (pp. 49–73).

GlobalABC Roadmap for Buildings and Construction, 2020-2050. (2020). GlobalABC, IEA and UNEP. https://www.iea.org/reports/globalabc-roadmap-for-buildings-and-construction-2020-2050

Government of Canada, S. C. (2024). Crop production: Visualization tool. https://www150.statcan.gc.ca/n1/pub/71-607-x/71-607-x2020025-eng.htm

Grazieschi, G., Asdrubali, F., & Thomas, G. (2021). Embodied energy and carbon of building insulating materials: A critical review. Cleaner Environmental Systems, 2, 100032. https://doi.org/10.1016/j.cesys.2021.100032

He, Y., Lu, L., Struble, L. J., Rapp, J. L., Mondal, P., & Hu, S. (2014). Effect of calcium–silicon ratio on microstructure and nanostructure of calcium silicate hydrate synthesized by reaction of fumed silica and calcium oxide at room temperature. Materials and Structures, 47(1), 311–322. https://doi.org/10.1617/s11527-013-0062-0

Hedayatinia, F., Delnavaz, M., & Emamzadeh, S. S. (2019). Rheological properties, compressive strength and life cycle assessment of self-compacting concrete containing natural pumice pozzolan. Construction and Building Materials, 206, 122–129. https://doi.org/10.1016/j.conbuildmat.2019.02.059

Hess Pumice. (2024). https://hesspumice.com/downloads/down-infoPubs.html

High Calcium Hydrated Lime | Graymont. (2024). Graymont. https://www.graymont.com/en/products/hydrated-lime/high-calcium-hydrated-lime-0

Horszczaruk, E., Strzałkowski, J., Głowacka, A., Paszkiewicz, O., & Markowska-Szczupak, A. (2023). Investigation of Durability Properties for Lightweight Structural Concrete with Hemp Shives Instead of Aggregate. Applied Sciences (Switzerland), 13(14). Scopus. https://doi.org/10.3390/app13148447

Hussain, A., Calabria-Holley, J., Lawrence, M., & Jiang, Y. (2019). Hygrothermal and mechanical characterisation of novel hemp shiv based thermal insulation composites. Construction and Building Materials, 212, 561–568. https://doi.org/10.1016/j.conbuildmat.2019.04.029

Ip, K., & Miller, A. (2012). Life cycle greenhouse gas emissions of hemp–lime wall constructions in the UK. Resources, Conservation and Recycling, 69, 1–9. https://doi.org/10.1016/j.resconrec.2012.09.001

Issaadi, N., Nouviaire, A., Belarbi, R., & Aït-Mokhtar, A. (2015). Moisture characterization of cementitious material properties: Assessment of water vapor sorption isotherm and permeability variation with ages. Construction and Building Materials, 83, 237–247. https://doi.org/10.1016/j.conbuildmat.2015.03.030

Jahami, A., Zeaiter, N., & Cheaib, M. (2024). Reviewing the potential: A comprehensive review of natural fibers (NFs) in structural concrete and their multifaceted influences. Innovative Infrastructure Solutions, 9(4), 102. https://doi.org/10.1007/s41062-024-01384-x

Jami, T., Karade, S. R., & Singh, L. P. (2019). A review of the properties of hemp concrete for green building applications. Journal of Cleaner Production, 239, 117852. https://doi.org/10.1016/j.jclepro.2019.117852

Jiang, Y., Lawrence, M., Ansell, M. P., & Hussain, A. (2018). Cell wall microstructure, pore size distribution and absolute density of hemp shiv. Royal Society Open Science, 5(4), 171945. https://doi.org/10.1098/rsos.171945

Jirgensone, B., Birjukovs, M., Sinka, M., Jakovics, A., & Bajare, D. (2024). Hygrothermal performance of hempcrete in a multi-layer wall envelope. Journal of Building Engineering, 84, 108359. https://doi.org/10.1016/j.jobe.2023.108359

Kaboré, A., Maref, W., & Ouellet-Plamondon, C. M. (2024). Hygrothermal Performance of the Hemp Concrete Building Envelope. Energies, 17(7), Article 7. https://doi.org/10.3390/en17071740

Karimpour, M., Belusko, M., Xing, K., & Bruno, F. (2014). Minimising the life cycle energy of buildings: Review and analysis. Building and Environment, 73, 106–114. https://doi.org/10.1016/j.buildenv.2013.11.019

Khan, M. A. (2020). Physical and Microstructural Properties of Insulating Hempcrete Mixes and their Impact as Infill System on the Foundations due to Increase in Dead Load [Masters]. University of Manitoba.

Kinnane, O., Reilly, A., Grimes, J., Pavia, S., & Walker, R. (2016a). Acoustic Absorption of Hemp Walls with Ground Granulated Blast Slag. Int. J. Archit. Environ. Eng, 10(9), 1188–1191.

Kinnane, O., Reilly, A., Grimes, J., Pavia, S., & Walker, R. (2016b). Acoustic absorption of hemp-lime construction. Construction and Building Materials, 122, 674–682. https://doi.org/10.1016/j.conbuildmat.2016.06.106

Laborel-Préneron, A., Magniont, C., & Aubert, J.-E. (2018). Characterization of Barley Straw, Hemp Shiv and Corn Cob as Resources for Bioaggregate Based Building Materials. Waste and Biomass Valorization, 9(7), 1095–1112. https://doi.org/10.1007/s12649-017-9895-z

Lagouin, M., Magniont, C., Sénéchal, P., Moonen, P., Aubert, J.-E., & Laborel-préneron, A. (2019). Influence of types of binder and plant aggregates on hygrothermal and mechanical properties of vegetal concretes. Construction and Building Materials, 222, 852–871. https://doi.org/10.1016/j.conbuildmat.2019.06.004

Le, A. T., Gacoin, A., Li, A., Mai, T. H., Rebay, M., & Delmas, Y. (2014). Experimental investigation on the mechanical performance of starch–hemp composite materials. Construction and Building Materials, 61, 106–113. https://doi.org/10.1016/j.conbuildmat.2014.01.084

Liu, C. H. J., Pomponi, F., & D'Amico, B. (2023). The Extent to Which Hemp Insulation Materials Can Be Used in Canadian Residential Buildings. Sustainability (Switzerland), 15(19). Scopus. https://doi.org/10.3390/su151914471

Magniont, C., Escadeillas, G., Coutand, M., & Oms-Multon, C. (2012). Use of plant aggregates in building ecomaterials. European Journal of Environmental and Civil Engineering, 16(sup1), s17–s33. https://doi.org/10.1080/19648189.2012.682452

Magwood, C. (2016). Essential Hempcrete Construction, The complete step-by-step guide (Sustainable building essentials). New Society Publishers.

Mahmood, O., Kavgic, M., & Noel, M. (2024). Hygrothermal and mechanical characterization of novel hemp-lime composites with enhanced consistency. Construction and Building Materials, 450, 138720. https://doi.org/10.1016/j.conbuildmat.2024.138720

Marceau, S., & Delannoy, G. (2017). Durability of Bio-based Concretes. In S. Amziane & F. Collet (Eds.), Bio-aggregates Based Building Materials: State-of-the-Art Report of the RILEM Technical Committee 236-BBM (pp. 167–187). Springer Netherlands. https://doi.org/10.1007/978-94-024-1031-0_8

Martínez, B., Mendizabal, V., Roncero, M. B., Bernat-Maso, E., & Gil, L. (2024). Towards sustainable building solutions: Development of hemp shiv-based green insulation material. Construction and Building Materials, 414, 134987. https://doi.org/10.1016/j.conbuildmat.2024.134987

MasterLife SF 100 | Master Builders Solutions. (2024). https://www.master-builders-solutions.com/en-us/products/concrete-admixtures/silica-fume/masterlife-sf-100

Murphy, F., Pavia, S., & Walker, R. (2010). An assessment of the physical properties of lime-hemp concrete. BCRI Bridge Infrastructure Concrete Research University of Cork, Walsh, 431–438.

Néron, A. (2019). Workshop guide, hempcrete and lime plasters. DuChanvre.

Nguyen, T. T., Picandet, V., Carre, P., Lecompte, T., Amziane, S., & Baley, C. (2010). Effect of compaction on mechanical and thermal properties of hemp concrete. European Journal of Environmental and Civil Engineering, 14(5), 545–560. https://doi.org/10.1080/19648189.2010.9693246

Nguyen, T.-T., Picandet, V., Amziane, S., & Baley, C. (2009). Influence of compactness and hemp hurd characteristics on the mechanical properties of lime and hemp concrete. European Journal of Environmental and Civil Engineering, 13(9), 1039–1050. https://doi.org/10.1080/19648189.2009.9693171

Niyigena, C., Amziane, S., & Chateauneuf, A. (2018). Multicriteria analysis demonstrating the impact of shiv on the properties of hemp concrete. Construction and Building Materials, 160, 211–222. https://doi.org/10.1016/j.conbuildmat.2017.11.026

Nozahic, V., Amziane, S., Torrent, G., Saïdi, K., & De Baynast, H. (2012). Design of green concrete made of plant-derived aggregates and a pumice–lime binder. Cement and Concrete Composites, 34(2), 231–241. https://doi.org/10.1016/j.cemconcomp.2011.09.002

Oti, J., Kinuthia, J., & Kırgız, M. S. (2024). 18—Ecology-based green clay–hemp brick material made with ground granulated blast-furnace slag. In M. S. Kırgız (Ed.), Advance Upcycling of By-Products in Binder and Binder-Based Materials (pp. 357–372). Woodhead Publishing. https://doi.org/10.1016/B978-0-323-90791-0.00026-3

Pandini, N. T., Dias, D. P., & Rangel, J. V. S. (2020). Influence of the CaO/SiO2 molar ratio on the technological properties of alkali-activated fly ash mortar with quicklime. Engineering Research Express, 2(4), 045015. https://doi.org/10.1088/2631-8695/abc184

Panesar, D. K. (2019). 3—Supplementary cementing materials. In S. Mindess (Ed.), Developments in the Formulation and Reinforcement of Concrete (Second Edition) (pp. 55–85). Woodhead Publishing. https://doi.org/10.1016/B978-0-08-102616-8.00003-4

Pavía, S., & Aly, M. (2016). Influence of aggregate and supplementary cementitious materials on the properties of hydrated lime (CL90s) mortars. Materiales de Construcción, 66, 104. https://doi.org/10.3989/mc.2016.01716

Pavía, S., Walker, R., & McGinn, J. (2015). Effect of testing variables on the hydration and compressive strength of lime hemp concrete. Academic Journal of Civil Engineering, 33(2), 635–640.

Piot, A., Béjat, T., Jay, A., Bessette, L., Wurtz, E., & Barnes-Davin, L. (2017). Study of a hempcrete wall exposed to outdoor climate: Effects of the coating. Construction and Building Materials, 139, 540–550. https://doi.org/10.1016/j.conbuildmat.2016.12.143

Provis, J. L., Duxson, P., & van Deventer, J. S. J. (2010). The role of particle technology in developing sustainable construction materials. Advanced Powder Technology, 21(1), 2–7. https://doi.org/10.1016/j.apt.2009.10.006

Ra, J., Shin, S., & Kim, J. (2023). Experimental Study on the Properties of Autoclave Curing High-Strength Concrete According to CaO/SiO2 Ratio. Applied Sciences, 13(10), Article 10. https://doi.org/10.3390/app13106190

Rahim, M., Douzane, O., Tran Le, A. D., & Langlet, T. (2016). Effect of moisture and temperature on thermal properties of three bio-based materials. Construction and Building Materials, 111, 119–127. https://doi.org/10.1016/j.conbuildmat.2016.02.061

Rosa Latapie, S., Sabathier, V., & Abou-Chakra, A. (2024). Bio-based building materials: A prediction of insulating properties for a wide range of agricultural by-products. Journal of Building Engineering, 86, 108867. https://doi.org/10.1016/j.jobe.2024.108867

Saeidpour, M., & Wadsö, L. (2016). Moisture diffusion coefficients of mortars in absorption and desorption. Cement and Concrete Research, 83, 179–187. https://doi.org/10.1016/j.cemconres.2016.02.003

Saleh Ahari, R., Erdem, T. K., & Ramyar, K. (2015). Permeability properties of self-consolidating concrete containing various supplementary cementitious materials. Construction and Building Materials, 79, 326–336. https://doi.org/10.1016/j.conbuildmat.2015.01.053

Sassoni, E., Manzi, S., Motori, A., Montecchi, M., & Canti, M. (2014). Novel sustainable hemp-based composites for application in the building industry: Physical, thermal and mechanical characterization. Energy and Buildings, 77, 219–226. https://doi.org/10.1016/j.enbuild.2014.03.033

Seraj, S., Cano, R., Ferron, R. D., & Juenger, M. C. G. (2017). The role of particle size on the performance of pumice as a supplementary cementitious material. Cement and Concrete Composites, 80, 135–142. https://doi.org/10.1016/j.cemconcomp.2017.03.009

Shea, A., Lawrence, M., & Walker, P. (2012). Hygrothermal performance of an experimental hemp–lime building. Construction and Building Materials, 36, 270–275. https://doi.org/10.1016/j.conbuildmat.2012.04.123

Shewalul, Y. W., Quiroz, N. F., Streicher, D., & Walls, R. (2023). Fire behavior of hemp blocks: A biomass-based construction material. Journal of Building Engineering, 80, 108147. https://doi.org/10.1016/j.jobe.2023.108147

Shobeiri, V., Bennett, B., Xie, T., & Visintin, P. (2021). A comprehensive assessment of the global warming potential of geopolymer concrete. Journal of Cleaner Production, 297, 126669. https://doi.org/10.1016/j.jclepro.2021.126669

Sinka, M., Sahmenko, G., & Korjakins, A. (2014). Mechanical Properties of Pre-Compressed Hemp-Lime Concrete. Journal of Sustainable Architecture and Civil Engineering, 8(3), Article 3. https://doi.org/10.5755/j01.sace.8.3.7451

Sinka, M., Sahmenko, G., Korjakins, A., Radina, L., & Bajare, D. (2015). Hemp Thermal Insulation Concrete with Alternative Binders, Analysis of their Thermal and Mechanical Properties. IOP Conference Series: Materials Science and Engineering, 96(1), 012029. https://doi.org/10.1088/1757-899X/96/1/012029

Song, H., Kim, T., Hajimohammadi, A., Oh, J. E., & Castel, A. (2024). Detailed characterisation of hemp and hempcrete pore structures: Effects on thermal and acoustic properties. Cement and Concrete Research, 186, 107702. https://doi.org/10.1016/j.cemconres.2024.107702

Stanwix, W., & Sparrow, A. (2014). The hempcrete book, designing and building with hemp-lime. Green Books.

Strandberg-de Bruijn, P., & Johansson, P. (2014). Moisture transport properties of lime–hemp concrete determined over the complete moisture range. Biosystems Engineering, 122, 31–41. https://doi.org/10.1016/j.biosystemseng.2014.03.001

Tale Masoule, M. S., Bahrami, N., Karimzadeh, M., Mohasanati, B., Shoaei, P., Ameri, F., & Ozbakkaloglu, T. (2022). Lightweight geopolymer concrete: A critical review on the feasibility, mixture design, durability properties, and microstructure. Ceramics International, 48(8), 10347–10371. https://doi.org/10.1016/j.ceramint.2022.01.298

Tale Ponga, D., Sabziparvar, A., Cousin, P., Boulos, L., Robert, M., & Foruzanmehr, M. R. (2023). Retarding Effect of Hemp Hurd Lixiviates on the Hydration of Hydraulic and CSA Cements. Materials, 16(16), Article 16. https://doi.org/10.3390/ma16165561

The Paris Agreement. (2015, December). United Nation. https://unfccc.int/process-and-meetings/the-paris-agreement

T.Mabah, D. E., K.Tchakouté, H., Fotio, D., Rüscher, C. H., Kamseu, E., Bignozzi, M. C., & Leonelli, C. (2019). Influence of the molar ratios CaO/SiO2 contained in the sustainable microcomposites on the mechanical and microstructural properties of (Ca, Na)-poly(sialate-siloxo) networks. Materials Chemistry and Physics, 238, 121928. https://doi.org/10.1016/j.matchemphys.2019.121928

Tran-Le, A. D., Nguyen, S.-T., & Langlet, T. (2019). A novel anisotropic analytical model for effective thermal conductivity tensor of dry lime-hemp concrete with preferred spatial distributions. Energy and Buildings, 182, 75–87. https://doi.org/10.1016/j.enbuild.2018.09.043

Vyšvařil, M., Krebs, M., & Bayer, P. (2023). Dual use of pumice in lime mortars. Materials Today: Proceedings. https://doi.org/10.1016/j.matpr.2023.05.534

Walker, R. (2013). A Study of the Properties of Lime-Hemp Concrete with Pozzolans [PHD Thesis]. University of Dublin, Trinity College.

Walker, R., & Pavía, S. (2011). Physical properties and reactivity of pozzolans, and their influence on the properties of lime–pozzolan pastes. Materials and Structures, 44(6), 1139–1150. https://doi.org/10.1617/s11527-010-9689-2

Walker, R., & Pavía, S. (2014a). Influence of the Type of Binder on the Properties of Lime-Hemp Concrete. In C. Llinares-Millán, I. Fernández-Plazaola, F. Hidalgo-Delgado, M. M. Martínez-Valenzuela, F. J. Medina-Ramón, I. Oliver-Faubel, I. Rodríguez-Abad, A. Salandin, R. Sánchez-Grandia, & I. Tort-Ausina (Eds.), Construction and Building Research (pp. 505–514). Springer Netherlands.

Walker, R., & Pavía, S. (2014b). Moisture transfer and thermal properties of hemp–lime concretes. Construction and Building Materials, 64, 270–276. https://doi.org/10.1016/j.conbuildmat.2014.04.081

Walker, R., & Pavía, S. (2015). Thermal performance of a selection of insulation materials suitable for historic buildings. Building and Environment, 94, 155–165. https://doi.org/10.1016/j.buildenv.2015.07.033

Walker, R., Pavia, S., & Mitchell, R. (2014). Mechanical properties and durability of hemp-lime concretes. Construction and Building Materials, 61, 340–348. https://doi.org/10.1016/j.conbuildmat.2014.02.065

Wang, L., Lenormand, H., Zmamou, H., & Leblanc, N. (2021). Effect of variability of hemp shiv on the setting of lime hemp concrete. Industrial Crops and Products, 171, 113915. https://doi.org/10.1016/j.indcrop.2021.113915

Wang, X., Li, C., Chen, G., Lin, H., Wu, W., Wang, Q., & Lan, Q. (2024). Effect of CaO/SiO2 and Al2O3/SiO2 on the chloride permeability of one-part alkali-activated nickel slag concrete. Construction and Building Materials, 411, 134348. https://doi.org/10.1016/j.conbuildmat.2023.134348

Williams, J., Lawrence, M., & Walker, P. (2017). Projection formed and precast hemp-lime: Better by design? Academic Journal of Civil Engineering, 35(2), Article 2. https://doi.org/10.26168/icbbm2017.38

Williams, J., Lawrence, M., & Walker, P. (2018). The influence of constituents on the properties of the bio-aggregate composite hemp-lime. Construction and Building Materials, 159, 9–17. https://doi.org/10.1016/j.conbuildmat.2017.10.109

World Energy Outlook 2022 (p. 523). (2022). International Energy Agency. https://www.iea.org/reports/world-energy-outlook-2022

Zerrouki, R., Benazzouk, A., Courty, M., & Ben Hamed, H. (2022). Potential use of matakaolin as a partial replacement of preformulated lime binder to improve durability of hemp concrete under cyclic wetting/drying aging. Construction and Building Materials, 333, 127389. https://doi.org/10.1016/j.conbuildmat.2022.127389

Zeyad, A. M., Magbool, H. M., Tayeh, B. A., Garcez de Azevedo, A. R., Abutaleb, A., & Hussain, Q. (2022). Production of geopolymer concrete by utilizing volcanic pumice dust. Case Studies in Construction Materials, 16, e00802. https://doi.org/10.1016/j.cscm.2021.e00802

Appendix A

a. Physical and chemical properties of hydrated lime (*High Calcium Hydrated Lime | Graymont*, 2024).

Physical state and appearance:	Solid- fine powder
Colour:	White
Odour:	Sweet soil-like odour
pH:	12.45 saturated solution at 25℃
Relative density:	2.3- 2.4
Solubility:	Water: 0.165 g /100 ml at 20℃
Decomposition temperature:	540℃

b. Physical and chemical properties of metakaolin provided by the manufacturer (*Advanced Cement Technologies*, 2025).

Physical state and appearance:	Solid- fine powder
Colour:	Off-white
Odour:	Odourless
pH:	4-8 (at 20℃)
Specific gravity:	2.60
Apparent density:	400 kg/m^3
Melting range:	1400-1800 ℃
Brightness:	80-82 Hunter L
Water solubility:	Insoluble
Decomposition temperature:	400-550℃

c. Physical and chemical properties of pumice according to the company's datasheet (*Hess Pumice*, 2024).

Physical state and appearance:	Solid- fine powder
Colour:	White
GE brightness:	84
pH:	7.2
Specific gravity:	2.35
Bulk density of loose:	1120 kg/m^3 (max)
Loss on ignition:	5% max
Water soluble substance:	0.15%
Softening point:	900℃

d. Silica fume's physical and chemical properties (*MasterLife SF 100 | Master Builders Solutions*, 2024).

Physical state and appearance:	Solid- fine powder
Colour:	Dark grey
Odour:	Odourless
pH:	6-8
Specific gravity:	2.2
Density:	2100-2300 kg/m^3
Melt/freezing point:	1550-1700℃
Water solubility:	insoluble

e. Physical and chemical specifications of slag according to the distributor's Mill Certificate.

Physical state and appearance:	Solid- fine powder
Colour:	Light grey
Odour:	Slight sulphur odour
Specific gravity:	2.91
Melt/freezing point:	1425℃
Water solubility:	insoluble

f. Portland Cement's specifications according to the company's datasheet (*Ciment Quebec*, 2024).

Physical state and appearance:	Solid- fine powder
Colour:	Grey
Odour:	Odourless
pH in water:	12-13
Specific gravity:	3.2
Boiling point:	Over 1000℃
Water solubility:	Slightly soluble- 0.1-1%
Flammability limit:	Non-flammable and non-combustible